To the Graduate Council:

I am submitting herewith a thesis written by Ting Song entitled "Electron Beam Cured Resins for Wood Composites." I have examined the final electronic copy of this thesis for form and content and recommend that it be accepted in partial fulfillment of the requirements for the degree of Master of Science, with a major in Polymer Engineering.

Timothy G. Rials

Major Professor

We have read this thesis
and recommend its acceptance:

David P. Harper

Kevin M. Kit

Accepted for the Council:

Anne Mayhew

Vice Chancellor and
Dean of Graduate Studies

(Original signatures are on files with official student records.)

ELECTRON BEAM CURED RESINS FOR WOOD COMPOSITES

A Thesis Presented for the

Master of Science Degree

The University of Tennessee, Knoxville

Ting Song

August 2005

ACKNOWLEDGEMENTS

I am especially grateful to Dr. George F. Dorsey, for his guidance and patience over the past two years. Besides presenting his advice in the research work, he presents me, a curious international student, a bridge to the American social lives and customs.

Special appreciation is extended to Dr. Timothy G. Rials, my major advisor, for his help and suggestion in the research and studies.

Particular thanks go to Dr. William Tze, William Moschler, and Chris Helton, for their considerable time and effort in helping me to complete this work.

Thanks also go to Dr. David Harper and Dr. Kevin Kit, who provided helpful suggestions in the thesis.

Many thanks go to all of the people in Tennessee Forest Products Center, who offered help and encouragement in the past two years.

Acknowledgements also go to the US Department of Energy for financial support, as well as IBA SteriGenics International, UCB and Sartomer, for e-beam access and materials they provided.

ABSTRACT

Adoption of rapid, low temperature electron beam curable resin systems provide a great potential for energy saving to the wood composites industry. Other considerable advantages benefit from the radiation progression including: cost saving, reduction curing time, increased throughout capacity, minimal volatile emissions, increased the design flexibility.

The research was mainly focused on radiation dose optimization, resin structure-property relationships investigation, and resin-wood bonds evaluation. Resin chemical, physical, and mechanical properties were explored in detail by means of various testing methods. The formulating studies were concentrated on the radiation curable monomers (polyfunctional and monofunctional) and their effects to the network performance. Mechanical evaluation of resin-wood bonds was carried out, and particular attention was paid to bondline investigation.

The research found that the radiation dose for a complete curing was in the range of 20 kGy to 40 kGy for most acrylate or methacrylate based resins. The resin formulating studies revealed that polyfunctional monomers increased brittleness of the resin matrix, whereas monofunctional monomers d improved energy dissipation in the polymer network. Investigation of the correlation of resin properties and bond performance indicated that energy dissipation of resin is an important factor affecting the mechanical performance of bonded joints. Thus the adhesive-wood bond strength can be manipulated by adjusting formulation. The study also showed no statistically significant correlations between wetting (indicated by contact angle and viscosity) and bond

mechanical properties. However, results showed a strong relationship between resin viscosity and penetration into the wood substrate. This suggests that formulation variables can be used to control the breadth of the interphase, and ultimately composite properties.

Finally, the experiments suggest that external, uncontrolled factors created by the conditions of joint preparation may have complicated analysis and interpretation of the data. Specifically, long times between resin application and subsequent cure may have led to over-penetration or other bondline defects.

TABLE OF CONTENTS

LIST OF TABLES

Table **Page**

LIST OF FIGURES

Figure **Page**

1 INTRODUCTION

The production of glued-wood assemblies, which accounts for almost a half of the US wood based industry, is a major consumer of heat energy. The heat energy is mainly used to dry the parent wood material, to assist in consolidation flat-pressed panel products, and to polymerize and cure the resin system. Most of these glued-wood assemblies, ranging from structural laminated beams, flat pressed panels to furniture assemblies and non-structural wood assemblies, are referred to as wood composites. Controlling moisture content of the wood furnish materials is a vital procedure in the manufacturing plant and requires considerable process heat. A high moisture level can generate an excess steam vapor pressure internal to the wood product leading to so-called "internal blows". A lack of moisture control eventually results in an inferior product quality and wastage of natural resources. Therefore, a large amount of heat energy is required in the wood composites production to dry the wood furnish materials and control the substrates moisture level.

Development of rapid, low-temperature electron beam curable resin systems provides a great potential for energy saving to the wood composites industry. Moisture content, which needs to be closely monitored during hot pressing, is not as important in electron beam curing. The parent wood materials are allowed to have a higher level of moisture content without having impact on the electron radiation curing progress. Therefore a great deal of energy is saved due to less drying (Sturgeon, 1989). Cross-linking of polymers in composites by means of electron beam radiation requires less energy than thermo-chemical curing on account of the low temperature and shortened

curing time (Ivanov, 1992). Thus a large amount of overall energy saving is foreseen by introducing electron beam technology to the wood composite industry.

European wood products and paper manufacturers are taking advantage of the cost reduction by the aid of electron beam in production. The economic study of the electron beam curing process in the US aerospace manufacturing sector has demonstrated that a substantial energy saving comes with 25% to 65% cost reduction (Lopata, 1999). The precedence of e-beam cured fiber reinforced epoxy composite for the aerospace industry is a piece of powerful evidence that e-beam curable resin system is superior to the current thermosetting resin system. The advantages are: reducing energy consumption, lowing production cost, increasing the throughput, minimizing the heat-driven emission of volatile organics, improving various end-use performance, eliminating thermal degradation of woods, suppressing the residual stress caused by the incomparable thermal expansion, and eliminating toxic cross-linking agents (Singh, 2001).

The production of structural panel and engineered wood products, which include glue laminated timber, laminated veneer lumber, medium density fiberboard, oriented strand board and particle board, is one the most rapidly growing areas of forest products. But the steadily increasing prices and more limited availability of wood adhesives become a serious challenge for the wood products industry (White, 1995). However, the expected expansion in wood composites production provides a significant opportunity to incorporate this energy saving technology and electron beam curable resin systems into wood-composite manufacturing.

The main objective of this research was to evaluate a variety of radiation curable resins within different chemical families, explore the optimum radiation dose, study resin

structure-property relationships, and explore resin-wood interaction. The radiation dose for a complete curing of a polymeric matrix was optimized for all resins. The dynamic mechanical properties as well as bulk mechanical properties were explored. Further formulation studies were conducted to assess monomers (polyfunctional and monofunctional) effect on the overall performance of the cured products. With the knowledge of chemical, physical and mechanical properties of the candidate resins, efforts were devoted to investigate resin-wood bonding. The mechanical behavior of the resin-wood bonds was evaluated and compared. The correlation between resin properties and bond performance was also studied. Additionally, surface properties and resin-wood bondline were investigated and related to the mechanical performance of bonds.

2 LITERATURE REVIEW

Research into electron beam radiation processing of polymeric materials was launched about 50 years ago and is currently receiving extensive attention. It is already proven to be an energy saving and environmentally friendly technology, in comparison to the conventional processing technique. The e-beam radiation methods have instigated industrial interest in applications ranging from tailoring material structure and properties, through the modification of bulk and surface properties of materials. Such interests together with the extensive research encourage a steady growth of commercial radiation process in the industry.

The application of this high energy radiation technology has been expanded by a variety of choices of electron beam machines (electron accelerators). Although the cost of the radiation source is as high as the conventional processing machine, the operating cost is lower (Singh, 1992). Based on years' experiences, the electron accelerators are recognized for reliability comparable to the extruders in the plastic industry (Singh, 1992). Without the radioactive isotope, their safety level is high exclusive of the isotope disposal problem. One compelling attribute of electron accelerators is that electron beams can be switched off when not in use. Other appealing advantages benefit from e-beam radiation are: low temperature operation, shortened life cycle, reduced health concerns, improved material handling, greater design flexibility, considerable operation control, reduced manufacturing cost, improved products performance, and higher production throughput.

As a result of decades of research and numerous benefits of e-beam radiation to polymeric materials, this technology has been turned to commercial uses in diverse fields:

curing of coatings and paints, vulcanization of rubber mixes, production of heat-shrink and heat-expanding products, manufacturing fiber-matrix composites, grafting, sterilization, plastic recycling, making radiation-resistant composites, surface modification and so on. With active and consistent research in the radiation of polymeric materials under investigation, new products through possible innovative radiation technology will continue to invade the marketplace.

2.1 Electron Beam Radiation

2.1.1 Electron Beam Processing

The electron beam radiation process can be simply separated into two procedures: primary and secondary radiation-chemical processes (Ivanov, 1992). The primary process is the ionization and excitation process. Fast electrons with typical energies in magnitude of keV or MeV lose their energy to target molecules of the irradiated substrates by inelastic collisions, forming excited molecules and secondary electrons (Mehnert, 1995). The secondary radiation-chemical process is the redistribution of originally absorbed energy (Ivanov, 1992). The secondary electrons and excited molecules dissipate their energy to the other molecules in the neighborhood, forming radicals, ions, electrons, molecules and atoms in the excited state. Consequently, the chemical bonds are broken with the formation of ions and radicals. Thus chemical changes in substrates can be initiated by the interaction between activated fragments of molecules or by the interaction between activated ones and non-activated molecules that are not subjected to radiation.

The absorbed energy can not completely degenerate into chemical changes, although such changes are of first importance in polymeric systems. A small percentage

of energy will transform to thermal energy, exhibiting as a heat increase in the matrix (Ivanov, 1992). Therefore, thermal effects are accompanied with chemical transformations in the e-beam radiation process.

2.1.2 Electron Energy and Dose

One of the most important parameters governing the radiation process is the radiation degree and intensity, which is defined as "dose" in radiation chemistry (Singh, 1992). The absorbed radiation dose is the ratio of the radiation energy (dE) to the irradiated substrate in an elementary volume to the mass (dm),

$$D = \frac{dE}{dm} \tag{1}$$

The unit of this measurement is termed as gray (Gy) in the SI unit,

$$1Gy = \frac{1J}{kg} = \frac{6.24 \times 10^{15} ev}{g} \tag{2}$$

The radiation dose absorbed can be conveniently determined by any type of dosimeters, depending on the radiation chemical effects. As the thermal effect is always accompanying with the radiation absorption, it can also be applied as a fundamental method of dose measurement.

Based on the dose concept, the electron energy is expressed as follows:

$$P = (D/3600)(M/t)(1/F_p) \tag{3}$$

where P is the electron beam power (kW), D is the absorbed dose in kGy (1000Gy), M is the mass of irradiated substrate (kg), t is the irradiation time (h), and Fp is the power utilization efficiency. The ratio of M/t is the throughput (kg/h). The maximum throughput capacity of a particular electron accelerator can be estimated from equation 3.

The absorbed dose is proportional to the electron current, which is the number of electrons accelerated per second. Their relationship can be expressed as follows:

$$I = (D/K_0)(A/t)(1/F_i) \quad (4)$$

where I is the emitted beam current (mA), D is the dose (kGy) at the irradiated area of A (m^2), t is the exposure time, F_i is the beam current utilization efficiency, and K_0 is the area processing coefficient. The ratio of A/t is the throughput rate of the irradiated area in the processing.

2.1.3 Electron Accelerators

The electron accelerator plays an important role in the radiation processing of polymeric materials. A typical direct-current accelerator is comprised of a voltage generator, a electron gun, a accelerator tube, a scan horn, and a control system. Worldwide, there is approximately a magnitude of 1000 electron accelerators in industrial use (Clough, 2001).

The low energy accelerators with energy less than 300 keV are used in industry mainly for surface coating or printing, where only a low penetration is needed. The medium energy accelerators with energy ranging from 300 keV to 4 MeV are used for processing thicker materials, such as thicker plastic and rubber sheets, plastic pipes and tubes, wire and cable insulations. The high energy accelerators with energy higher than 4 MeV are applied for food irradiation and sterilization. With energy up to 10 MeV, the electron accelerator is employed in the production of wood-plastic composites (Ivanov, 1992).

Electron beam has a limited penetration compared to gamma radiation, but it has much higher energy utilization efficiency. The irradiated substrate can absorb all irradiation energy from the electron beam. Although gamma rays are penetrating, the much lower radiation dose severely slows down the processing rate. The penetration of electron beam in materials is almost proportional to the energy of the electrons. With the availability of high energy electron accelerators, e-beam provides a deeper penetration as well as stronger electron current and dose, further leading to a greater throughput capacity.

2.2 Radiation Induced Polymers Transformation

Initiated by very reactive electrons, there are several types of chemical reactions occurred at the irradiated substrate, mainly including crosslinking, grafting, and degradation. Polymerization of monomers simultaneously happens together with above reactions, but the industry interest is small with very few practical applications.

2.2.1 Grafting

Grafting polymerization can take place when radical sites form at the polymer backbone. Grafting induced by electron beam has received wide attention in the last decade, although the practical application in a large scale is not very much. The ability to modify surface properties of a material while retaining its bulk properties is an appealing feature of the e-beam radiation. Surface properties that have been successfully improved through the radiation grafting include: wettability, printability, dyeability, adhesion, biological or chemical compatibility, surface conductivity, flammability, chemical resistance, water absorption, and hydrophobic quality and so on (Clough, 2001).

2.2.2 Degradation

Upon exposure to high energy radiation, degradation occurs by chain scission causing a decrease in molecular weight. Undesirable degradation leads to inferior product quality and shortened shelf life. On the contrary, chain scission can also be applied as a radiation treatment when properly used. The most popularized application of chain scission is ameliorating the processing characteristics of polymers. The melt flow of polypropylene can be improved by adjusting the molecular weight distribution through radiation chain scission. The electron beam degradation of polytetrafluoroethylene (PTFE) is a successful example, which has already been employed in the commercial processes. The reduction in particle size and molecular weight of PTFE by e-beam allows it to be incorporated into coatings or inks.

Radiation sterilization of disposable plastic medical items is an important application of e-beam processing in the industry, which is still growing in many industrialized countries. Plastic recycling by e-beam radiation is also an area actively gaining much attention. This fast, cheap, safe, and green technology with many available innovations undergoing investigations has a strong potential in the future market.

2.2.3 Cross-linking

Irradiated by high energy electrons, reactive liquids rapidly convert to solids through polymerization and cross-linking. Radiation cross-linking is a well-established technology applied into different fields with great economic and environmental impact. Radiation cross-linking of wire and cable insulation is one of the largest industry utilization (Singh, 1992). Food wrapping and tubing for electric connection are another two examples commonly seen. Superior to thermo-chemical cross-linking, radiation

cross-linking bestows products with unique properties, such as heat shrink products, and recently self-regulating heat tape (Clough, 2001). Curing of coatings and inks is a rather mature technology and has been successfully commercialized with a still growing trend (Hoyle, 1989). Other radiation cross-linking applications are pipes, tubing, and automobile tires. More recently, electron beam curing of composites has been receiving extensive attention. Many researchers in different countries devoted their efforts in this area and have acquired many successful accomplishments. The successful production of e-beam curable fiber-reinforced epoxy composites in aerospace stimulated more efforts from laboratories and industries (Lopata, 1999). Moreover, the cost and manufacture studies demonstrate that the e-beam curing is associated with numerous advantages compared to conventional thermo-chemical curing (Singh, 2001).

2.3 Electron Beam Curing

Radiation curing is the largest commercial application of electron beam in polymeric systems. With continuous contribution from a variety of laboratories in different countries, the new products and various innovations in e-beam technology have been widely reported (Berejka, 2002; Singh, 2001). Additionally, industry interest in this field seems continue to grow. Numerous advantages as well as potential products ensure high competency of e-beam technology in today's competitive marketplace. Due to the importance of radiation curing and its relevancy to our research, the primary focus of the following review is radiation curing.

2.3.1 Curing Mechanism

Radiation curing originated from the observation 50 years ago that polyethylene was converted to insoluble gel upon radiation (Clough, 2001). Before this discovery, cross-linking had been thought to be only possible with the aid of chemical agents in polymers with suitable reactive functional groups, such as sulfur vulcanization of rubber. The discovery of radiation curing introduced a new concept of cross-linking that formation of covalent bonds between polymer chains is practicable without chemical agents. Since then, a large amount of research emerged, further leading to commercial applications throughout the world.

E-beam curing proceeds via a free radical mechanism or a cationic mechanism, according to chain initiation and propagation.

Acrylated or methacrylated monomers and oligomers show a typical free radical addition polymerization after initiated by high energy electrons (Sui, 2002). Like the classic radical polymerization, both initiating radicals and propagating radical chains are sensitive to oxygen inhibition. Further reaction with oxygen terminates the propagation chains. Polyester acrylates (or methacrylates), polyurethane acrylates (or methacrylates), and epoxy acrylates (or methacrylates) are typical curable formulations widely used in the radiation industry. Acrylate or methacrylate monomers, called reactive thinners, can also form into a polymeric network with oligomers after curing. The properties of the network, such as viscosity and cross-linking density, can be modified by adding different monomers. However, the principal constituents (oligomers) primarily determine the product properties, such as solvent resistance, high gloss, scratch resistance, and variable adhesion.

Another class of monomers and oligomers, which shows a typical cationic polymerization through e-beam radiation, is mainly epoxies (Sui, 2002). Like the typical cationic polymerization, cations and cationic propagating chains are sensitive to water. One characteristic that distinguishes the cationic polymerization from free radical polymerization is the stability of the initiated species. Cycloaliphatic epoxies and aliphatic epoxies with other epoxidized oil are frequently used in radiation industry. In comparison with other curable formulations, the network formed by epoxy resins present favorable properties, such as low shrinkage, high chemical resistance, high gloss, and good adhesion.

2.3.2 Principal Applications

Many important applications of radiation curing have already been successfully commercialized, as mentioned earlier. In the last decade, the main interest in radiation curing is focused on composites. Since then, many promising findings have been reported. Here, electron beam curing of composites, especially plastic-wood composites, will be briefly reviewed.

Three main types of composites, which are polymer- and wood- based products treated by e-beam radiation, have been studied and produced. They are wood-plastic composites (WPC), wood fiber reinforced plastics (WFRP), and laminated WPCs (Singh, 1992).

The radiation-processed wood-plastic composites were studied as early as 1960 and were commercialized in 1970s (Singh, 1992). Taking advantage of the high porosity of wood structure, wood panels are impregnated with cross-linkable monomers, such as

styrene, acrylate or methacrylate, and are subjected to e-beam exposure. The impregnated WPC is produced with many improved properties. The hardness, tensile strength, compression and shear strength are impressive, compared to the original wood. The dimension stability, shrinkage reduction, and resistance to biological degradation are greatly improved compared to original wood panels.

The interest in using wood fibers as fillers or reinforcements in plastics is under continuously growth. WFRP is radiation-processed by dispersing wood or cellulose fibers in the polymer matrix (Clough, 2001). Specific additives, including adhesion promoters and coupling agent, are applied to promote adhesion between fibers and matrix.
The mechanical performance is improved by the incorporation of strong fibers.

Laminated wood-plastic composites are produced by e-beam coating of cross-linkable resins on the wood based agglomerates (Singh, 1992). Either one coating layer or multiple coating layers can be employed. E-beam processing of laminated WPCs has been converted into industry scale as early as 1970s. More coating lines have been built since then, demonstrating that the e-beam radiation of laminated WPCs is a commercial success with economic impact.

2.3.3 Advantages of Electron Beam Curing

The comparison between the radiation curing and convent thermo-chemical curing has been frequently carried out in the literature (Berejka, 2002). It has been proven that the processes of radiation curing require less energy than conventional operations. Less than one third of energy is required to form the same density of the polymeric network by radiation, as compared to chemical curing (Ivanov, 1992). Other numerous

advantages are also competing: low temperature, reduced curing time, reduced volatile emissions, greater design flexibility, simplified processing steps, more latitude process control, considerable cost savings, and increased throughput rate (Sui, 2002). In no doubt, the trend to convert this low cost green technology into industry scale will be ever rising.

2.4 The Theory of Adhesion

The function of adhesives is to bond two substrates together so strongly that adhesives or substrates fail before the two surfaces are pulled apart. This description states the essential requirement of adhesives.

2.4.1 Forces Involved in Adhesion

The state of adhesion between two surfaces is sustained by interfacial forces that may comprise interlocking action or valence forces or both (Blomquist, 1981). Interfacial forces, also called adhesive forces, originate from the forces between atoms or molecules of two different materials. Cohesive forces hold adjacent molecules together in the same material. Both forces contribute to the strength of bonded joints. If adhesive forces are the weakest, adhesion failure occurs at the interface between the adhesive and substrate. If cohesive forces of the adhesive are the weakest, cohesion failure occurs within the adhesives.

The forces can be classified into two groups: the primary forces and the secondary forces. The primary forces, also called short range forces, arise from chemical bonding. Chemical bonding comprises interlinking between molecules of the adhesive and molecules of the substrate by covalent, ionic or metallic bonds. The secondary forces, also called long range forces, originate from physical attraction. Van der Waals forces or

hydrogen bonds may be formed between different types of molecules when two materials have an intimate contact.

Depending on the nature of the materials, the interaction between the adhesive and substrate may involve either chemical bonding or physical attraction. Physical attraction is more important to adhesion in many cases, although it is difficult to determine (Petrie, 2000).

2.4.2 Mechanisms of Adhesion

There is no single theory of adhesion which explores all interactions between the adhesive and the substrate in a comprehensive way. Several existing theories provide different perspectives for a better understanding of the work of adhesives. Each theory is applicable for certain application or particular substrates in certain circumstances. But none of them are universally applicable.

2.4.2.1 Mechanical Interlocking

The surface of a solid material is never perfectly smooth but presents crevices, peaks and valleys. If the viscosity of the adhesive is not too high, the liquid adhesive can flow and fill into these micro-cavities on the substrate. When the adhesive solidifies, the substrates are held together by a mechanical anchor. Due to porosity nature of wood, textiles and paper, mechanical interlocking play an important role during bonding (Blomquist, 1981). On the other hand, this mechanism is not applicable for substrates whose surfaces are smooth and glossy, such as glass. Plastics can be etched to boost the roughness and increase the contact area for the adhesive penetration and locking into the substrate.

2.4.2.2 Adsorption Theory

The adsorption theory states that adhesion results from intermolecular attraction when adhesive molecules are absorbed onto the substrate. The two materials should have an intimate contact for these forces to develop. The contact condition can be explored by wetting properties which comprises two actions: spreading and penetration. Once good wetting is established between the adhesive and substrate, the permanent adhesion is developed through molecular attraction. The forces involved in adhesion include: covalent, electrostatic, metallic, and van der Waals (Petrie, 2000).

2.4.2.3 Diffusion Theory

The diffusion theory states that adhesion arises from the inter-diffusion of molecules in the adhesive and substrate (Blomquist, 1981). The extent of diffusion relies on the chemical compatibility of the two materials and the penetrability of the substrate. When both the adhesive and substrate are polymeric and have compatible molecular movement, the diffusion theory is quite applicable. If the substrate has a high density and has limited compatibility with the adhesive, the diffusion theory is not appropriate. Interpenetration potentially contributes to the adhesion properties of wood.

2.4.2.4 Weak-Boundary-Layer Theory

This theory suggests that true interfacial failure rarely occurs. When bond failure seems to occur at the interface, it is actually a cohesive failure of a weak boundary layer (Petrie, 2000). The weak boundary layers originate from the adhesive, the substrate, the circumstance, or a combination of any of the three. And they could be developed in any procedures of joints processing, such as adhesive applying or even in the service.

2.5 Techniques Used in the E-beam Curing Study

A large amount of research work has been carried out in the area of e-beam curing by different laboratories. The extensive literature work promotes a better understanding of curable resins as well as the radiation process. Most of the research focuses on radiation dose optimization, resin system formulation, and property testing (Cadinot, 1994).

The optimum radiation dose for curing a resin matrix was mainly determined by dynamic mechanical analyses (DMA). Glass transition temperature, measured under different radiation dose by DMA, was regarded as a conversion index of the specific resin system. Other techniques, infrared spectroscopy and differential scanning calorimetric, were also used (Patacz, 2000).

The formulating curable resin was the emphasis of the research. Curable oligomers are the base ingredients which determine the fundamental properties of the products. A variety of cross-linkable resins were investigated, including acrylated or methacrylated oligomers, epoxies, vinyl ethers. Curable monomers, which are called reactive thinners, were also formulated and studied.

A variety of testing was employed to determine physical, chemical, thermal and mechanical properties. Viscosity, surface tension, and solids content were measured on liquid resins before curing. Shrinkage, cross-linking density, glass transition temperature, shear strength, flexural strength, elongation and other useful properties were measured on the cured matrix. The correlation between structure formation and final properties were explored.

3 MATERIALS AND EXPERIMENTS

3.1 Materials

The material information is listed in table 1 for oligomers and table 2 for monomers, most of which are based on acrylate and methacrylate. These radiation curable materials were from UCB Radcure and Sartomer. Totally, 120 different resins were made as either individual oligomers or blends added with monomers for further electron beam curing and testing.

Liquid resins were drawn and sealed into one ml plastic syringes. Care must be taken to avoid bubbles forming during the processing. Then syringe samples were shipped to IBA SteriGenics in San Diego, California for electron beam radiation. The electron accelerator used is rated at 12 MeV and 8 kW with a six ms pulse at 180 Hz.

The cured resins were removed from syringes for dimension and weight measurements. Color, relative hardness or flexibility were also examined and recorded.

All materials were used without further purification.

3.2 Experiments

3.2.1 Viscosity Measurement

Viscosity was measured on a Brookfield HBDV-III Ultra Cone/Plate Viscometer. A CPE-52 cone spindle was selected to allow a wide range of measurement. A Fisher 3016 Isotemp Refrigerated Circulator was connected to the viscometer to assure the measurements were accomplished at 25°C. The measurements were only carried out until the temperature attained equilibrium and were performed 5 times.

Table 1. Oligomers.

Code	Designation	Chemical family
R01	Ebecryl 3720	Bisphenol-A epoxy diacrylate
R02	Ebecryl 3708	Bisphenol-A epoxy diacrylate
R03	Ebecryl 860	Epoxidized Soya oil tetraacrylate
R04	Ebecryl 8402	Aliphatic urethane diacrylate
R05	Ebecryl 4827	Aromatic urethane diacrylate
R06	Ebecryl 450	Fatty acid modified polyester hexaacrylate
R07	Ebecryl 830	Polyester hexaacrylate
R08	Ebecryl3720-HD20	Bisphenol-A epoxy diacrylate
R09	Ebecryl3720-TM20	Bisphenol-A epoxy diacrylate
R10	Ebecryl3720-TM40	Bisphenol-A epoxy diacrylate
R11	Ebecryl 8800	Aliphatic urethane acrylate
R12	Ebcryl8800-20R	Aliphatic urethane acrylate
R13	Ebecryl 6602	Aromatic urethane triacrylate
R14	Ebecryl 4866	Aliphatic urethane triacrylate
R15	CN104	Epoxy acrylate
R16	CN135	Low viscosity acrylate /methacrylate
R17	CN137	Low viscosity acrylate
R18	CN292	Low viscosity polyester acrylate oligomer
R19	CN302	Polybutadiene urethane diacrylate
R20	CN961	Resilient aliphatic urethane acrylate
R21	CN961A80	Resilient aliphatic urethane acrylate
R22	CN961I75	Resilient aliphatic urethane acrylate
R23	CN961B75	Resilient aliphatic urethane acrylate
R25	CN962	Flexible aliphatic urethane acrylate
R26	CN962L50	Flexible aliphatic urethane acrylate
R27	CN963E75	Hard aliphatic urethane acrylate
R28	CN966H50	Aliphatic urethane acrylate
R29	CN983	Hard aliphatic urethane acrylate
R30	CN983B88	Hard aliphatic urethane acrylate
R31	CN985B88	Urethane acrylate blended with SR238
R32	CN9001	Aliphatic urethane acrylate monomer
R33	CNUVE151	Modified epoxy diacrylate
R34	SR213	1,4-butanediol diacrylate
R35	SR368D	Tris(2-hydroxyethyl)isocyanurate triacrylate diluted
R36	SR399	Dipentaerythritol pentaacrylate
R38	SR9003	Propoxylated(2) neopentyl glycol diacrylate
R39	SR9012	Trifunctional acrylate ester
R40	CN1963	Urethane dimethacrylate
R41	SR206	Ethylene glycol dimethacrylate

Table 1. Continued.

Code	Designation	Chemical family
R42	SR239	1,6-hexanediol dimethacrylate
R43	SR252	Polyethylene glycol dimethacrylate
R44	SR297	1.3-butylene glycol dimethacrylate
R46	SR540	Ethoxylated(4)bisphenol-A dimethacrylate
R47	SR9009	Trifunctional methacrylate ester
R48	CN150	Bisphenol-A diglycidyl dimethacrylate
R49	SB500K60	Aromatic acid methacrylate half ester
R50	CHDMDVE	Cyclohexanedimethanol divinyl ether
R51	Vectomer 1312	Aromatic ester multifunctional vinyl ether
R52	Vectomer 4010	Bis-[4-(vinyloxy)butyl]isophthalate
R53	Vectomer 4060	Bis[4-(vinyloxy)butyl]adipate
R54	Vectomer 5015	Tris[4-(vinyloxy)butyl] trimellitate
R59	TR46D24-20	Ethoxylated(4)bisphenol-A dimethacrylate/VE4010
R60	TR13D24-20	Aromatic urethane triacrylate/Ve4010
R61	TR51D01-75	Aromatic ester multifunctional vinyl ether diluted with TRPGDA
R62	CD501	Propoxylated(6) trimethylolpropane triacrylate
R63	SR494	Ethoxylated(4) pentaerythtitol tetraacrylate
R64	TR31D35-60	Urethane acrylate bended with SR238 & SR368D
R65	TR53D01-75	Bis[4-(vinylocxy)butyl] adipate diluted with TRPGDA
R66	TR54D01-75	Tris[4-(vinyloxy)butyl] trimellitate
R67	SR601	Ethoxylated(4)bisphenol-A diacrylate
R68	TR11D04-10	Aliphatic urethane acrylate
R69	TR11D04-20	Aliphatic urethane acrylate
R70	TR11D04-40	Aliphatic urethane acrylate
R71	TR01R05-10	BPA/epoxy aromatic urethane diacrylate
R72	TR71D04-20	BPA/epoxy aromatic urethane diacrylate
R73	TR01R05-20	BPA/epoxy aromatic urethane diacrylate
R74	TR73D04-20	BPA/epoxy aromatic urethane diacrylate
R75	TR29R04-20	Aliphatic urethane diacrylate
R76	TR29R04-40	Aliphatic urethane diacrylate
R77	TR04R29-40	Aliphatic urethane diacrylate
R78	TR04R29-20	Aliphatic urethane diacrylate
R79	TR75D04-20	Aliphatic urethane diacrylate
R80	TR76D04-20	Aliphatic urethane diacrylate
R81	TR77D04-20	Aliphatic urethane diacrylate
R82	TR78D04-20	Aliphatic urethane diacrylate

Table 1. Continued.

Code	Designation	Chemical family
R83	TR13R05-10	Aromatic urethane diacrylate
R84	TR13R05-20	Aromatic urethane diacrylate
R85	TR13R05-30	Aromatic urethane diacrylate
R86	TR13R05-50	Aromatic urethane diacrylate
R87	TR83D04-20	Aromatic urethane diacrylate
R88	TR84D04-20	Aromatic urethane diacrylate
R89	TR85D04-20	Aromatic urethane diacrylate
R90	TR86D04-20	Aromatic urethane diacrylate
R120	TR14D12-10	Aliphatic urethane triacrylate
R121	TR14D12-15	Aliphatic urethane triacrylate
R122	TR14D12-20	Aliphatic urethane triacrylate
R123	TR14D23-10	Aliphatic urethane triacrylate
R124	TR14D23-15	Aliphatic urethane triacrylate
R125	TR14D23-20	Aliphatic urethane triacrylate
R126	TR14R16-20	Aliphatic urethane triacrylate
R127	TR14R16-30	Aliphatic urethane triacrylate
R128	TR14R16-40	Aliphatic urethane triacrylate
R129	TR33D12-10	Modified epoxy diacrylate
R130	TR33D12-15	Modified epoxy diacrylate
R131	TR33D12-20	Modified epoxy diacrylate
R132	TR33D36-10	Modified epoxy diacrylate
R133	TR33D36-15	Modified epoxy diacrylate
R134	TR33D36-20	Modified epoxy diacrylate
R135	TR33R16-20	Modified epoxy diacrylate
R136	TR33R16-30	Modified epoxy diacrylate
R137	TR33R16-40	Modified epoxy diacrylate
R138	TR49D12-5	Aromatic acid methacrylate half ester
R139	TR49D12-10	Aromatic acid methacrylate half ester
R140	TR49D12-15	Aromatic acid methacrylate half ester
R141	TR49D36-5	Aromatic acid methacrylate half ester
R142	TR49D36-10	Aromatic acid methacrylate half ester
R143	TR49D36-15	Aromatic acid methacrylate half ester
R144	TR49R16-10	Aromatic acid methacrylate half ester
R145	TR49R16-20	Aromatic acid methacrylate half ester
R146	TR49R16-30	Aromatic acid methacrylate half ester
R147	TR14L-15	Aliphatic urethane triacrylate
R148	TR33L-15	Modified epoxy diacrylate
R149	TR33L-20	Modified epoxy diacrylate
R150	TR49L-15	Aromatic acid methacrylate half ester

Table 2. Monomers.

Code	Designation	Chemical Name
D1	TRPGDA	Tripropylene glycol diacrylate
D2	TMPTA-N	Trimethylopropane triacrylate
D3	TMPTMA	Trimethylopropane trimethacrylate
D4	HDODA	1,6-hexanediol diacrylate
D5	EOEOEA	2(2-ehtoxyethoxy)ethyl acrylate
D6	TMPEOTA	TMP-ethoxy triacrylate
D8	CD501	Propoxylated(6)trimethylopropane triacrylate
D9	SR213	1,4-butanediol diacrylate
D10	SR494	Ethoxylated(4)pentaerythritol tetraacrylate
D12	SR506(IBOA)	Isobornyl acrylate
D13	SR9003	Propoxylated(2)neopentyl glycol diacrylate
D14	SR9012	Trifunctional acrylate ester
D15	SR206	Ethylene glycol dimethacrylate
D16	SR239	1,6-hexanediol dimethacrylate
D17	SR252	Polyethylene glycol dimethacrylate
D18	SR297	1,3-butylene glycol dimethacrylate
D19	SR423A	Isoborny methacrylate
D20	SR540	Ethoxylated(4) bisphenol-A dimethacrylate
D21	SR9009	Trifunctional methacrylate ester
D22	SR344	Polyethylene glycol 400 diacrylate
D23	CHDMDVE	Cyclohexanedimethanol divinyl ether
D24	Vectomer 4010	Bis-(4-vinyloxybutyl)isophthalate
D25	Vectomer 4060	Bis-[4-(vinyoxy)butyl] adipate
D35	SR368D	Tris(2-hydroxyethyl)isocyanurate triacrylate diluted
D36	GENOMER 1122	Urethane monoacrylate
L	V-PYROL	N-vinyl-2-pyrrolidone

3.2.2 Surface Tension

The surface tensions of liquid resins were determined on a Thermo Cahn WinDCA 322 at room temperature. Rectangular clean glass plates were used for this Wilhelmy method. This micro-technique was described elsewhere (Petrie, 2000). The force of the plate stretching the liquid surface was recorded by the inner electron balance, and the data were automatically converted to results. Three measurements were performed on the same resin and averaged to give a surface tension value.

3.2.3 Contact Angle

The contact angle between resins and maple surface was determined on the same Thermo Cahn WinDCA 322 at room temperature. This thermodynamic quantity signifies the interaction between a liquid and a solid at the contact area. The measurements give the information on the tendency of the liquid to spread over the solid surface.

Fresh maple was cut into thin smooth rectangular pieces as substrates to contact with a particular resin. Three values of contact angle of a resin against the maple surface were averaged and reported.

3.2.4 Shrinkage

Shrinkage determined in this work is based on the direct measurement of specimen dimension. Since geometry shape changes of cured resin were not observed in syringes, isotropic volume shrinkage is assumed. Hence, a linear shrinkage was defined by measuring the diameter of the cylindrical resins:

$$LinearShrinkage(\%) = \frac{D_0 - D}{D_0} \times 100 \quad (5)$$

where D_0 is the initial diameter of the syringe and D is the diameter of the cured rods. All of the measurements were carried out at room temperature.

3.2.5 Solvent Swelling

Solvent swelling is widely used to determine the swelling ratio, sol fraction. Ally alcohol was used as a solvent for the swelling studies.

The swelling ratio Q can be measured by volume change:

$$Q = \frac{V_{sw}}{V_d} = \frac{\frac{W_d}{\rho_p} + \frac{W_{sw} - W_d}{\rho_s}}{\frac{W_d}{\rho_p}} \tag{6}$$

where V_{sw} and V_d are the volume of the swollen and dry polymers, ρ_p and ρ_s are the density specified for polymer and solvent, W_d and W_{sw} are the weight of dry and swollen polymers, respectively.

The sol fraction can be calculated as follows:

$$SolFraction = \frac{W_0 - W_d}{W_0} \times 100\% \tag{7}$$

where W_0 is the original weight of specimens.

Swelling studies were carried out by immersing the cured specimens in small bottles containing nearly 20 ml of solvents kept at 25°C. The samples were cut circularly from the cured rods to maximize the surface area for solvent extraction. All of the samples were weighed to the nearest 0.01 mg throughout the experiment. After solvent extraction, the swollen specimens were removed from the bottles, blotted to remove solvents, and weighed. Then the swollen samples were subjected to oven-dry and re-

weighed. The procedures were repeated until constant weight readings resulted. This implied the swelling equilibrium has been reached.

3.2.6 Dynamic Mechanical Analysis

Dynamic mechanical analysis (DMA) is the most frequently employed technique compared to others. Dynamic mechanical properties of cured resins were measured using a PerkinElmer Diamond DMA controlled by a liquid nitrogen cooling accessory. All materials were tested in bending mode (dual cantilever) with sinusoidal oscillation at 1 Hz frequency at a scanning rate of 3°C/min.

Dynamic mechanical analysis (DMA), also called dynamic mechanical thermal analysis (DMTA) or dynamic rheology, refers to the same technique and instrument in which the behavior of a sample under oscillating load are monitored against temperature, time, or frequency (Menard, 1999).

Materials can behave in two extreme ways. A purely elastic material, in which the stress is proportional to the strain and the slope is denoted E (Young's modulus), follows Hook's law. A purely viscous material, in which the stress is proportional to the strain rate and the slope is denoted viscosity η, follows Newton's law. Most polymeric materials exhibit combination behaviors. The DMA technique analyzes these viscoelastic behaviors into separate moduli values: elastic or storage modulus E' and loss modulus E". The storage modulus represents the elastic component of the material and the loss modulus represents the viscous damping component. The ratio of loss modulus to storage modulus is tan δ (tangent of phase angle), indicating the damping ability of the material. All DMA measurement falls within the linear viscoelastic region of the test specimens.

Inside this region, the modulus is constant and strain can be recovered. Beyond this linear region, erroneous results may be caused in DMA analysis.

The elastic behavior of polymer at the rubber plateau, which can be detected from DMA spectra, was described by the theory of rubber elasticity about 60 years ago (Flory, 1943). Kuhn introduced the fundamental assumption that chain displacement caused by deformation act like macroscopic elements of a homogeneous isotropic material. Then he derived the famous equation which relates Young's modulus E at small deformation to molar density of network strands ν, by

$$E = 3\nu RT = {}^{3\rho RT}\!/_{M_c} \tag{8}$$

where ρ is the density of the rubber, T is the absolute temperature of the rubber plateau, and M_c is the number-average molecular weight between cross-links. This equation was further simplified with the assumption of density equaling to 1 for most organic polymers (Aharoni, 1986). Thus the molecular weight between cross-links can be calculated by an inverse relation to E, as following:

$$M_c = {}^{3RT}\!/_{E} \tag{9}$$

3.2.7 Three-Point Bending

Three-point bending was carried out using an Instron 5567 following procedures B described in the ASTM D790 standard. The diameter of the cured rods was measured three times around the circumference at center and at span support positions. With the average diameter value, a 4 mm/min of crosshead motion rate was calculated from the equation described by the procedure B. Restricted by the length of the rods, a 16:1 of

support span-to-depth ratio required by the standard can not be met. Instead, a 34.1 mm span was set for all specimens (about 7.5:1 span-to-diameter ratio).

Flexural strength, which is the maximum flexural stress sustained by the specimen during the bending test, was automatic measured by the instrument during the test and recorded. The energy to break the specimen, which is defined by the area under the stress-strain curve in units of energy per unit volume, was integrated and evaluated. Both flexural properties were recorded and reported. Only one measurement was performed due to the limited sample numbers.

3.2.8 Infrared Spectroscopy − ATR

FT-IR attenuated total reflectance spectroscopy was conducted using a PerkinElmer Spectrum One instrument equipped with a single bounce, diamond ATR accessory. Each spectrum was produced by 32 scans at a resolution of 4 cm^{-1}. Four spectra were collected around the circumference of the cured rods with approximate 90° increments. Then the collected 4 spectra of each resin were averaged for further analysis.

3.2.9 Infrared Spectroscopy − Imaging

FT-IR imaging, which is a useful problem solving tool for heterogeneous systems, was adopted for bondline study. FT-IR imaging was carried out using a PerkinElmer Spectrum Spotlight spectrometer equipped with imaging system. The scan was operated in reflectance mode with a pixel resolution of 6.25 microns. The spectra were collected in the infrared region of 650 cm^{-1} to 2000 cm^{-1}, with 32 scans at a resolution of 8 cm^{-1}.

Due to the heterogeneity of bondline as observed under the microscope, care was taken to locate a scan area displaying both adhesives and substrates. Three images from

different positions along the bondline were collected for further investigation.

3.2.10 Shear Test of Resin-Poplar 3-Plywood

The strength properties of adhesives in 3-plywood construction were tested on the MTI Universal Testing Systems following the ASTM D906 standard. Yellow poplar veneers of 0.0929 m^2 (12 inches square) and 0.0032 m (1/8 inch) thickness were used as the substrates for further evaluation. Liquid resins were rolled out on the veneer by a brayer with 74 g/m^2 loading rate. The resinated veneers were sandwiched between polyurethane foams, and subsequently plywood sheets. Then the fixture was compressed together by tightening screws. Finally, the plywood fixtures were cured at IBA SteriGenics in San Diego at 80 kGy radiation dose.

All test specimens were cut as required by standard. Then 3-plywood samples were grouped and tested into two categories, lathe checks opening and lathe checks close, according to the lathe check orientation in the core veneer. The tests were accomplished at a rate of 0.02 mm/s (0.05 in/min) with a load scale of 22680 kg (50000 pounds).

The percentage of wood failure in joints after shear tests was estimated according to the ASTM D5266 standard. A transparent ruler was employed as an aid to estimate the area of torn wood fibers.

3.2.11 Shear Test of Resin-Maple Blocks

The strength properties of adhesives in the maple block construction were tested on the same MTI Universal Testing Systems following the ASTM D906 standard. Maple panels around 0.3×0.05×0.02 m(3/4×2×12 inch) were used for this shear test. Resin loading was 214 g/m^2 for first two sets and changed to 68 g/m^2 for subsequent sets

(Sellers, 1985). Two panels were held together by bolts to provide pressure to the bondline. Again, resin/maple blocks were cured at IBA SteriGenics in San Diego.

The cured samples were cut to maple blocks as required by standard. Eight specimens for each resin were cut from two pairs of panels, and subsequently tested at 0.08 mm/s (0.2 in/min) crosshead speed with a load scale of 22680 kg (50000 pounds). The test results were recorded and averaged for further evaluation.

Moisture content of the maple blocks was measured for each set according to ASTM D4442. Specimens were weighed before oven dry at 105°C for twenty four hours. Then they were removed from the oven and re-weighed. The specimens were placed in the oven again. The procedures were repeated until a constant weight was reached.

The percentage of wood failure in joints after shear tests was estimated according to the ASTM D5266 standard. A transparent ruler was used to estimate the area of torn wood fibers. Shallow wood failure, which is easily confused with adhesion failure, was carefully inspected. The percentage of wood failure was averaged for each resin and reported together with the average shear stress at failure.

4 RESULTS AND DISCUSSION − PRELIMINARY SCEENING

4.1 Electron Beam Curable Resins

Most of the electron beam curable resins chosen in this project cover three chemical families, epoxy, ester, and urethane, all of which are based on acrylate or methacrylate. A few others are vinyl ether. Altogether, 90 different resins or blends grouped to different sets, from Set A to Set J, were subjected to preliminary screening tests. These resins with a total of 1600 individual samples were cured under the electron beam at radiation dose that ranges from 2 kGy to 160 kGy. Around 600 of cured samples were tested using a PerkinElmer Pyris Diamond Dynamic Mechanical Analyzer in the bending (dual cantilever) mode at a scanning rate of 3°C/min.

4.1.1 Dynamic Mechanical Properties

In this work, all of the resins were tested in a wide range of temperature: from -100°C to their rubbery plateau temperature (vary with different resins). A variety of information was acquired from each scan to better understand every resin candidate. Figure 1 shows the typical DMA spectrum and analysis. The acquired information includes all of the following: the E'_{25} (storage modulus at 25°C), the E' onset temperature (the discontinuous change in temperature from the glass region into the transition), the E' offset temperature (the discontinuous change in temperature from the transition region to the rubbery region), the E'_{min} (storage modulus at the rubbery plateau), the temperature at tanδ peak and the temperature at E" peak (loss modulus). The latter two are frequently quoted as the glass transition temperature (T_g). In this work all of the T_g refers to the temperature at tan δ peak.

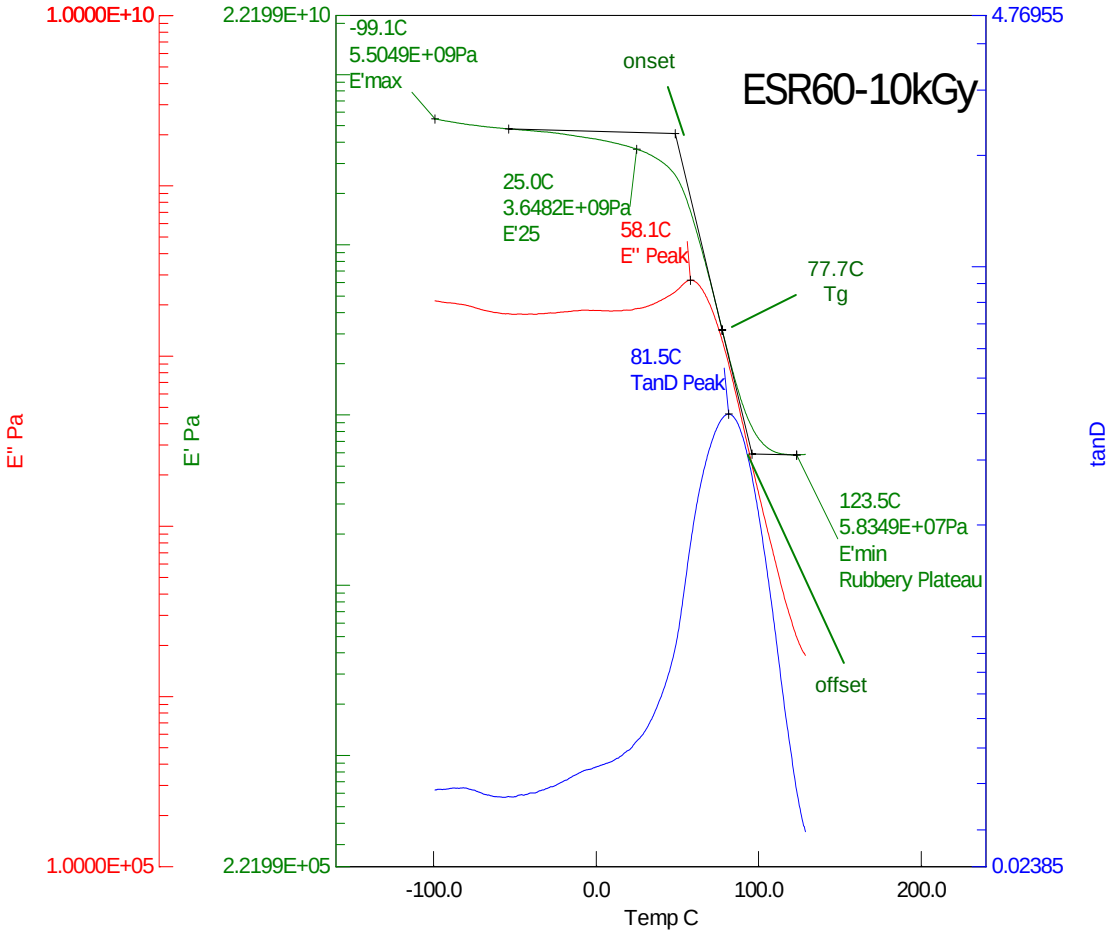

Figure 1. Typical Dynamic Spectrum and Analysis.

The dynamic mechanical properties vary greatly from resin to resin. Of all studied materials, E'_{25} ranges from 3 MPa to 6 GPa; T_g ranges from -60°C to 200 °C. The data show all resins exhibit a large variety of both chemistry and physical properties.

Table 3 simply summarizes the T_g, E'_{25} and E'_{min} of resins (cured at 80 kGy) based on DMA results, which are regarded as the critical guideline for the whole research.

4.1.2 Effect of Radiation Dose

Glass transition temperature (T_g) is of first importance to thermosetting polymers for various reasons. Many attempts have been made to correlate this important glass transition temperature to their molecular structure. Several authors have reported T_g data in correlation with conversion. Of various equations, the empirical DiBenedetto's equation that describes T_g as a function of conversion is widely used in the literature to fit experimental data (Hale, 1991).

In this work, T_g was adopted as a monitor for the curing degree as a response to radiation dose. T_g data of four different resins were collected and plotted against radiation dose shown in figure 2. These four resins are: R18 (low viscosity polyester acrylate oligomer), R22 (resilient aliphatic urethane acrylate), R33 (modified epoxy diacrylate), R61 (aromatic ester multifunctional vinyl ether diluted with TRPGDA). All four plots show T_g steadily increase to the plateau as the radiation dose increases. Such plots roughly indicate the amount of dose to achieve complete curing. For R18 and R22, the optimum curing dose (complete curing dose) is around 20 kGy; for R33, the dose seems to be in the range of 20 to 40kGy; for R61, the curing dose appears to be higher than 40 kGy. For most resins that are acrylate (or methacrylate) based epoxy, ester and urethane,

Table 3. Dynamic Mechanic Properties Summary.

Code	Chemical family	T_g(°C)	E'_{25}(GPa)	E'_{min}(GPa)
R01	Bisphenol-A epoxy diacrylate	131	4.00	0.0883
R02	Bisphenol-A epoxy diacrylate	27.8	0.138	0.0101
R03	Epoxidized soya oil tetraacrylate	52.3	0.652	0.0413
R04	Aliphatic urethane diacrylate	50.3	1.89	0.0337
R05	Aromatic urethane diacrylate	23.3	0.0836	0.0132
R06	Fatty acid modified polyester hexaacrylate	61.1	1.67	0.735
R07	Polyester hexaacrylate	116	5.10	0.634
R08	Bisphenol-A epoxy diacrylate	144	3.56	0.179
R09	Bisphenol-A epoxy diacrylate	155	3.88	0.223
R10	Bisphenol-A epoxy diacrylate	177	4.04	0.565
R11	Aliphatic urethane acrylate	64.9	1.79	0.0387
R12	Aliphatic urethane acrylate	69.6	1.64	0.0389
R13	Aromatic urethane triacrylate	123	3.93	0.136
R14	Aliphatic urethane triacrylate	108	3.24	0.0524
R15	Epoxy acrylate	120	4.24	0.0749
R16	Low viscosity acrylate /methacrylate	21.6	0.0176	0.00290
R17	Low viscosity acrylate	38.5	1.18	0.0187
R18	Low viscosity polyester acrylate oligomer	69.4	2.57	0.192
R19	Polybutadiene urethane diacrylate	-61.6	0.0152	0.00640
R20	Resilient aliphatic urethane acrylate	47.2	0.692	0.0167
R21	Resilient aliphatic urethane acrylate	63.2	1.14	0.0246
R22	Resilient aliphatic urethane acrylate	61.6	1.06	0.0236
R23	Resilient aliphatic urethane acrylate	71.0	1.24	0.0575
R25	Flexible aliphatic urethane acrylate	-1.7	0.0627	0.00930
R26	Flexible aliphatic urethane acrylate	120	2.39	0.00420
R27	Hard aliphatic urethane acrylate	109	3.61	0.0692
R28	Aliphatic urethane acrylate	-10.0	0.00330	0.00290
R29	Hard aliphatic urethane acrylate	151	4.23	0.0639
R30	Hard aliphatic urethane acrylate	155	4.36	0.0924
R31	Urethane acrylate blended with SR238	199	3.96	0.202
R32	Aliphatic urethane acrylate monomer	52.5	0.722	0.0155
R33	Modified epoxy diacrylate	56.2	3.86	0.0138
R34	1,4-butanediol diacrylate	111	2.65	0.868
R35	Tris(2-hydroxyethyl)isocyanurate triacrylate diluted	74.9	4.95	2.17
R36	Dipentaerythritol pentaacryalte	-7.3	5.99	4.65
R38	Propoxylated(2) neopentyl glycol diacrylate	71.9	2.39	0.110

Table 3. Continued.

Code	Chemical family	T_g(°C)	E'_{25}(GPa)	E'_{min}(GPa)
R39	Trifunctional acrylate ester	70.2	5.09	2.79
R40	Urethane dimethacrylate	136	4.75	0.124
R41	Ethylene glycol dimethacrylate	87.9	4.63	2.58
R42	1,6-hexanediol dimethacrylate	-82.4	2.56	1.31
R43	Polyethylene glycol dimethacrylate	-22.6	0.0270	0.0262
R44	1.3-butylene glycol dimethacrylate	81.6	3.51	1.66
R46	Ethoxylated(4)bisphenol-A dimethacrylate	126	3.32	0.108
R47	Trifunctional methacrylate ester	-1.7	2.72	1.35
R48	Bisphenol-A diglycidyl dimethacrylate	148	4.94	0.0757
R49	Aromatic acid methacrylate half ester	121	3.55	0.0384
R59	Ethoxylated(4)bisphenol-A dimethacrylate/VE4010	93.4	3.30	0.0908
R60	Aromatic urethane triacrylate/Ve4010	101	3.68	0.0937
R61	Aromatic ester multifunctional vinyl ether /TRPGDA	70.7	1.79	0.107
R62	Propoxylated(6) trimethylopropane triacrylate	52.0	1.56	0.119
R63	Ethoxylated(4) pentaerythtitol tetraacrylate	115	3.13	0.563
R64	R31 diluted with SR368D	187	4.02	0.100
R65	Bis[4-(vinylocxy)butyl] adipate / TRPGDA	69.2	2.27	0.128
R66	Tris[4-(vinyloxy)butyl] trimellitate	74.6	2.66	0.132
R67	Ethoxylated(4)bisphenol-A diacrylate	84.4	3.06	0.0724
R68	Aliphatic urethane acrylate	71.9	1.68	0.0465
R69	Aliphatic urethane acrylate	84.0	1.79	0.0731
R70	Aliphatic urethane acrylate	89.0	1.86	0.127
R71	BPA/epoxy aromatic urethane diacrylate	124	3.90	0.0817
R72	BPA/epoxy aromatic urethane diacrylate	138	3.33	0.163
R73	BPA/epoxy aromatic urethane diacrylate	117	3.91	0.0776
R74	BPA/epoxy aromatic urethane diacrylate	132	3.29	0.150
R76	Aliphatic urethane diacrylate	116	3.43	0.0537

Table 3. Continued.

Code	Chemical family	T_g(°C)	E'_{25}(GPa)	E'_{min}(GPa)
R78	Aliphatic urethane diacrylate	72.00	2.51	0.0409
R80	Aliphatic urethane diacrylate	125	3.26	0.109
R82	Aliphatic urethane diacrylate	82.1	2.49	0.0824
R85	Aromatic urethane diacrylate	102	3.09	0.0744
R89	Aromatic urethane diacrylate	110	2.85	0.0599

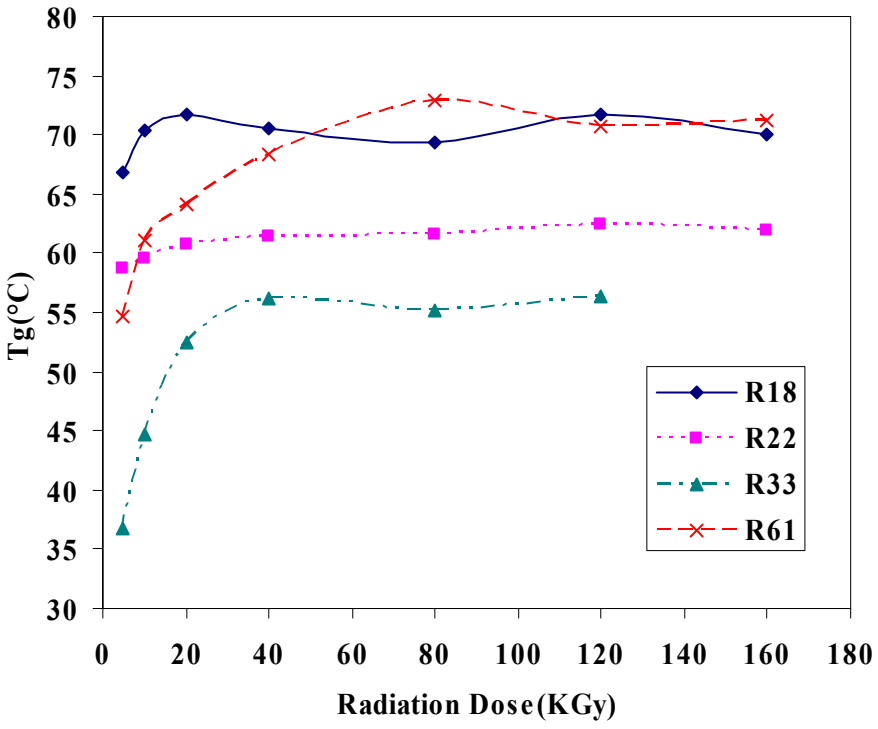

Figure 2. Effect of Radiation Dose on Tg.

the radiation dose for full curing is in the range of 20 to 40 kGy. For vinyl ether (such as R61), the radiation dose is higher. Some vinyl ether can not be cured within the range of our radiation dose, such as R50 and R51.

For oligomers containing acrylate or methacrylate groups, a low radiation dose is required to form a polymer network. This feature suggests that a lower exposure level can be considered in the practice, since it is not always necessary to achieve a full cure.

4.1.3 Effect of Diluents

4.1.3.1 Difunctional Monomers

Adding diluents to viscous base resins results in both physical and chemical property changes. The effect of difunctional monomer diluents on dynamic mechanical properties was studied during the screening tests. The two specific difunctional monomers formulated are: HDODA (1,6-hexanediol diacrylate) and TRPGDA (tripropylene glycol diacrylate). The effect of HDODA ratio on the variation of dynamic mechanical properties of R11 (aliphatic urethane acrylate) is shown in Figure 3. It is obvious that both T_g and E'_{min} increase with HDODA ratio. On the other hand, E'_{25} drops firstly with a small ratio of diluent, and then rises with increase amount of diluent. The observation indicates that the cross-linking density is amplified by introducing HDODA.

Figure 4 shows the effect of HDODA and TRPGDA on the variation of dynamic mechanical properties of resins at 20% ratio. Similar trends in figure 3 are also found in figure 4. Compared to base resins, both T_g and E'_{min} exhibit an increase with difunctional monomer, while E'_{25} shows a decrease with the difunctional monomers.

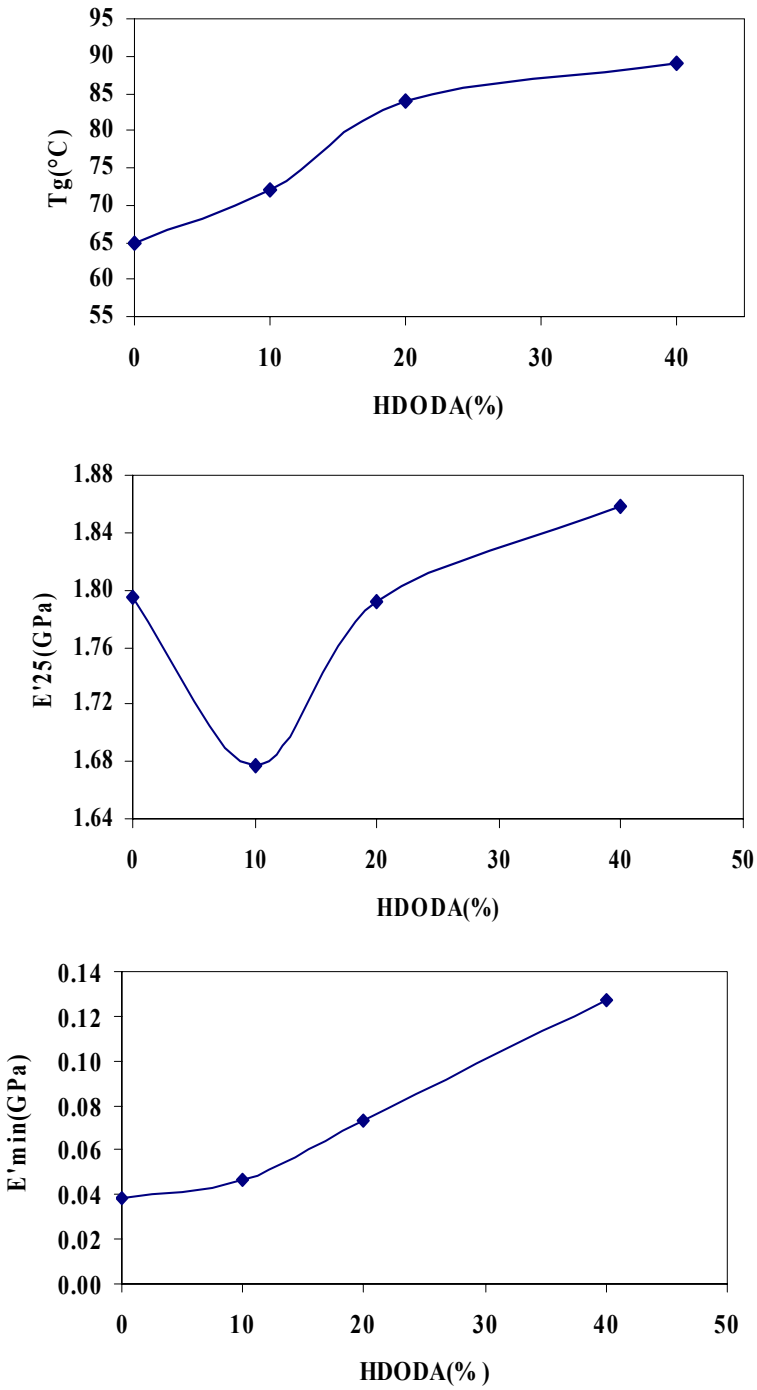

Figure 3. Effect of HDODA on the Dynamic Mechanical Properties of R11.

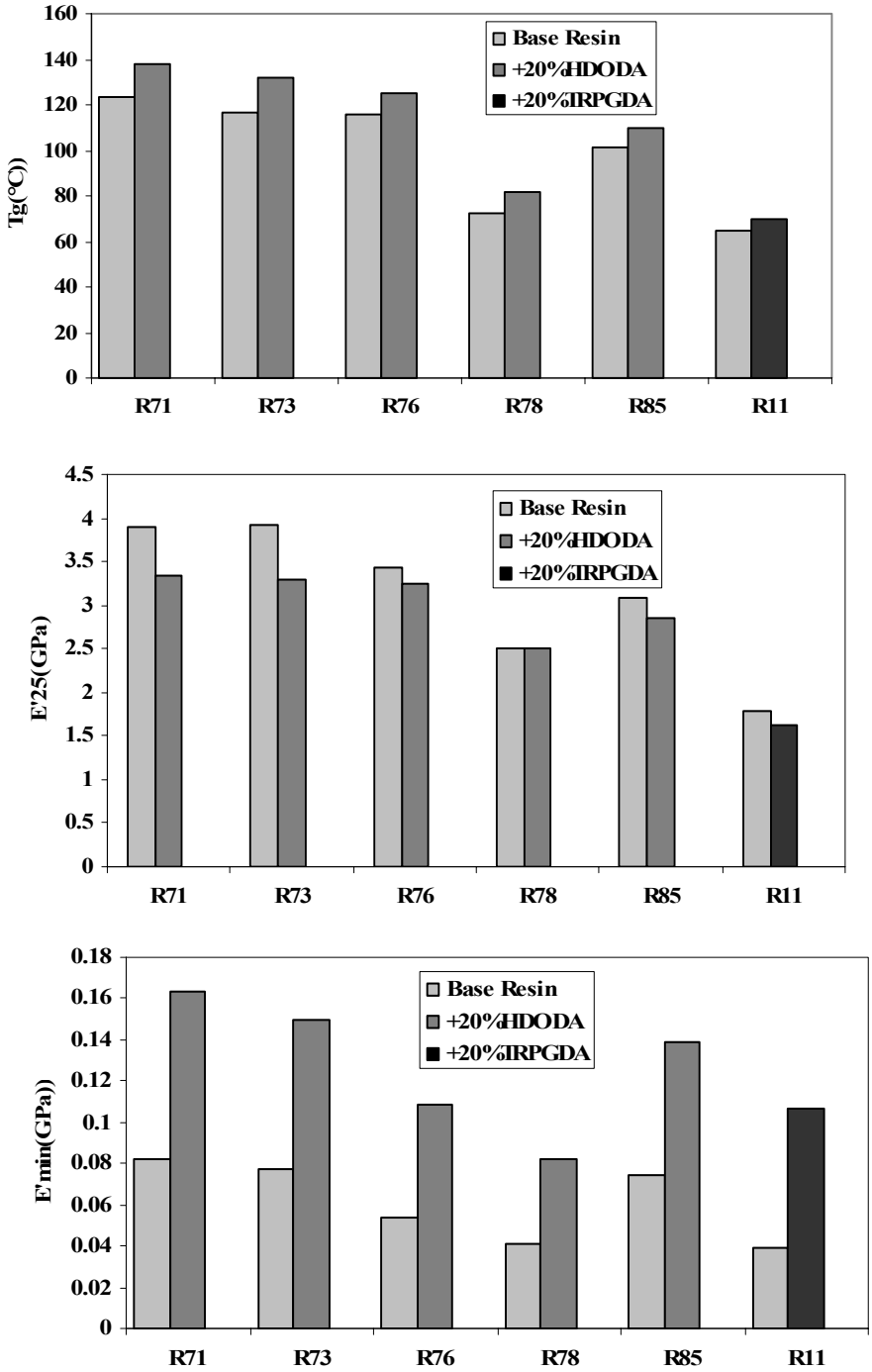

Figure 4. Effect of HDODA on the Dynamic Mechanical Properties of Selected Resins

4.1.3.2 Trifunctional Monomers

The effect of trifunctional monomer on the resin property was also studied. Figure 5 plots TMPTA (trimethylopropane triacrylate) affecting dynamic mechanic properties of R01 (bisphenol-A diacrylate). Figure 3, 4 and 5 show that both the difunctional and trifunctional monomers increase the cross-linking density of the cured resins.

4.2 Resin-Wood Bonds

With a better understanding of the properties of the candidate resins, as well as their response to the radiation dose, the attempts to study resin-wood bondline were initiated.

The major difficulty was selecting an appropriate standardized test which would permit comparisons of a wide variety of adhesives with minimized substrate variables. Another challenge is to design an applicable resin-wood fixture which would permit sufficient access of the electron beam to adhesive bondline. Two ASTM standards were chosen: ASTM D906 (standard test method for strength properties of adhesives in plywood type construction in shear by tension loading) and ASTM D905 (standard test method for strength properties of adhesive bonds in shear by compression).

4.2.1 Shear Properties of Resin-Poplar 3-Plywood

The 3-plywood construction specimens were prepared with selected resins, cured at 80 kGy dose, and then tested in shear by tension loading according to ASTM D906. The commercial product G-2 epoxy formulated to bond wood was also included for the reference. The test results were illustrated in figure 6.

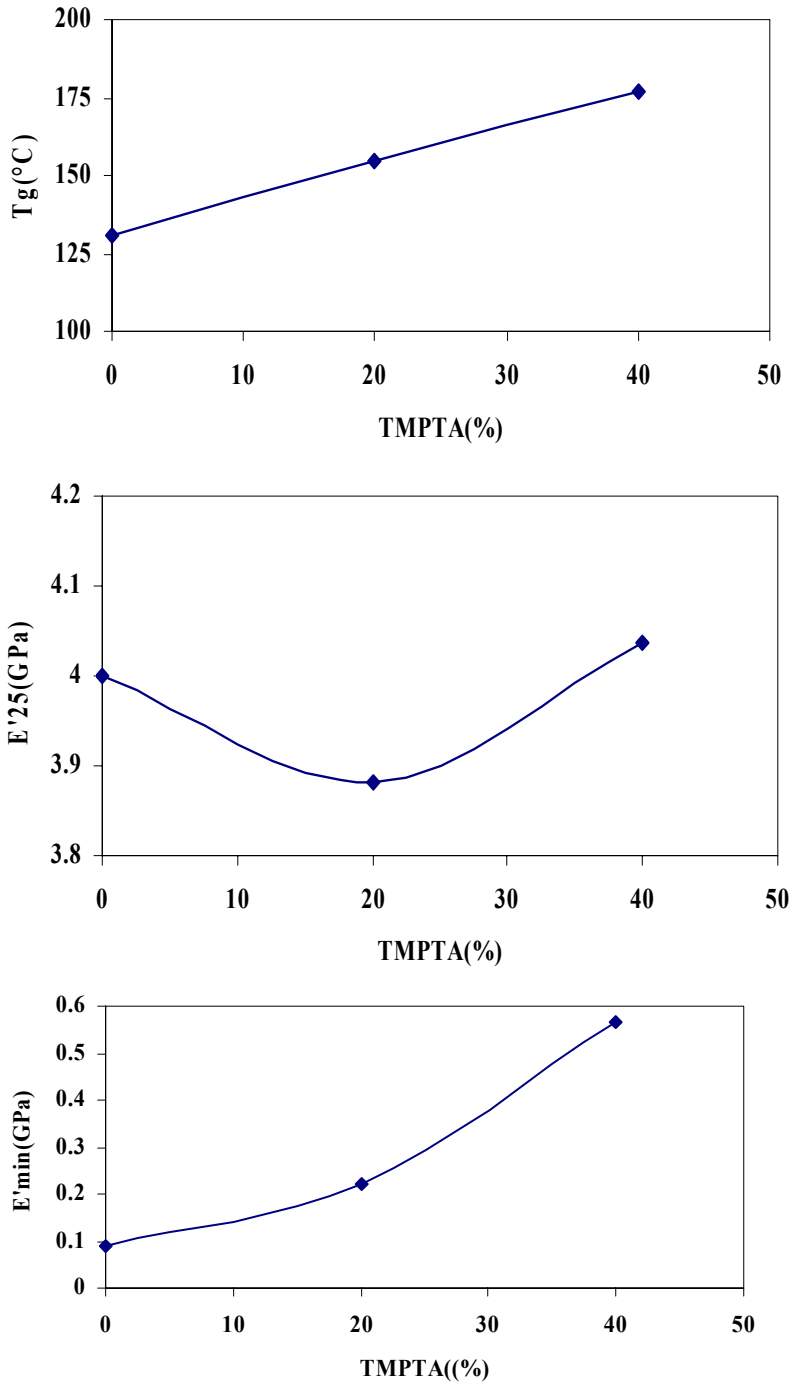

Figure 5. Effect of TMPTA on the Dynamic Mechanical Properties of R01.

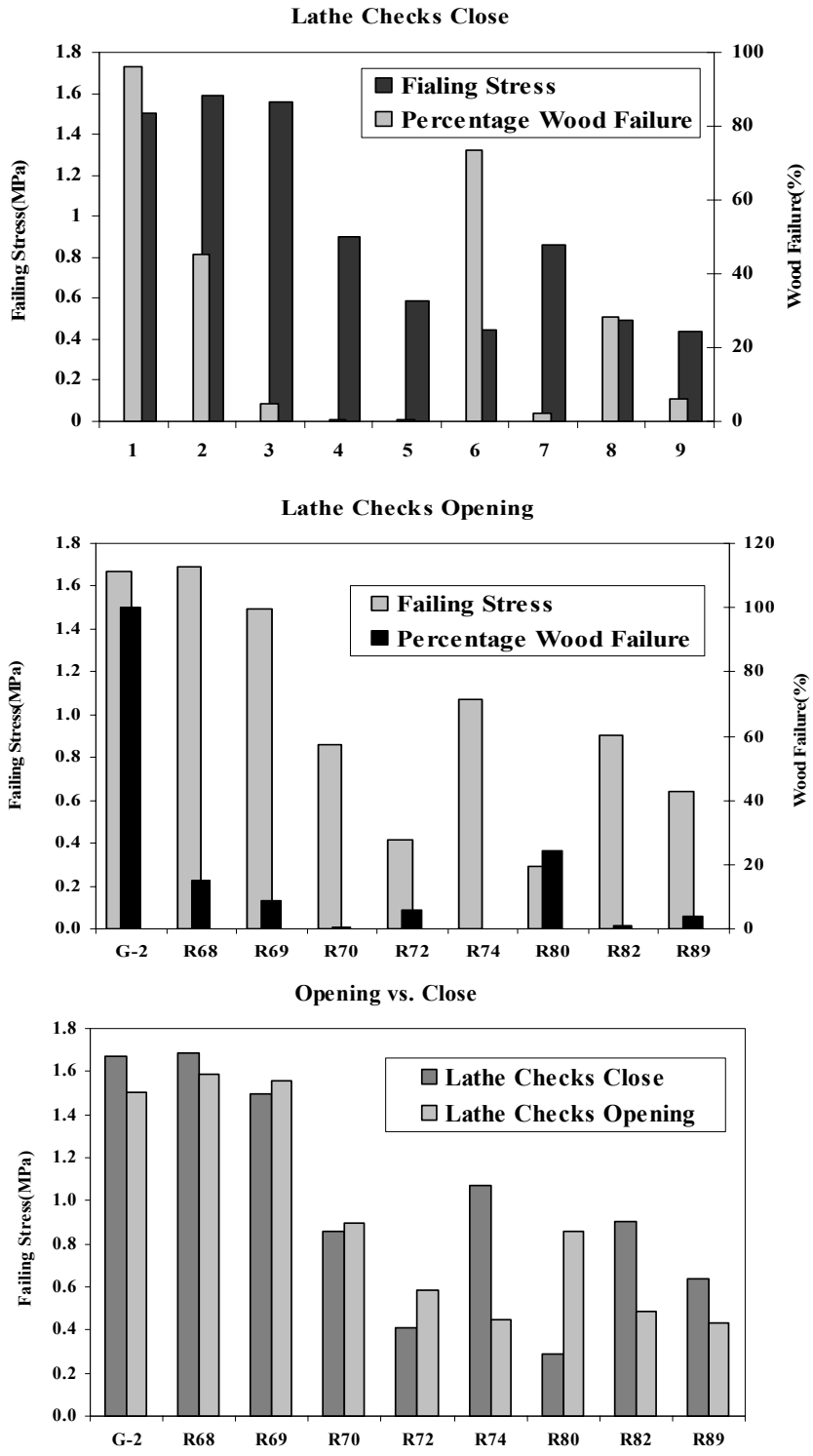

Figure 6. Shear Test Results of Plywood.

According to the orientation of lathe checks in the transverse core veneer, all 3-plywood specimens were grouped and tested to two major categories: lathe checks opening and lathe checks close respectively. Figure 7 displays the tendency of lathe checks to open or close when the specimens are subjected to tension (Sellers, 1985). Thus different levels of failing stress can be observed between two groups and sometime this difference can be as high as 50 percent.

Based on comparisons of failing stress and percentage wood failure in figure 6, R68 seems comparable to the reference G-2 epoxy. But the comparison results were doubted due to many uncertain variables during the entire sample preparation and testing processes. Firstly, the ASTM D906 requires birch wood that is free of defects as the adherend. With the only available choice, yellow polar during the test, its weak strength causes peculiar data. Furthermore, selecting veneers that are free of knots, cracks or distorted grain is impossible, which inevitable leads to inferior results. Secondly, the resin loading rate was 74 g/m^2 for plywood samples (Sellers, 1985). Due to the low density of poplar, over penetration left insufficient amount of resins on veneer surface, especially the lathed surface. The bondline appears unsatisfactory and some specimens were failed before the test. Thirdly, some processing procedures like adhesives application, cutting of plywood for the desired test geometry, and samples loading to the testing machine, inevitably result in cracks. The top specimen in figure 8 exemplifies one type of failure before test when the test sample was loaded. Fourthly, the bulk mechanical strength of the core veneer is the critical factor affecting the joints quality. Test results, however, found around 1/5 of the specimens failed at the center veneer, as displayed by the bottom specimen in figure 8. Finally, the failing stress of the specimens with close

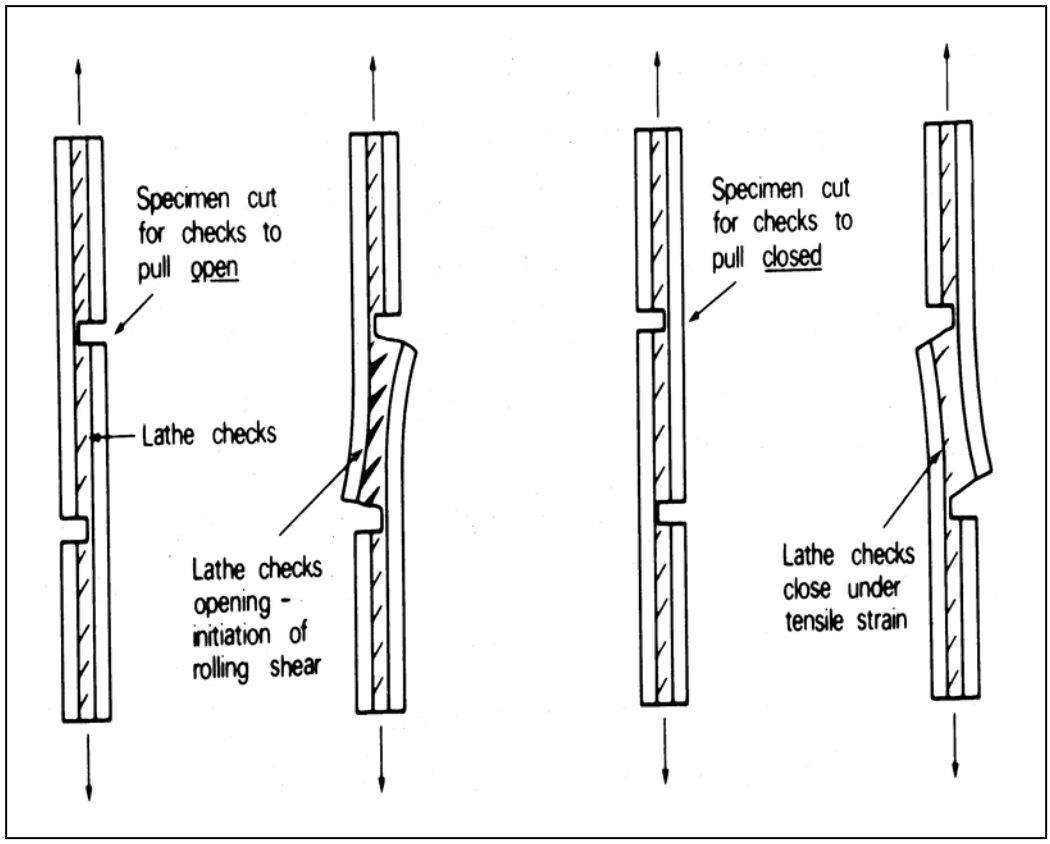

Figure 7. Plywood Specimens with Open and Closed Lathe Checks.

Notch Failure

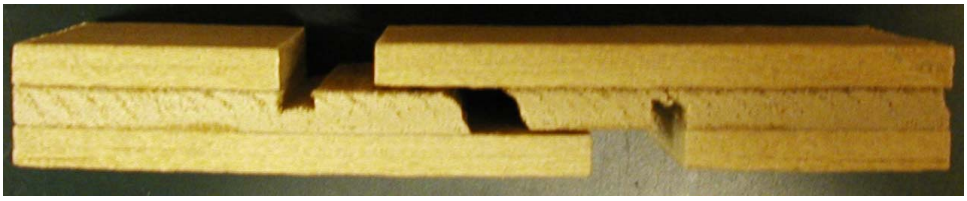

Core Veneer Failure

Figure 8. Two Types of Plywood Failure.

lathe checks should be higher than that of opening lathe checks, as mentioned above. Referring to figure 6 again, half of the resin-wood bondline (R69, R70, R72, and R80) show the opposite results, namely the failing stress of specimens with open lathe checks is superior to that of close one. All of the above factors indicate that yellow poplar is not strong enough to accomplish the bondline strength evaluation. Thus strength testing of adhesive bond in plywood construction is not continued.

4.2.2 Shear Properties of Resin-Maple Blocks

The maple block specimens were prepared with selected resins, cured and then tested to ASTM D905. Hard maple employed as a substrate in the test is requested by the standard and is also highly recommended by the literature (Blomquist, 1981).

Compared to yellow poplar, sugar maple is more adequate as a substrate for the adhesive bonds tests. With less variability, selecting maple blocks that are free from knots, decay and unusual discolorations is effortless. As one the strongest species, sugar maple has shear strength of 15.9 MPa (2306 psi), compared to 13.0 MPa for yellow birch and 7.6 MPa for Douglas-fir (Blomquist, 1981). Moreover, due to its high density, a resin loading rate of 68 g/m^2 ensures satisfactory bondline without over penetration problem. Sample processing, such as cutting and loading, is also relative easy because of its high strength and high density.

4.2.2.1 Effect of Radiation Dose

Figure 9 plots the evolution of failing stress of resin-maple bonds with the increment of radiation dose. The failing stress increases continuously with the exposure level. No plateau is observed in the observation range due to insufficient radiation doses

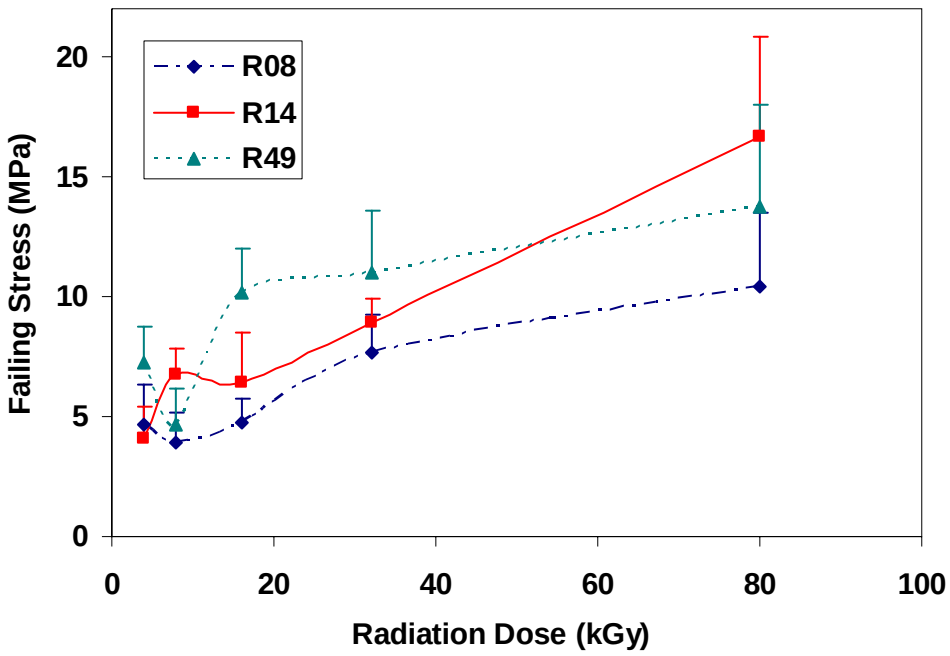

Figure 9. The Evolution of Failing Stress with Radiation Dose.

employed. Nevertheless, the apparent observation is that a radiation dose of 40 kGy can not fully cure resin-maple bonds. This behavior differs from the curing behavior of neat resin seen in figure 2.

The difference in curing progresses between neat resins and resin-wood bonds is within reasonable explanation. Loss of energy as electron beam penetrates the thick wood block is a possible attribute. Another potential factor is the dilution of reactive functional groups of resin in the presence of the wood, with reference to bulk resin reaction.

4.2.2.2 Correlation with Dynamic Mechanical Properties

In the preliminary screening period, two sets (Set G and Set J) of maple blocks with their respective resins were prepared, cured at 80 kGy radiation dose and tested. The carpenter's wood glue Commercial poly (vinyl acetate) was also included in the adhesive bond test as a reference. The tests results were displayed in figure 10. The distinction between Commercial poly (vinyl acetate) and other candidates is obvious. The reference Commercial poly(vinyl acetate)-maple has the highest failing strength (up to 27.4 MPa) with 63 percentage wood failures; while other resin-maple have inferior performance with cohesive failure or adhesive failure.

The performance of resin-maple bonds can be traced to the resin structure characteristics, such as the type of molecules, molecular weight and structure, cross-linking density, etc. The attempt to correlate the dynamic mechanical properties of neat resin to the shear strength of maple bonds is presented in figure 11. To minimize the variability, the data shown in the figure are for the urethane family only. The line is included to highlight the qualitative trend, and was not generated from any numerical model. The greater shear strength is associated with low E'_{min}. As E'_{min} increases,

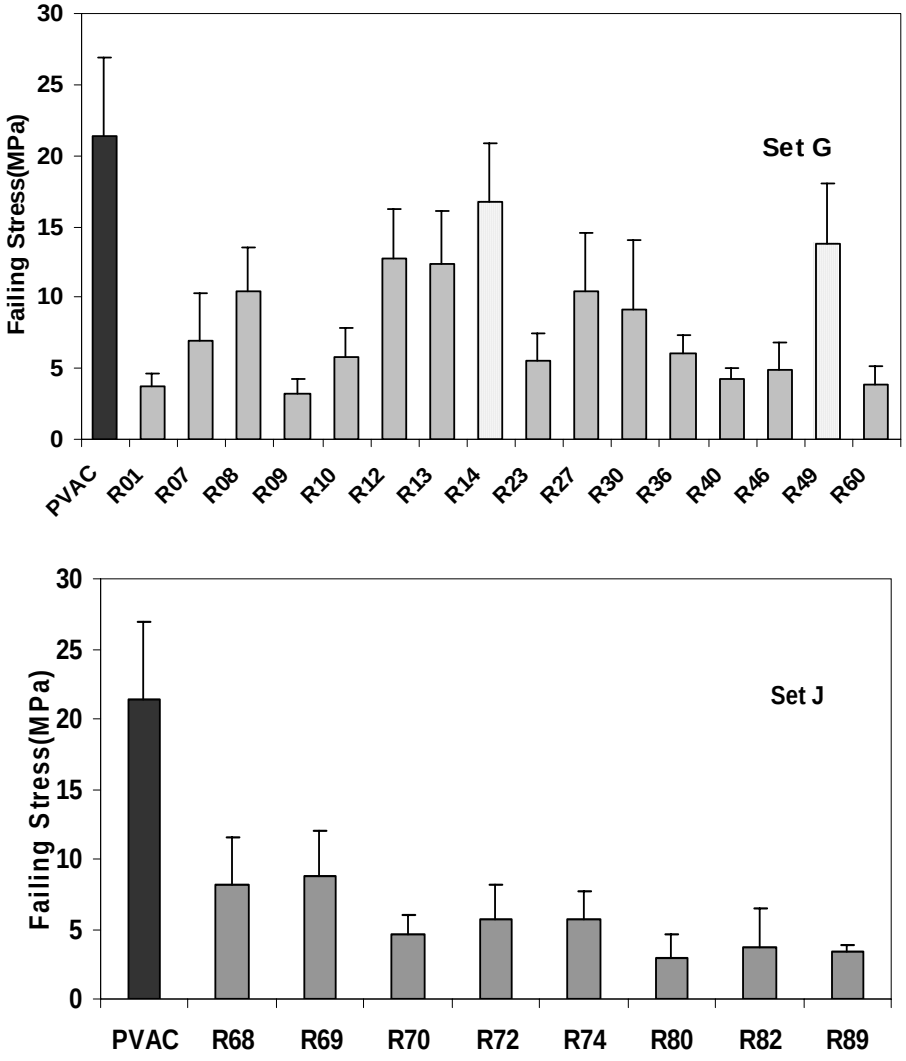

Figure 10. Shear Test Results of Set G and Set J.

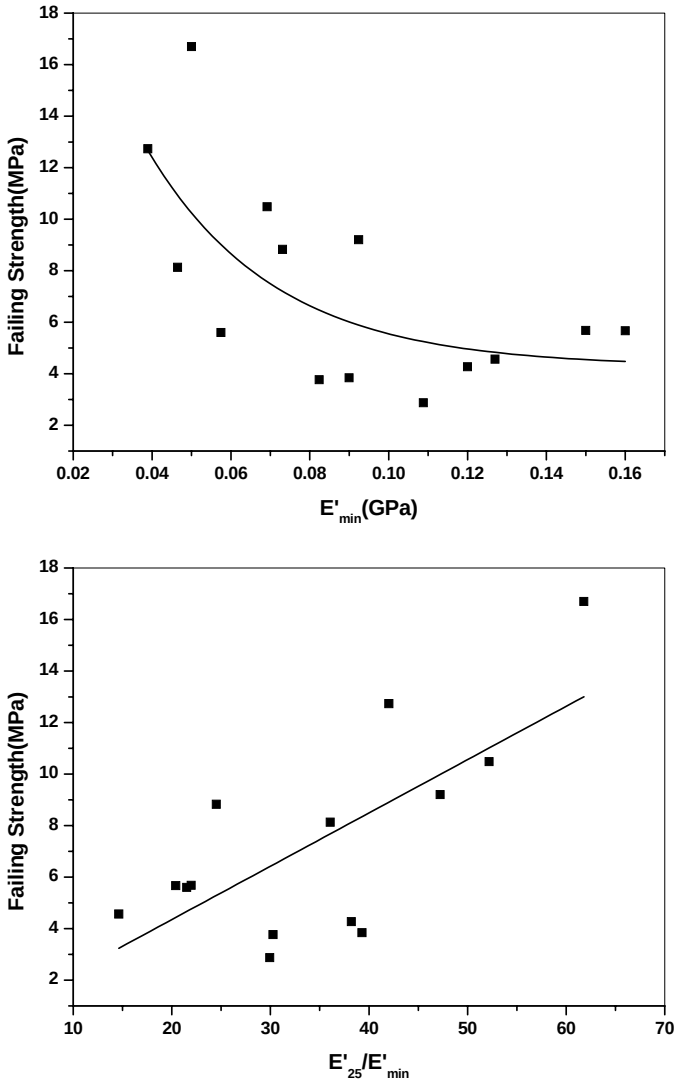

Figure 11. The Failing Stress vs. Dynamic Mechanical Properties.

the shear strength decreases. The plot of shear strength against E'_{25}/ E'_{min} suggest that high failing stress of bonded joints is related to the large ratio of E'_{25} to E'_{min}.

Table 4 lists the dynamic mechanical properties of resins for the shear test of maple blocks (Set G & J). Mechanical behavior of bonds made with R14 (aliphatic urethane triacrylate) and R49 (aromatic acid methacrylate half ester) stand out among all resins. These two candidates possess moderate E'_{25}, low E'_{min} and largest values of E'_{25}/ E'_{min}.

The correlation study is indicating if relate E'_{min} to the cross-linking density. The lower E'_{min}, the lower cross-linking density. As the cross-linking density decreases, the effective chains between cross-links are freer to assume more configurations. Therefore, the dissipative property of resins is improved, indicated by low E'_{min}. When subjected to external forces, the bonded joints exhibit higher shear strength as improved energy dissipation into resin matrix.

Table 4. Dynamic Mechanical Properties of Resins in Shear Tests (Set G & J).

Code	Failing Stress (MPa)	E'_{25}(GPa)	E'_{min}(GPa)	E'_{25}/ E'_{min}
GMR01	3.73	4.00	0.0883	45
GMR07	6.98	5.10	0.634	8
GMR08	10.4	3.56	0.179	20
GMR09	3.27	3.88	0.223	17
GMR10	5.80	4.04	0.565	7
GMR12	12.7	1.64	0.0389	42
GMR13	12.3	3.93	0.136	28
GMR14	16.7	3.24	0.0524	62
GMR23	5.60	1.24	0.0575	22
GMR27	10.5	3.61	0.0692	52
GMR30	9.20	4.36	0.0924	47
GMR36	6.02	5.99	4.65	1
GMR40	4.27	4.75	0.124	38
GMR46	4.87	3.32	0.108	30
GMR49	13.8	3.55	0.0384	93
GMR60	3.84	3.68	0.0937	39
JMR68	8.13	1.68	0.0465	36
JMR69	8.83	1.79	0.0731	25
JMR70	4.56	1.86	0.127	15
JMR72	5.67	3.33	0.163	20
JMR74	5.68	3.29	0.150	22
JMR80	2.87	3.26	0.109	30
JMR82	3.76	2.49	0.0824	30
JMR89	3.45	2.85	0.0599	48

5 RESULTS AND DISCUSSON − POTENTIAL RESINS

5.1 Potential Resins

With the knowledge from preliminary screening studies, R14 and R49 obviously stand out as potential resins for further exploration. Referring back to all dynamic mechanical data in table 3, R33 (modified epoxy diacrylate) shows prospective properties comparable to R14 and R49. These three were chosen as base resins in the later work.

The previous study of diluent effect indicates that addition of difunctional and trifunctional monomer into resins results in diminished stiffness (reduced E'_{25}) and amplified brittleness (increased E'_{min}). This conclusion suggests the use of monofunctional monomer which has the ability of improving flexibility and adhesion of radiation curable products. Two monofunctional monomers indicated by the vendor, IBOA (Isobornyl acrylate) and GENOMER 1122 (urethane monoacrylate), meet our desired criterion and were adopted. R16 (low viscosity acrylate/methacrylate) was selected as toughener because of its especially low level of E'_{min}.

5.1.1 Dynamic Mechanical Properties

In order to index the appropriate magnitude of E'_{25}, E'_{min} and T_g, G-2 epoxy and Commercial poly (vinyl acetate) were run on DMA. G-2 was cured in the oven at 100 °C for 24 hours. Commercial poly(vinyl acetate) (PVAC)was room temperature cured for 48 hours and then heated to 100 °C for another 24 hours. The DMA data of references and bases are listed in table 5 (cured at 80 kGy). The new formulations derived from the three base resins as well as two diluents and toughener are listed in table 6 with their important DMA data (obtained at 80 kGy) listed in table 7.

Table 5. Dynamic Mechanical Properties of Potential Resins and References.

Code	Chemical family	T_g(°C)	E'_{25}(GPa)	E'_{min}(GPa)
R14	Aliphatic urethane triacrylate	108	3.24	0.0524
R33	Modified epoxy diacrylate	56.2	3.86	0.0138
R49	Aromatic acid methacrylate half ester	121	3.55	0.0384
R16	Low viscosity acrylate/methacrylate	21.6	0.0176	0.0029
G-2	Reference	66.8	2.92	0.0106
PVAC		50.1	3.05	0.000100

Table 6. New Formulations Based on Potential Resins.

Code	Chemical family	Base resin	2nd Component
R120	Aliphatic urethane triacrylate	90%R14	10%D12
R121	Aliphatic urethane triacrylate	85%R14	15%D12
R122	Aliphatic urethane triacrylate	80%R14	20%D12
R123	Aliphatic urethane triacrylate	90%R14	10%D36
R124	Aliphatic urethane triacrylate	85%R14	15%D36
R125	Aliphatic urethane triacrylate	80%R14	20%D36
R126	Aliphatic urethane triacrylate	80%R14	20%R16
R127	Aliphatic urethane triacrylate	70%R14	30%R16
R128	Aliphatic urethane triacrylate	60%R14	40%R16
R129	Modified epoxy diacrylate	90%R33	10%D12
R130	Modified epoxy diacrylate	85%R33	15%D12
R131	Modified epoxy diacrylate	80%R33	20%D12
R132	Modified epoxy diacrylate	90%R33	10%D36
R133	Modified epoxy diacrylate	85%R33	15%D36
R134	Modified epoxy diacrylate	80%R33	20%D36
R135	Modified epoxy diacrylate	80%R33	20%R16
R136	Modified epoxy diacrylate	70%R33	30%R16
R137	Modified epoxy diacrylate	60%R33	40%R16
R138	Aromatic acid methacrylate half ester	95%R49	5%D12
R139	Aromatic acid methacrylate half ester	90%R49	10%D12
R140	Aromatic acid methacrylate half ester	85%R49	15%D12
R141	Aromatic acid methacrylate half ester	95%R49	5%D36
R142	Aromatic acid methacrylate half ester	90%R49	10%D36
R143	Aromatic acid methacrylate half ester	85%R49	15%D36
R144	Aromatic acid methacrylate half ester	90%R49	10%R16
R145	Aromatic acid methacrylate half ester	80%R49	20%R16
R146	Aromatic acid methacrylate half ester	70%R49	30%R16
R147	Aliphatic urethane triacrylate	85%R14	15%L
R148	Modified epoxy diacrylate	80%R33	20%L

Table 6. Continued.

Code	Chemical family	Base resin	2nd Component
R149	Modified epoxy diacrylate	85%R33	15%L
R150	Aromatic acid methacrylate half ester	85%R49	15%L

Table 7. Dynamic Mechanical Properties of New Formulations.

Code	Chemical family	T_g(°C)	E'_{25}(GPa)	E'_{min}(GPa)
R120	Aliphatic urethane triacrylate	110	3.59	0.0463
R121	Aliphatic urethane triacrylate	110	3.57	0.0448
R122	Aliphatic urethane triacrylate	110	3.38	0.0424
R123	Aliphatic urethane triacrylate	96.0	3.85	0.0470
R124	Aliphatic urethane triacrylate	90.1	3.85	0.0424
R125	Aliphatic urethane triacrylate	85.5	3.79	0.0391
R126	Aliphatic urethane triacrylate	83.0	4.10	0.0390
R127	Aliphatic urethane triacrylate	72.3	3.88	0.0347
R128	Aliphatic urethane triacrylate	62.7	3.78	0.0278
R129	Modified epoxy diacrylate	57.6	3.79	0.0114
R130	Modified epoxy diacrylate	58.2	3.68	0.0105
R131	Modified epoxy diacrylate	59.5	3.64	0.0101
R132	Modified epoxy diacrylate	53.3	3.71	0.0119
R133	Modified epoxy diacrylate	51.4	3.74	0.0120
R134	Modified epoxy diacrylate	49.2	3.53	0.0109
R135	Modified epoxy diacrylate	48.4	3.67	0.0114
R136	Modified epoxy diacrylate	44.5	3.23	0.0107
R137	Modified epoxy diacrylate	40.2	2.27	0.00950
R138	Aromatic acid methacrylate half ester	121	3.44	0.0374
R139	Aromatic acid methacrylate half ester	124	3.34	0.0354
R140	Aromatic acid methacrylate half ester	125	3.02	0.0327
R141	Aromatic acid methacrylate half ester	114	3.51	0.0371
R142	Aromatic acid methacrylate half ester	106	3.51	0.0362
R143	Aromatic acid methacrylate half ester	97.4	3.54	0.0334
R144	Aromatic acid methacrylate half ester	108	3.43	0.0400
R145	Aromatic acid methacrylate half ester	94.8	3.36	0.0395
R146	Aromatic acid methacrylate half ester	82.9	2.96	0.0372
R147	Aliphatic urethane triacrylate	122	3.91	0.0491
R148	Modified epoxy diacrylate	80.5	3.83	0.0195
R149	Modified epoxy diacrylate	88.4	3.82	0.0200
R150	Aromatic acid methacrylate half ester	112	3.58	0.0288
G-2	Reference	66.8	2.92	0.0106
PVAC		50.1	3.05	0.000100

5.1.2 Effect of Radiation Dose

The cure progression of potential resins with increasing radiation level is addressed here by means of FTIR spectrum, which has been repeatedly reported in the literature as a determination of the extent of reaction (Coqueret, 2003).

The curing progress can be evaluated by the attenuation bands in the FTIR spectroscopy. With the presence of acrylate groups in all resins, 3 main absorption bands are applicable for quantitative analysis (Ruiz, 2002), which are centered at: 810 cm^{-1} (corresponding to C=C bond out of plan deformation), 1410 cm^{-1} (corresponding to stretching of $=CH_2$), and 1640 cm^{-1} (corresponding to stretching of C=C). The acrylate absorption at 810 cm^{-1} has been proved more accurate by reason of free of vicinity disturbance and high intensity. The strong absorption at 1720 cm^{-1} related to the carbonyl function is not involved in the curing reaction and can be used as an internal standard.

The FTIR spectra of R14 and R49 with different radiation dose are shown in Figure 12 and 13 correspondingly. Both spectra show continuous attenuation of absorbance peak at 810 cm^{-1} with the increase of exposure level. It is worth noting that the absolute quantitative analysis of spectra is restricted at higher exposure due to the weakness of absorption and limited contact between specimen and the infrared diamonds. Figure 14 plots the ratio of the peak absorbance of double bond at 810 cm^{-1} to that of 1720 cm^{-1} peak as a function of radiation dose. A rapid decline in the concentration of C=C functionality up to 10 kGy is visually apparent. Upon continuous exposure to higher dose, the gradually leveled curve indicates the completely consumption of the reaction groups, hence suggesting the end of curing.

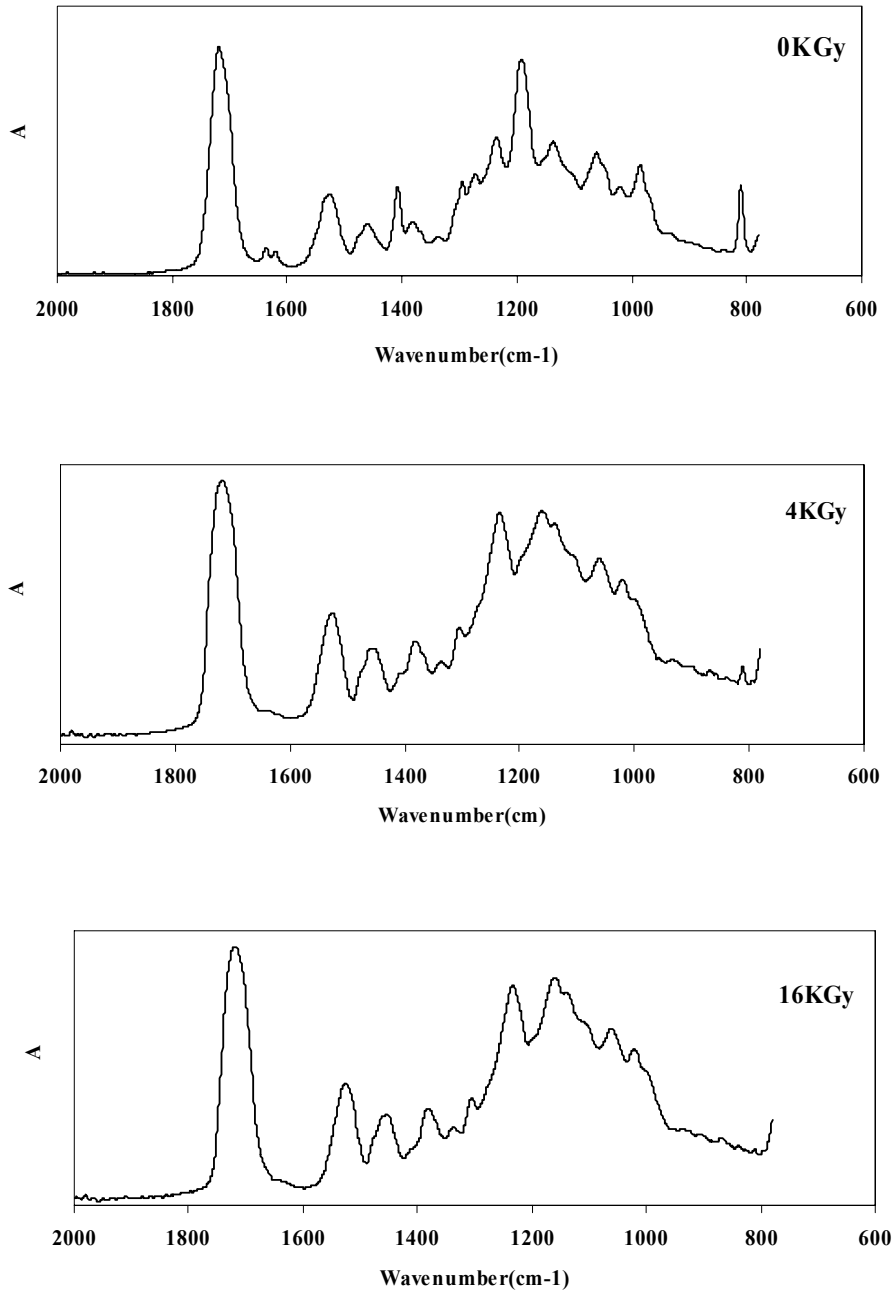

Figure 12. IR Spectra of R14 with Exposure to Different Doses.

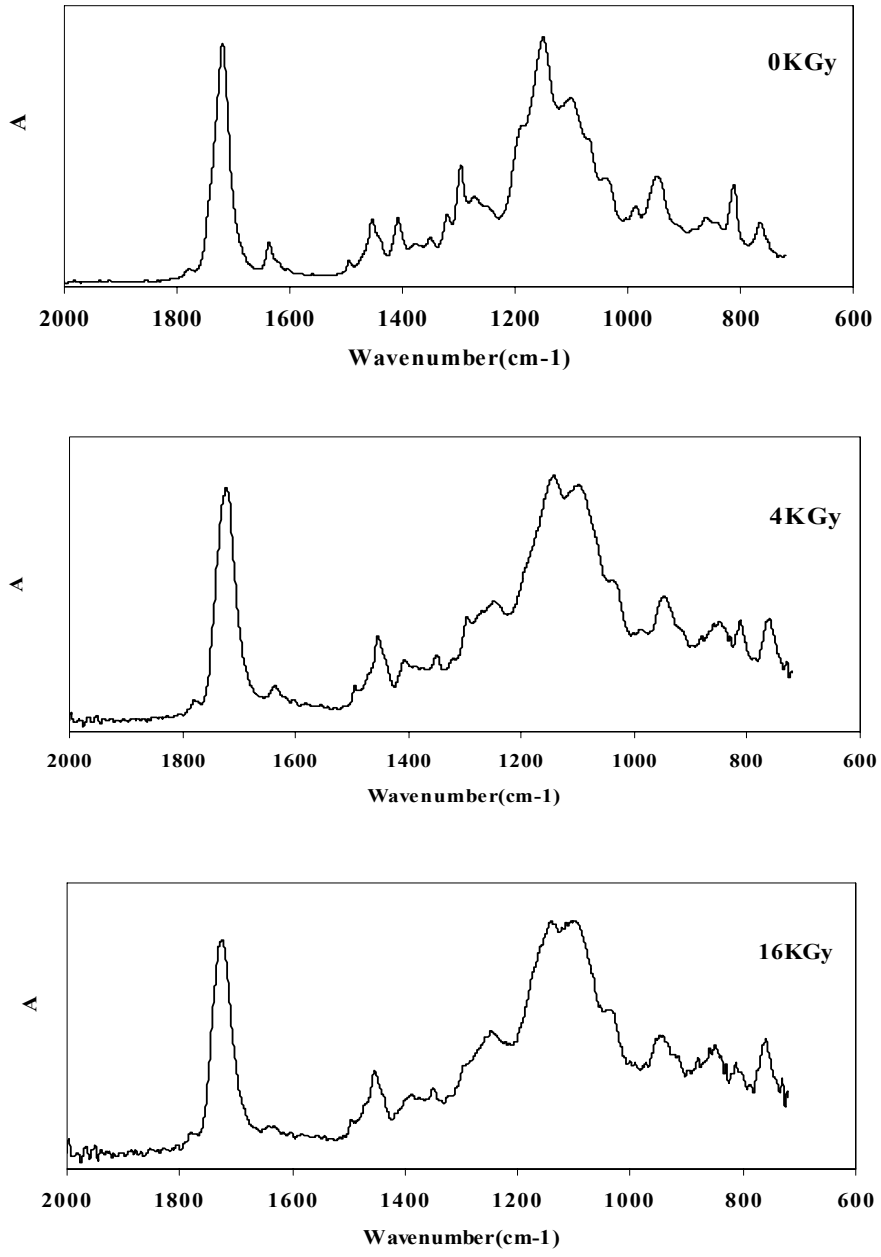

Figure 13. IR Spectra of R49 with Exposure to Different Doses.

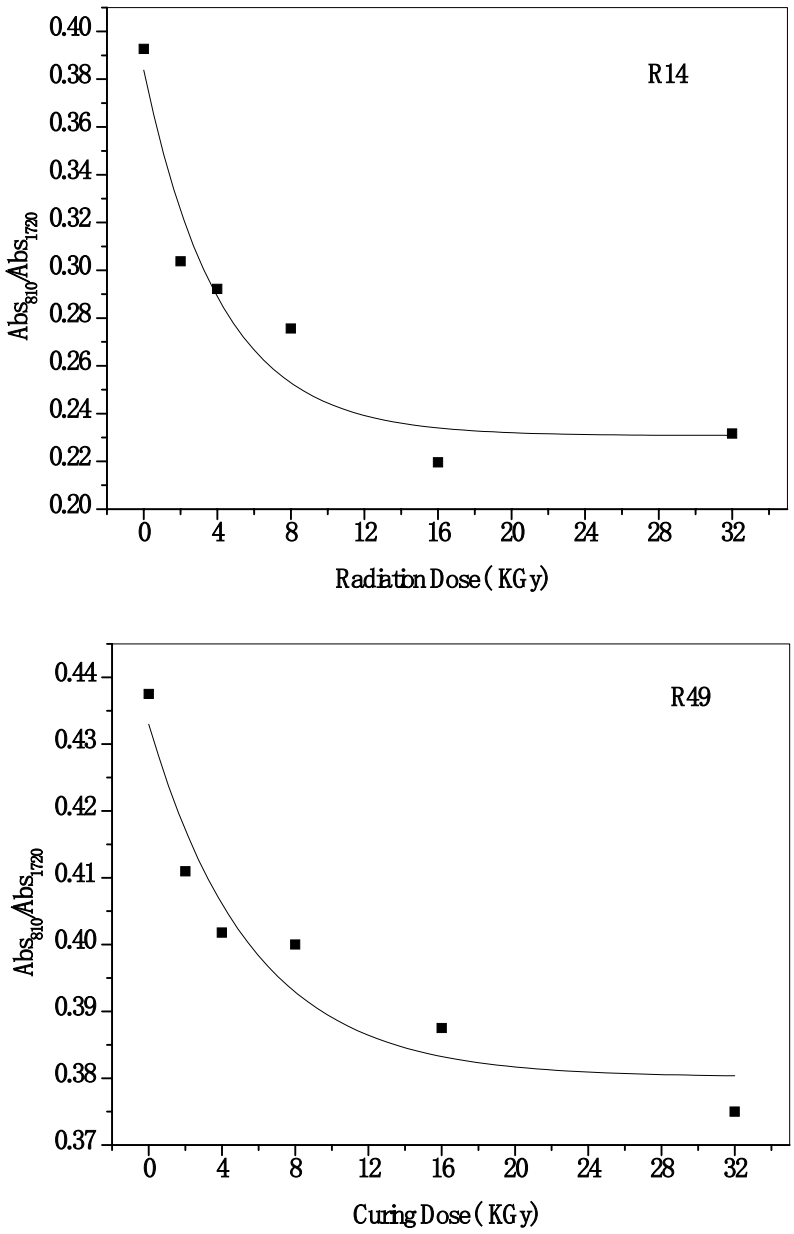

Figure 14. Decrease of Acrylic Functionality as a Function of Radiation Doses.

The general trend in T_g variation of both base or new formulations is in consistent with the observation from IR spectra, shown in figure 15. After exposed to around 10 kGy, a big shift in T_g of 3 potential resins is detected, which reflects a significant increase in cross-linking among polymer chains. Upon further exposure to doses exceeding 20 kGy, there is little impact on T_g of R14, R49, R123 and R125 resins. For R33 and R128, the optimum radiation dose seems to be around 40 kGy. This suggests the development of network is essentially ended around 20 kGy to 40 kGy for acrylate based curable resins.

5.1.3 Effect of Diluent and Toughener

IBOA (isobornyl acrylate), GERNOMER 1122 (urethane monoacrylate) and R16 (low viscosity acrylate/methacrylate) were formulated to 3 base resins to adjust the dissipative properties. The effects of the above three components on the variation of the dynamic mechanical properties are displayed in figure 16, 17 and 18.

The E'_{25} values of all formulations are reduced with reference to their base materials, except R14 derivatives. All three additives exert a small extent of stiffening on R14 based formulations with a little increase of E'_{25}. Regarding variation of T_g, IBOA has a slight positive effect on resins with 2°C to 4 °C increment; while GERNOMER 1122 and R16 have a varied negative effect on different base materials.

It is worth noting that E'_{min} of all new formulations is decreased compared to their base resins. The reduced rubbery plateau modulus indicates decreased cross-linking density. The extent of modification on E'_{min} varies with different additives as well as base resins, which can be obviously observed in figure 19. Among the 3 additives, IBOA

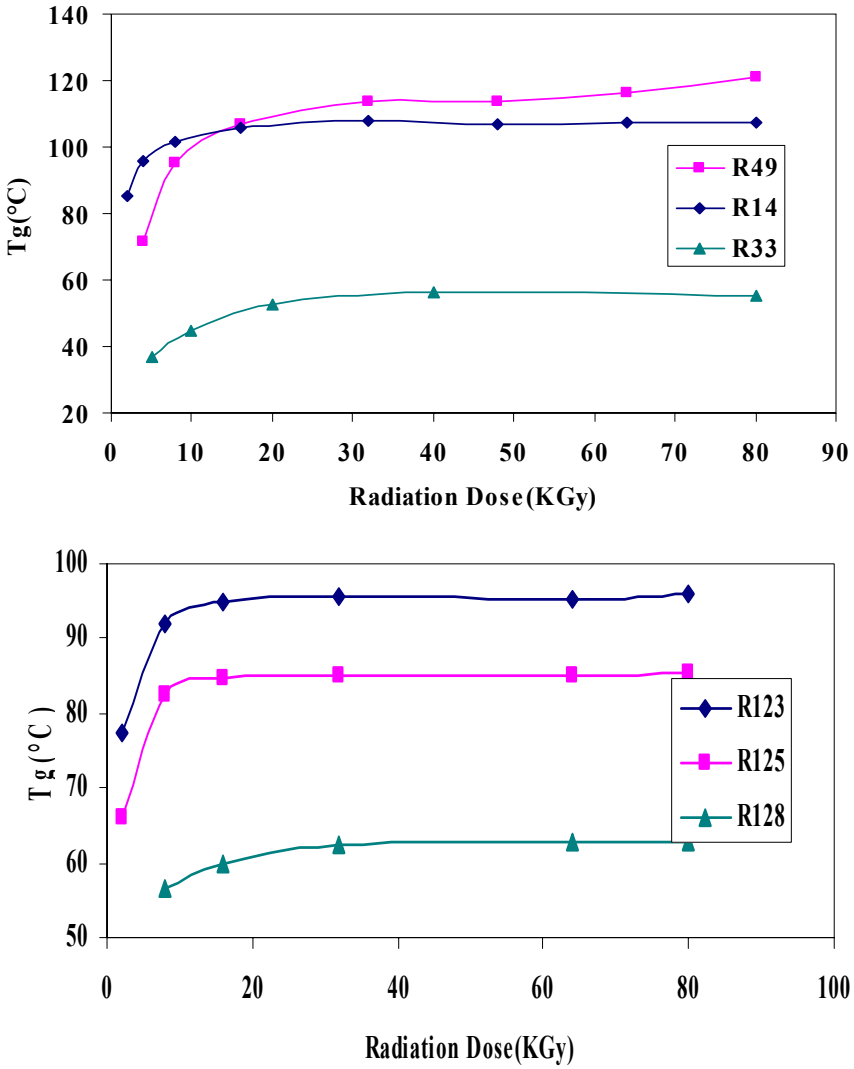

Figure 15. Effect of Radiation Dose on Tg of Base and New Resins.

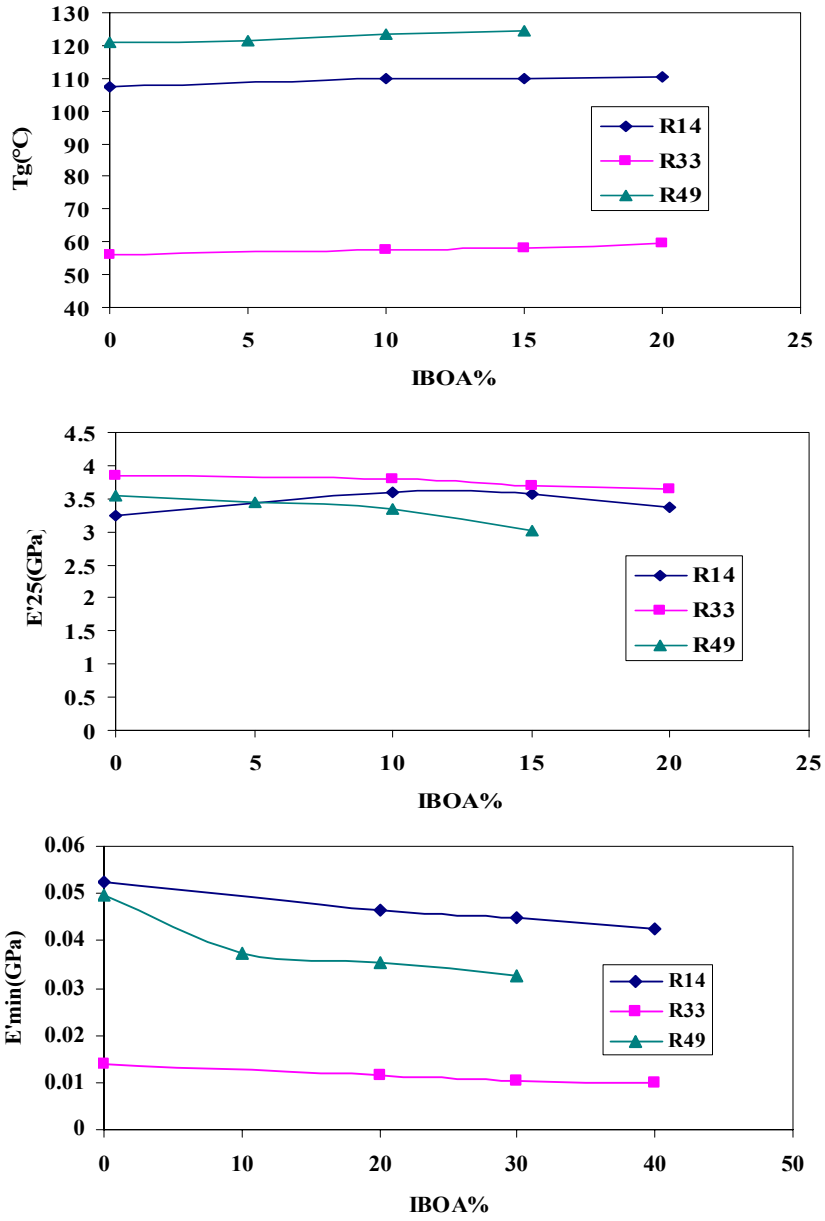

Figure 16. Effect of IBOA on Dynamic Mechanical Properties of Base Resins.

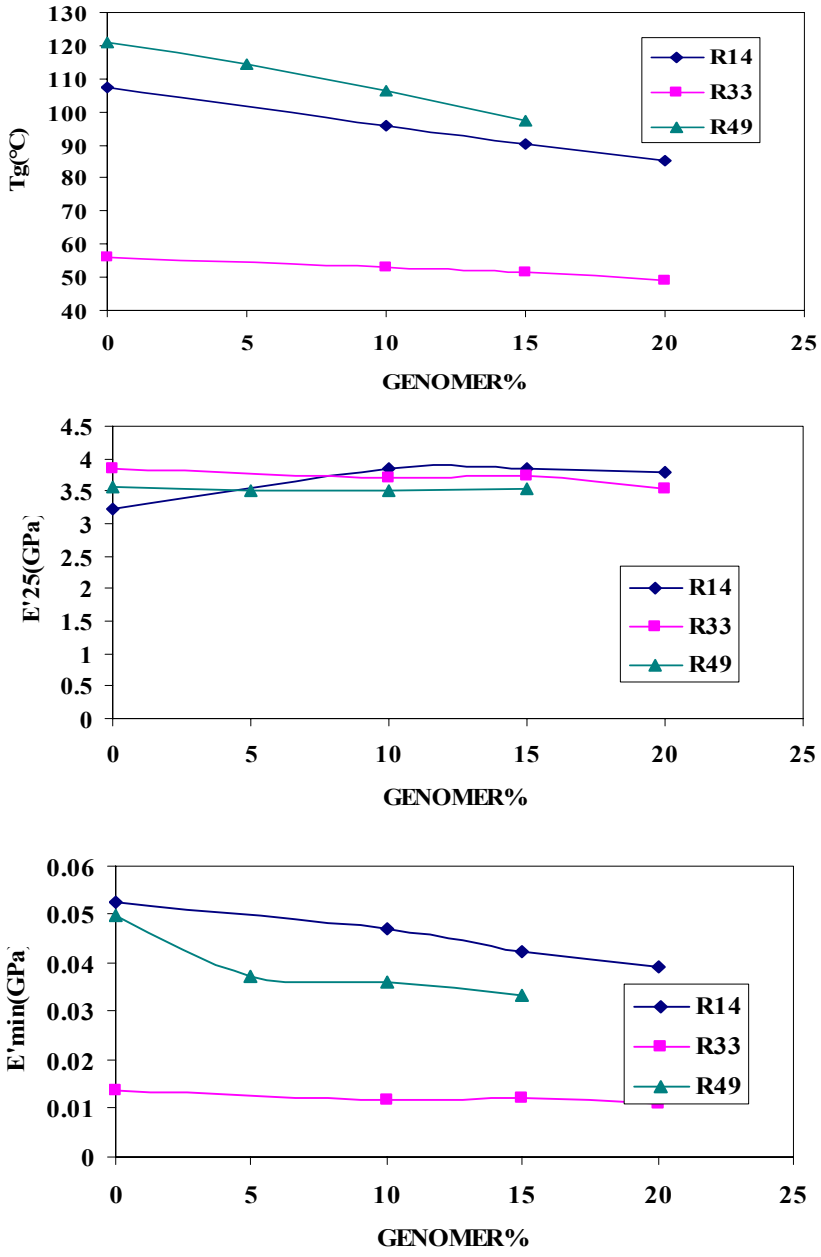

Figure 17. Effect of GENOMER on Dynamic Mechanical Properties of Base Resins.

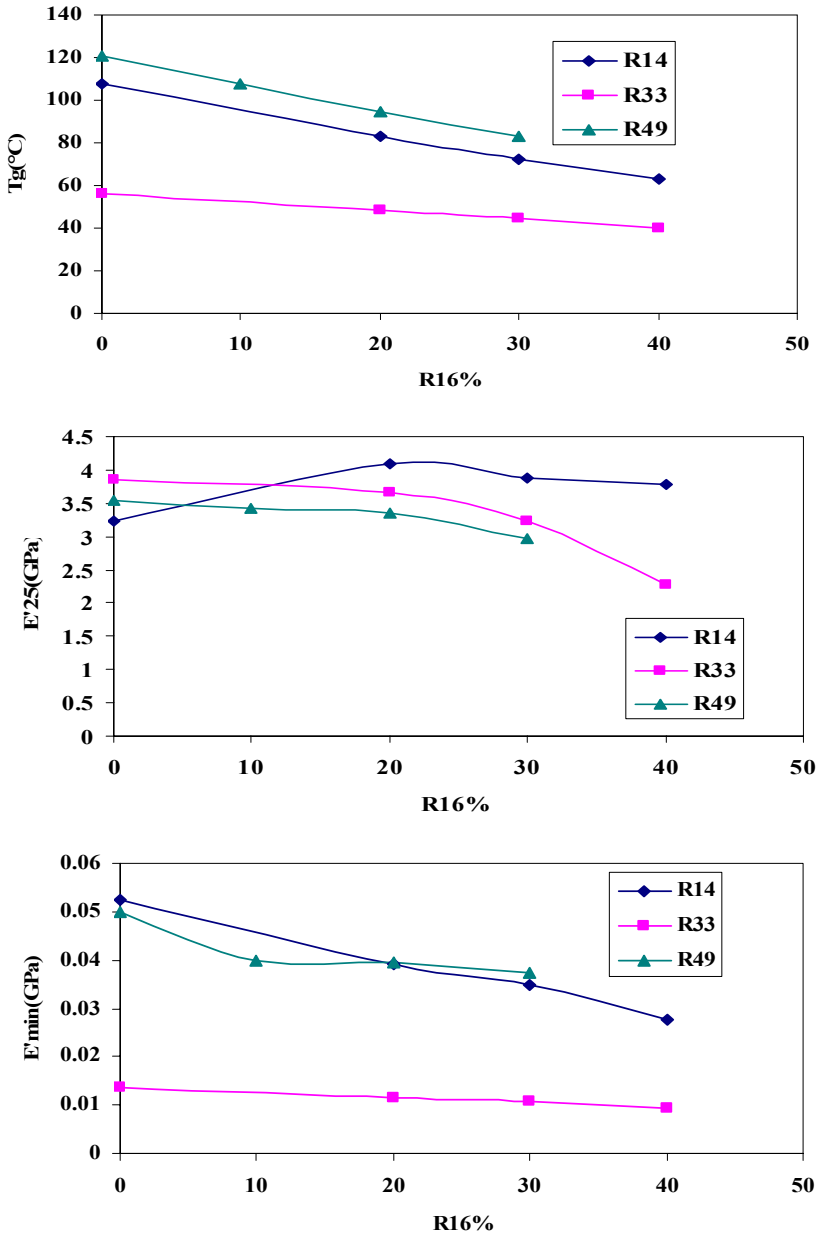

Figure 18. Effect of R16 on Dynamic Mechanical Properties of Base Resins.

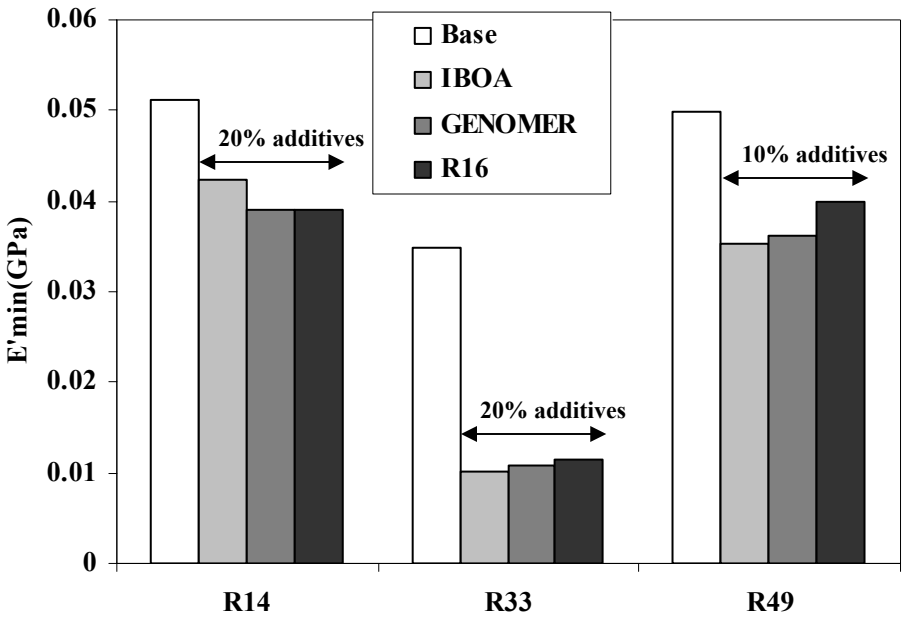

Figure 19. Effect of Additives on E'min of Bases.

works the best with R33 and R49 base resins; whereas it works worst with R14.

Other than E'_{min} and E'_{25} which are studied in detail, considerable attentions should also be addressed to T_g, which is an essential physical property for thermosetting polymers for theoretical and practical reasons. The concept of T_g is a temperature range of polymers transiting from a glass state to a rubbery state. The knowledge of T_g helps understanding the degree of molecules motion, which is an elementary concern in polymer properties and applications.

Polymers with lower T_g values are tougher, more flexibility and impact resistant but accompanied with inferior tensile strength and elastic moduli. Polymers with higher T_g values are stiffer, stronger and more creep resistant but at the expense of increased brittleness. For adhesive practical application, T_g should be above the upper service temperature for good bond performance. Thus, various sealants and adhesives are specially formulated for optimized performance over a particular temperature range.

As T_g affects the polymer end-use temperature, the relationship between T_g and service temperature should always be considered by the formulator along with other physical properties. However, T_g is not an absolute and sole criterion for assessing the suitability of the adhesives.

R33 itself as well as its derivatives has rather low T_g values, compared to other resins. This disadvantage restricts resin further application, although they possess adequate storage moduli at both room temperature and the rubbery plateau temperature. Some techniques that can adjust T_g while maintaining other desirable mechanical properties should be studied in future research. IBOA may be a good example, but the extent of improvement on T_g need to be further enhanced.

5.1.4 Flexural Properties

Physical property testing is a series of important mechanical tests which determines the mechanical response of samples to acting forces under certain loading regimes. All testing methods provide particular information for further resin evaluation, such as shear strength, elastic modulus, and impact resistance. Each testing result is helpful for polymer structure-property understanding.

The cylindrical geometry of our cured resins limits the option of testing methods. After consideration, the three-point bending method was selected and carried out, following procedures B described in the ASTM D790 standard. Flexural strength and the energy to break the specimen, which are the most interested physical properties related to cured resins, were recorded and evaluated. Both flexural properties for new formulations and reference G-2 are listed in table 8.

Flexural stress-strain relation of R14 is plotted in figure 20, and the flexural properties of the R14 derivatives are presented in figure 21. R14 has a rather high deformation up to the fracture point without yielding. With reference to G-2 epoxy, R14 exhibits a higher flexural strength and a lower energy to break. With the addition of diluent and toughener, the flexural strength of all R14 derivatives was lessened to different degree, especially those blended with R16. But the energy to break is significantly improved by R16. R128, which is R14 blended with 40% of R16, shows no break at all. It suggests that dissipative property of R14 is ameliorated with the toughener

R16, but at the expense of the inferior flexural strength. R33 and its derivatives are the most flexible ones which exhibit yield point and very large extension without break. Its stress-strain curve exhibits peculiarity with two yield points, plotted in figure

Table 8. Flexural Properties of Base and Derivative Resins.

Code	Base Resin	Flexural Strength (MPa)	Energy to Break (MJ/m^3)
R14	R14	189	2212
R120		176	1621
R121		175	1940
R122		172	2059
R123		167	980
R124		169	1840
R125		160	2550
R126		159	2623
R127		134	2761
R128		93	No break
R147		192	2492
R33	R33	103	No break
R129		109	
R130		105	
R131		110	
R132		79	
R133		60	
R134		40	
R135		36	
R136		9	
R137		4	
R148		152	
R149		161	
R49	R49	172	2339
R138		159	2233
R139		131	574
R140		146	949
R141		165	1550
R142		132	742
R143		134	1095
R144		149	2336
R145		113	1122
R146		94	923
R150		157	1677
G-2	Reference	124	2410

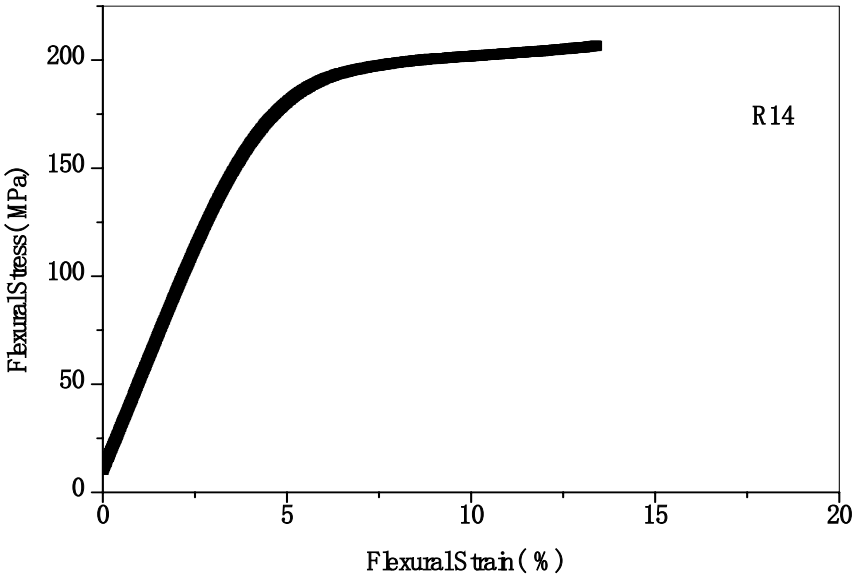

Figure 20. Flexural Stress-Strain Curve of R14.

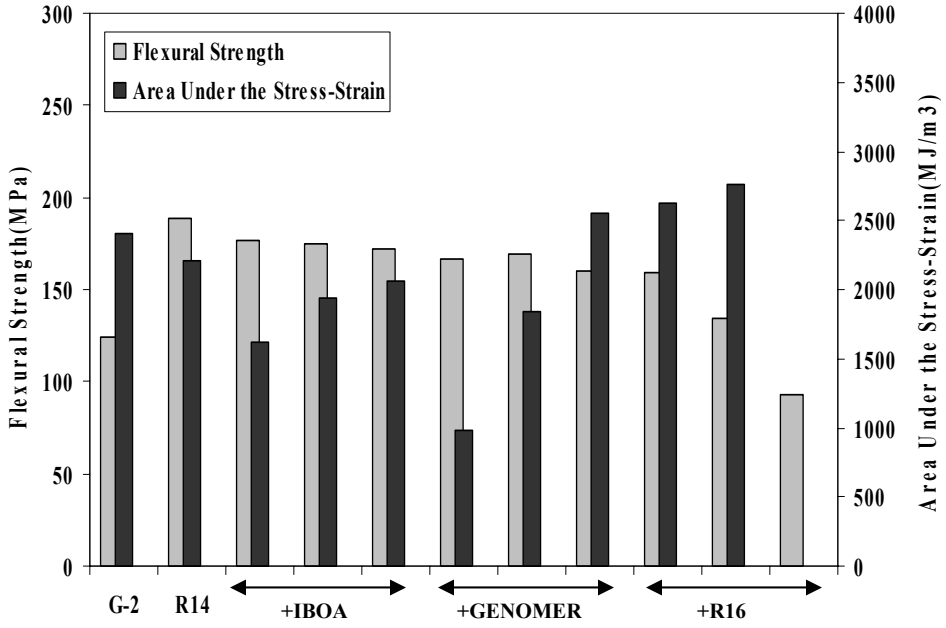

Figure 21.Flexural Properties of R14 Derivatives.

22. No explanation for this behavior is provided for now. In figure 23, R33 exhibits lower flexural strength compared to G-2. The additive effects on the flexural properties of R33 differ from those of R14. IBOA shows positive effect on R33 with slight improvement on flexural strength. GERNOMER and R16 deteriorate flexural strength to a dramatic extent.

Figure 24 recorded the bending test of R49. It deformed to a large extent until break without yielding. In figure 25, R49 displays higher flexural strength and comparable energy to break with reference to G-2. But all 3 additives show negative effect on flexural properties. Especially, the energy to break of R49 derivatives decreases to a low level compared to the base resin (R49).

5.1.5 Cross-linking Density

5.1.5.1 Rubber-Like Elasticity

By introducing cross-linking to molecules, the mechanical behavior of the polymers changes dramatically. The correlation between cross-linking density and viscoelastic behavior has been studied 50 years ago, which is a main aspect of rubber elasticity theory. In the cross-linking progression, the long polymer molecules attach to the cross-linking sites, restrict the degree of motion and lose their identity. At the end of curing, a single giant 3-dimensional network is formed with chains connected to each linked sites can shift to new positions, and the chains between them are somewhat free to adapt new configurations to decrease entropy. Table 9 lists the molecular weight between cross-links of cured resins exposed to 80 kGy, which are calculated to equation 9. Among three base resins, R14 the smallest M_c, while R33 shows the longest M_c values. But G-2 excels all three base materials.

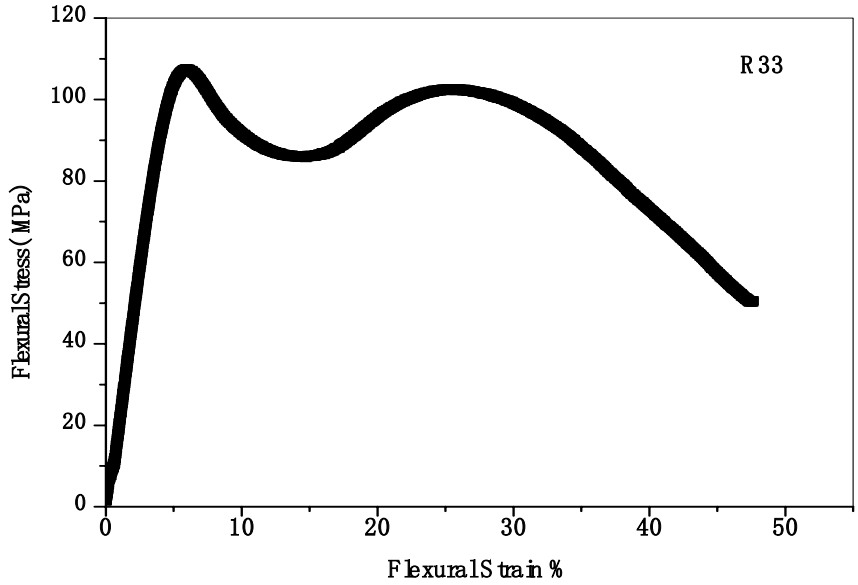

Figure 22. Flexural Stress-Strain Curve of R33.

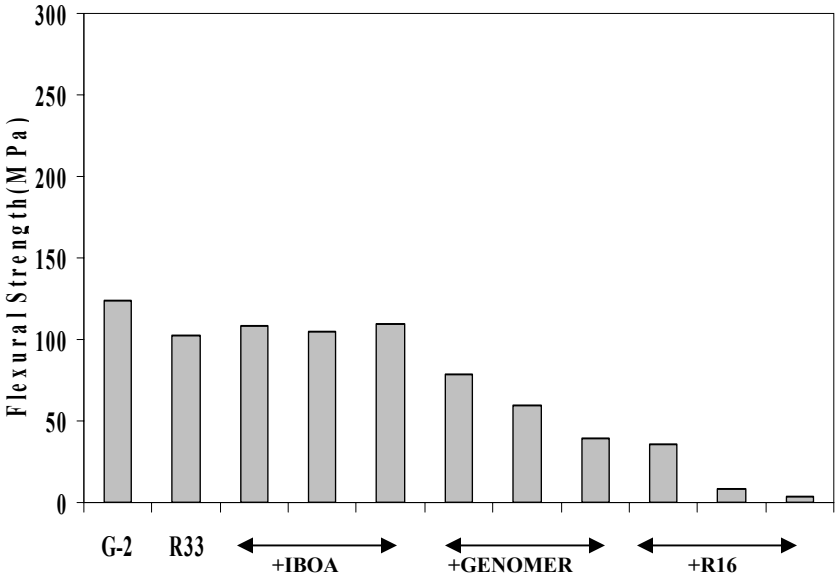

Figure 23. Flexural Properties of R33 Derivatives.

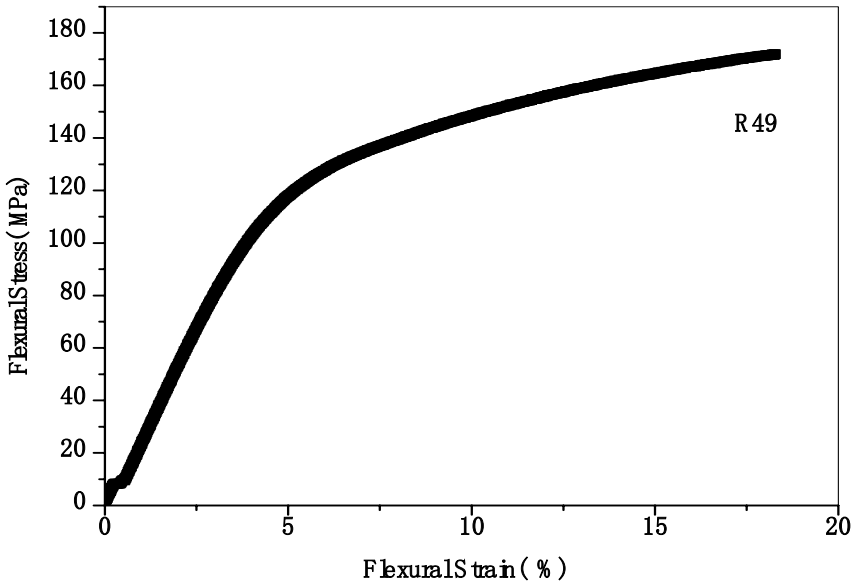

Figure 24. Flexural Stress-Strain Curve of R49.

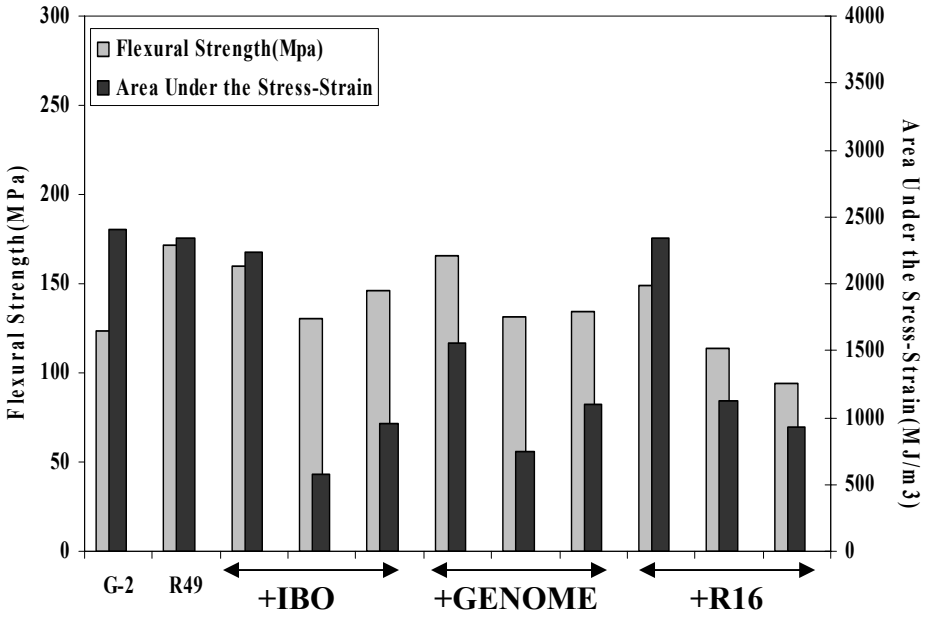

Figure 25. Flexural Properties of R49 Derivatives.

Table 9. Molecular Weight between Cross-Links from DMA Measurement.

Code	Base Resin	M_c (g/mol)
R14	R14	182
R120		220
R121		226
R122		240
R123		208
R124		228
R125		244
R126		244
R127		267
R128		327
R147		335
R33	R33	636
R129		775
R130		847
R131		885
R132		727
R133		724
R134		793
R135		752
R136		797
R137		885
R148		485
R149		484
R49	R49	381
R138		350
R139		369
R140		398
R141		352
R142		358
R143		385
R144		326
R145		323
R146		335
R150		451
G-2	Reference	851

Figure 26 displays the development of molecular weight between cross-links with the evolution of radiation dose for three base resins. It is found that the number average molecular weight is almost unchanged after the exposure level attains 20 kGy for R14 and R49. For R33, this radiation dose needs to be increased to around 40 kGy to obtain considerable molecular weight between cross-links. This behavior indicates that the formation of a giant 3-dimentional network is almost completed after 20 to 40 kGy of electron beam radiation. Again, this result confirms the observations from FTIR spectra and DMA analysis.

To better investigate the effect of diluents and toughener on the variation of molecular weight between cross-links, all data are plotted as bar charts in figure 27. All three additives have a positive effect on R14. The molecular weight between cross-links is stretched out from 200 g/mol to above 300 g/mol, with reference to R14's 182 g/mol. The same active effect of three additives is also observed with R33. The molecular weight between cross-links of R33 derivatives is modified to a range of 720 g/mol to high 800 g/mol, in comparison with 636 g/mol of R33. For R49, all additives show the depressing effect. The number-average molecular weight between cross-links decreases from 381 g/mol (R49) to roughly 320g/mol.

As the molecular weight between cross-links getting larger, the mid-portion of the chains is freer to assume more configurations. This can be related to improved toughness and ameliorated energy dissipation of polymers.

The theory of rubber elasticity is developed from the ideal network with Gaussian distribution of chains. Deviation of the real network from ideal network is always observed due to various network defects, such as hanged chain ends and entanglements.

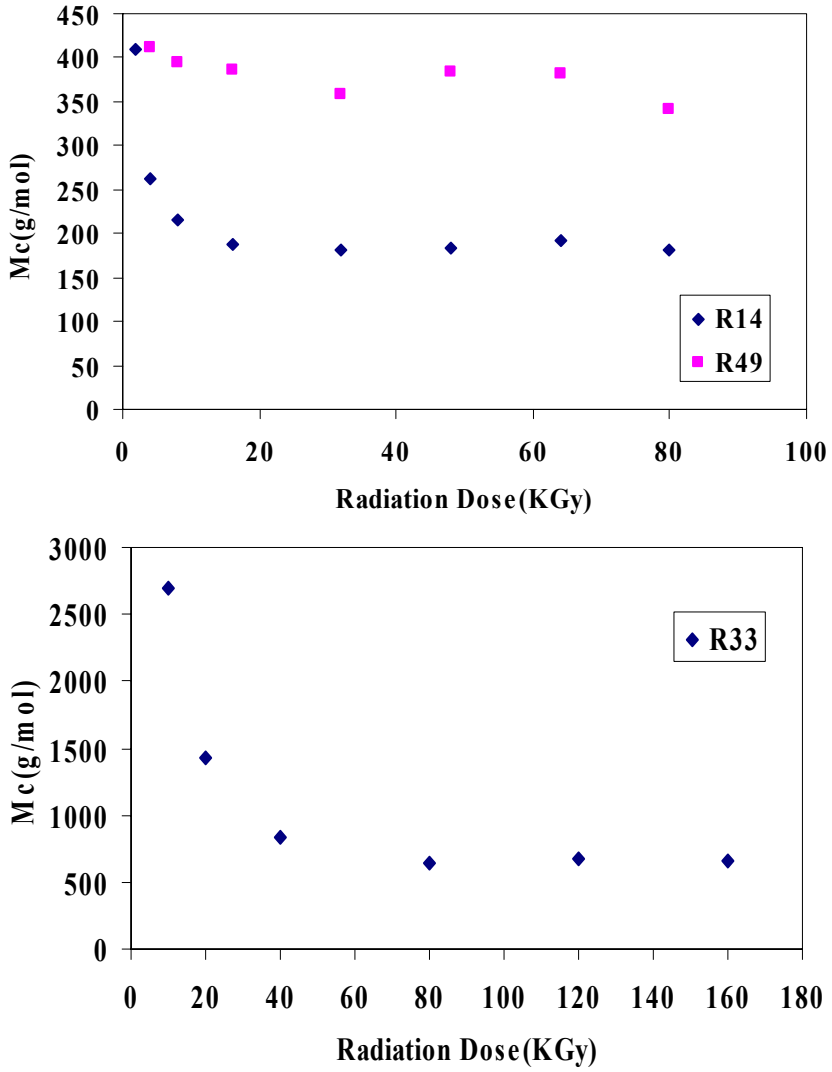

Figure 26. The Variation of Molecular Weight between Cross-Links as a Function of Radiation Dose.

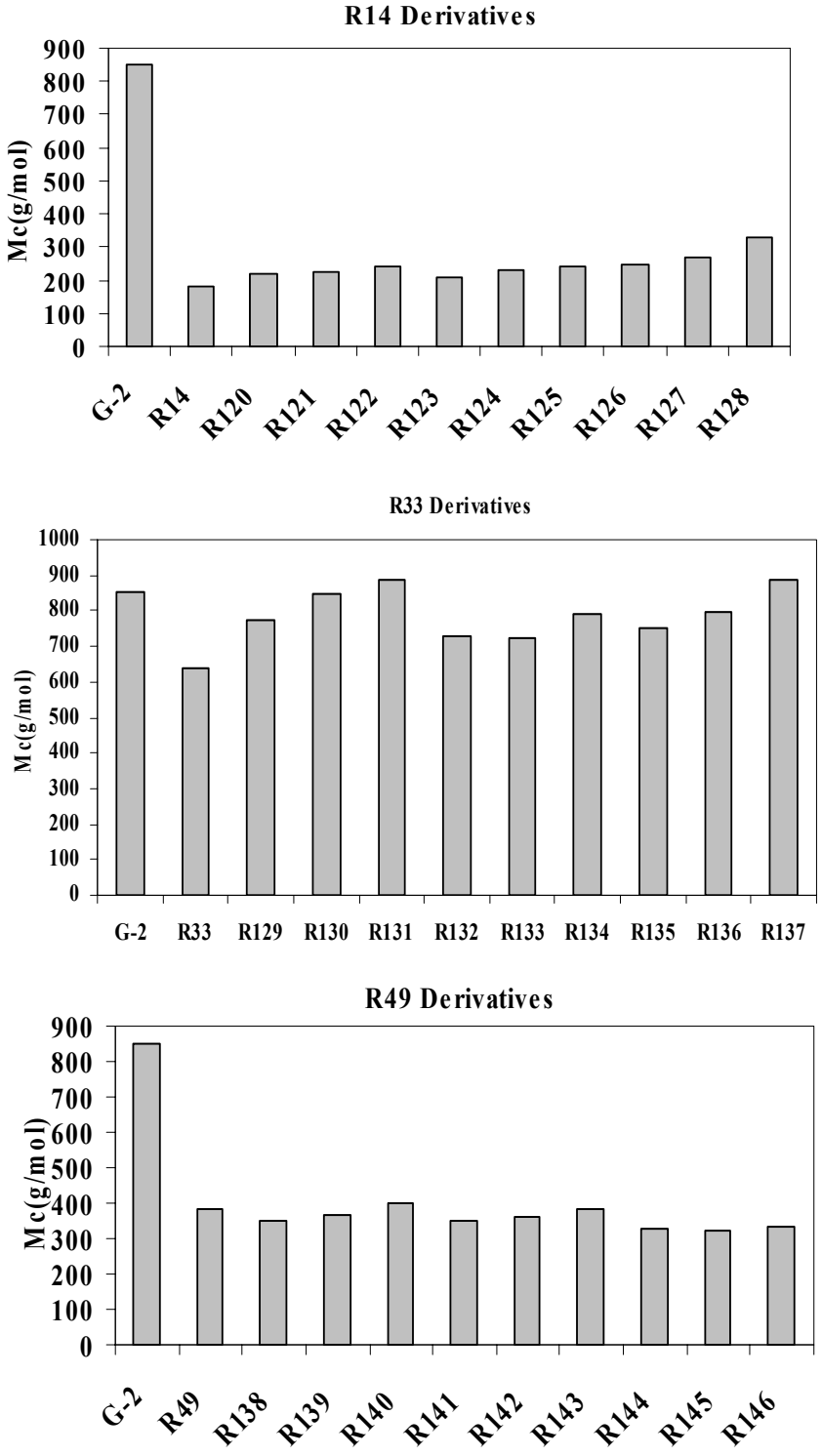

Figure 27. Effect of Additives on the Molecular Weight between Cross-Links.

Problems arise when applying the elasticity equation to the real network without any modification (Zosel, 1980).

5.1.5.2 Swelling Equilibrium

Solvent swelling studies were performed on three base resins with ally alcohol. The sol fraction values of three resins are rather low (table 10), indicating gel contents are high and resins are highly cross-linked. Although it took around 31 days to perform the sol swelling experiment, there was still uncertainty if the swelling equilibrium had been reached.

The highly cross-linked resins and limited surface per sample likely prevented the solvents from penetrating into the network. Thus the swelling equilibrium is difficult to attain and hence seemingly depicted as a lower sol extraction level, as stated in the ASTM D2765 standard. The resins used for solvent swelling were cured at 80 kGy, which means a complete curing was attained as previously analyzed. The tightly bound network rigorously restricts the sol extraction. For better solvent-network interaction, samples are normally made into porous films for swelling studies, widely reported in the literature (Errede, 1986; Liao, 1997). In our study, the preparation of film samples is impracticable because of limitations imposed by the operating conditions. Big pieces of samples cut from the cured rods were employed instead of film samples, which lead to the significantly reduced surface area per sample, and so resulting in an even less extraction level.

Table 10. Results of Solvent Swelling Experiments.

Code	Swelling Ratio	Sol Fraction (%)
R14	1.36	2.34
R33	1.33	6.65
R49	1.26	5.43

5.1.6 Shrinkage

Curing induced material shrinkage is a common phenomenon with various disadvantages. The main reason of shrinkage is the spatial distance reduction among molecules as they connect to each other during the curing process to finally form a single network. Shrinkage can cause a serious problem to adhesive-substrate bonds: voids, residual stress, and poor adhesion. Sometimes, un-neglected volume shrinkage induces significant residual stress which leads to debonding. When the residual stress is not high enough to initiate failure alone, it can precipitate premature cracking during mechanical loading.

The new formulations blended with R16 were not measured due to the remarkable shrinkage observed at the syringe end near the plunger. Therefore isotropic volumetric shrinkage, assumed in the previous shrinkage experiments, does not apply to R16 derivatives.

Figure 28 displays the variation of linear shrinkage with increasing amount of IBOA and GENOMER. Among the three base resins, R14 displays the highest linear shrinkage and R33 shows the lowest. By introducing two monofunctional monomers (IBOA and GENOMER), the shrinkage of R14 and R49 are slightly decreased. But a totally opposite effect is observed with R33, whose shrinkage is apparent.

There are two possible competing factors which lead to the variation of shrinkage. By introducing the liquid monomer with a larger free volume into the oligomer somehow compensates the shrinkage caused by cross-linking. On the other hand, the good affinity of polymer-solvent leads to two types of molecules invading each other's territory. Thus

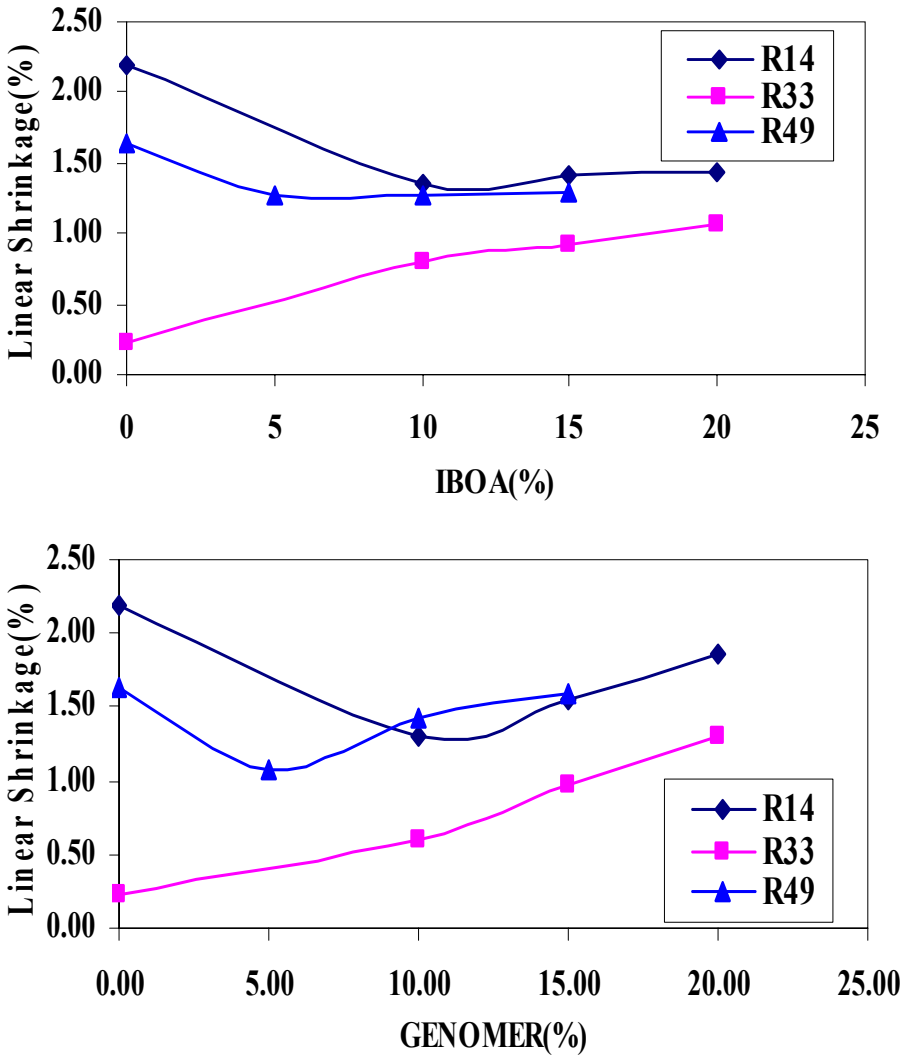

Figure 28. Effect of IBOA and GERNOMER on Shrinkage.

blending is not a simple addition of two components. Indeed, blending leads to the total volume shrink, which attributes to the increased shrinkage level.

A larger residual stress is expected in the thermal curing adhesive system due to the additional internal stress caused by thermal expansion, which is completely avoided in the electron beam curing systems. This internal stress arises from the difference between the thermal expansion coefficients of the adhesive and the substrate (Petrie, 2000). When these two coefficients are not comparable and the curing temperature is much higher than the service temperature, the substantial stress resulted can easily cause failure or premature crack.

5.2 Potential Resin-Wood Bonds

Evaluation of resin-maple bonds was continued. The resin selection was based on viscosity, one of the most important working properties. For each base-additive pair, one formulation was selected based on the minimum viscosity, for subsequent wood bonding. All resin-maple blocks were prepared as the same manner as previous sets, with 68 g/m^2 resin loading rate, 80 kGy curing and subsequent testing in accordance with the ASTM D905. One different procedure in this set was using an air torque wrench instead of manual wrench to tight the bolts for holding two panels together. The improved uniformity and higher pressure were intended to ensure better resin-wood good contact. G-2 epoxy was also included in the bonds preparation and shear testing as a reference. Estimation of percentage wood failure in the tested joints was performed in accordance with the ASTM D5266.

5.2.1 Shear Properties of Selected Resin-Maple Bonds

The shear stress at failure as well as the average wood failure is listed in table 11 and also plotted in figure 29 for better comparison. The standard deviation seems to be unfavorably large due to the limited number (8) of bonded specimens tested for each selected resin. The ASTM D905 standard requires at least 20 specimens in 4 joints to be tested. This requirement is impractical in the study because of the limited available quantity of resins and maple panels.

The shear test results of the 12 resins selected in Set L show a better consistency, compared to Set G and Set J. All but one (R140) of the resin-maple bonds exhibit shear strength higher than 6.9 MPa (1000 psi). On the other hand, 8 out of 16 resin-maple bonds in Set G and 2 out of 8 resin-maple bonds in Set J exhibit shear strength at failure beyond 6.9 MPa (1000 psi). An even more significant improvement is the presence of wood failure in 10 out of 12 resin-wood bonds, which was not observed in the former sets. Two resin-maple bonds, made with R128 and R134, show deep wood failure in joints while the other 8 resins displaying a shallow wood failure. Nevertheless, when averaged by 8 specimens, the average wood failure appears disappointingly low. The visual evidence of a deep wood failure is displayed in figure 30 for R128 and R134, in comparison with no wood failure for R122 and a fair wood failure for G-2 in figure 31.

5.2.1.1 Correlation with Resin Dynamic Mechanical Properties

From the dynamic mechanical data of 12 maple bonded candidates, storage moduli at room temperature are considerably consistent in a medium range between 3.9139 GPa and 2.2743 GPa. Conversely, E'_{25} values of Sets G and J distribute broadly from 5.9869 GPa to 1.2367 GPa. The rubber plateau moduli of the new formulations

Table 11. Shear Strength and Wood Failure of Set L.

Code	Shear Stress at Failure		Percentage Wood Failure	
	Failing Stress (MPa)	STDEV	Wood Failure (%)	STDEV
R122	8.64	3.30	0	0
R125	10.7	1.96	0	0
R128	11.1	2.24	5.63	9.36
R131	12.0	2.69	0.130	0.350
R134	13.1	2.68	3.63	5.71
R137	11.1	1.10	0.630	0.920
R140	4.73	2.62	0.500	0.760
R143	6.95	3.59	0.250	0.460
R146	10.6	3.38	0.880	1.36
R147	11.3	3.00	0.380	0.740
R148	10.8	4.86	0.500	0.760
R150	8.99	3.07	0.250	0.460
G-2	19.0	1.88	38.8	17.50

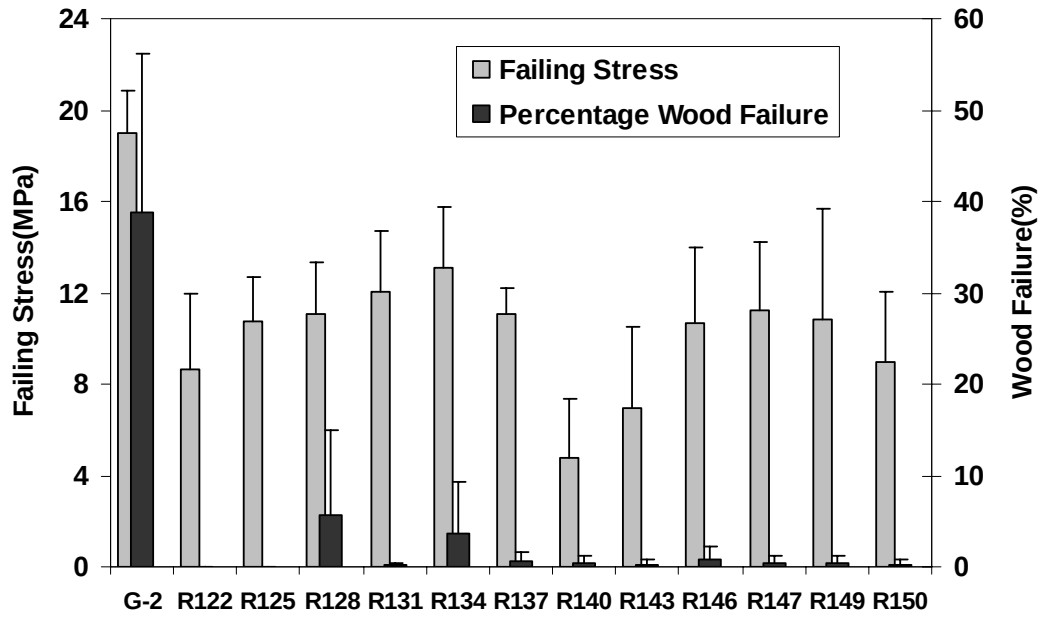

Figure 29. Shear Test Results of Set L.

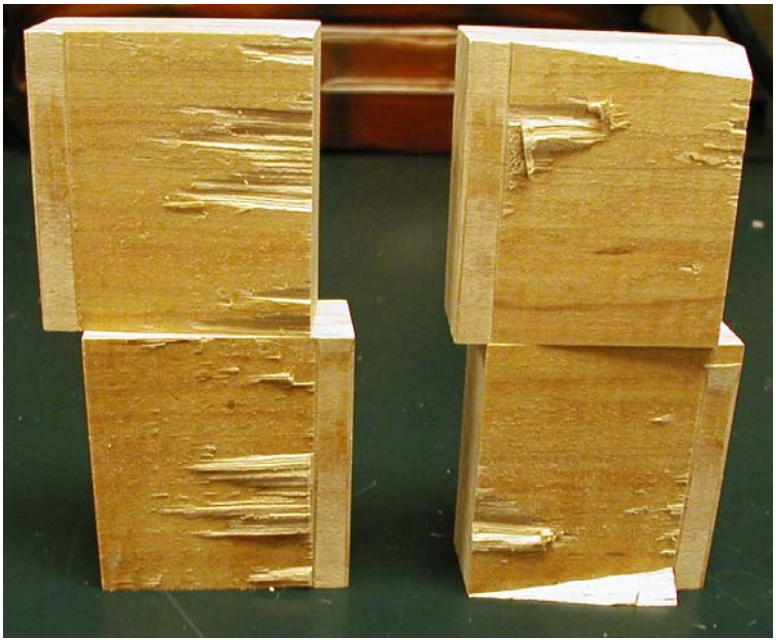

R128

R134

Figure 30. Deep Wood Failure of R128 and R134.

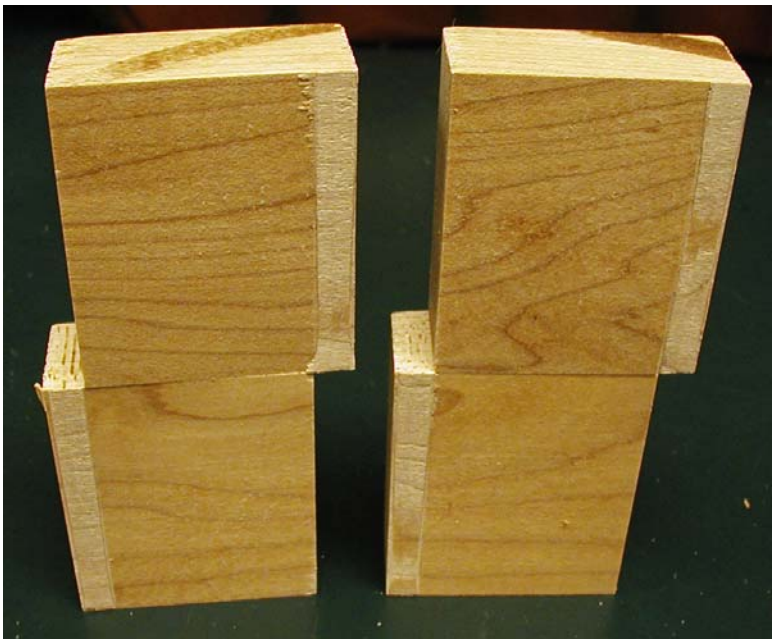

R122

G-2

Figure 31. No Wood Failure and Fair Wood Failure.

are reduced as intended to be. Their values distribute in a lower and more concentrated region from 0.0424 GPa to 0.0095 GPa. On the other hand, E'_{min} values of Sets G and J scatter widely from 4.6547 GPa to 0.0384 GPa. This observation shows that the consistency of dynamic mechanical properties is agreeable with the steady shear behavior of resin-maple bonds.

Table 12 lists the dynamic mechanical properties as well as the shear test results of the resin-wood bond. Due to the narrow distribution of E'_{25} and E'_{min}, the trend of failing stress with the changes in rubbery plateau modulus is not as clear as the tendency detected in the preliminary screening tests. However, with careful inspection, the same trend can be observed in the same chemical family (the same base resin): high shear strength appears to associate with low E'_{min} and large value of E'_{25}/ E'_{min}.

R128 (R14 blended with R16), which shows deep wood failure in the wood joints, has the lowest E'_{min} and largest E'_{25}/ E'_{min} among the R14 based candidates. This finding agrees with the initial formulation objectives: improve bonds behavior by amplifying resin dissipative property. Of peculiarity is R134, which shows deep wood failure, though it has the highest E'_{min} with the second large E'_{25}/ E'_{min} among the R33-based resins. This phenomenon can be explained with the fact that, R33 possesses rather low E'_{min}, while introducing additives induce small changes to the E'_{min} values for all R33 derivatives.

Based on the discussion above, other issues should be taken into account to clarify the differences of resin-wood bond behavior. E'_{min} of R49 is reduced to some degree by blending with diluents and toughener. But compared to R14, R33 and G-2, the E'_{min} values of R49-based formulations are still high. So no improvement was found for wood bonding using R49 candidates because of no significant improvement on toughness.

Table 12. Dynamic Mechanical Properties of Resins in Shear Tests (Set L).

Code	Base Resin	Failing Stress (MPa)	E'_{25}(GPa)	E'_{min}(GPa)	E'_{25}/ E'_{min}
LMR122	R14	8.64	3.38	0.0424	80
LMR125		10.7	3.79	0.0391	97
LMR128		11.1	3.78	0.0278	136
LMR147		11.3	3.91	0.0491	80
LMR131	R33	12.0	3.64	0.0101	360
LMR134		13.1	3.53	0.0109	324
LMR137		11.1	2.27	0.00950	239
LMR149		10.8	3.82	0.0200	197
LMR140	R49	4.73	3.02	0.0327	92
LMR143		6.95	3.54	0.0334	106
LMR146		10.6	2.96	0.0372	80
LMR150		8.99	3.58	0.0288	133

5.2.1.2 Correlation with Flexural Properties

The flexural properties of pure resins are a mechanical behavior controlled by the resin chemical structure. This mechanical behavior is also one of the main factors affecting adhesive bond performance. The correlation of the resin flexural properties with the resin-wood bond properties is studied by listing shear strength at failure as well as flexural properties of pure resins (table 13).

There is no clear relationship between shear stress of bonds and flexural strength of resins. One resin-maple bond with the best shear performance has a moderate resin flexural strength. Several other bonds that have a similar magnitude of failing stress, display a wide range of flexural strength from 50 MPa up to 200 MPa. High flexural strength of resins dose not ensure a decent resin-wood bond behavior. Hence, the resin flexural strength is not a dominant factor affecting the bond performance.

The effect of the flexural energy on the shear test of resin-maple bonds is clearer than that for the flexural strength. With the increasing magnitude of the flexural energy, there is more probability of high resin-wood failing stress. Although the exact relationship is uncertain, it is reasonable that a higher energy is beneficial to resin bonds. Again this observation is in agreement with the conclusion drawn at the preliminary screening stage: improve bond performance by increasing dissipative properties of resin system.

R128 is the most flexible resin among the R14-based resins with no break during the 3-point bending test. The deep wood failure and high failing stress of R128 can be attributed to its significant energy dissipation. R134, which derives from R33 with ductile behavior (no break), also results in a deep wood failure and moderate failing stress.

Table 13. Flexural Properties of Resins in Shear Tests (Set L).

Code	Base Resin	Failing Stress (MPa)	Flexural Strength (MPa)	Flexural Energy (MJ/m^3)
LMR122	R14	8.64	172	2059
LMR125		10.7	160	2550
LMR128		11.1	93	No break
LMR147		11.3	192	2492
LMR131	R33	12.0	110	No break
LMR134		13.1	40	
LMR137		11.1	4	
LMR149		10.8	161	
LMR140	R49	4.73	146	949
LMR143		6.95	134	1095
LMR146		10.6	94	923
LMR150		8.99	157	1677

R49 derivatives with both inferior flexural strength and break energy did not provide satisfactory bonding test results. Once again, this behavior suggests that the flexure break energy is more important than flexural strength in affecting resin-wood bond shear behavior.

5.2.1.3 Correlation with Molecular Weight between Cross-links

The above study shows the important role of energy dissipation to the mechanical performance of the resin-wood bonds. The molecular weight between cross-links can also be an index of dissipate property, in the perspective of the polymer network. A longer chain between the cross-links means more configurations can be adopted. Thus the energy dissipation (or say toughness) of the network improves.

Table 14 lists the bonds shear stress and molecular weight between cross-links (M_c). Thus the same tendency is observed: the bigger molecular weight between cross-links is beneficial to the shear performance of resin-wood bonds.

Table 14 shows R128 has the longest chain length between cross-links among the R14-based resins. Once again, it explains its superior bond behavior. With the presence of additives, the M_c value of R49 derivatives is reduced to a lower level compared to the base R49. Thus no favorable resin-wood bond behavior was observed in R49-based formulations because of no improved property of energy dissipation (or toughness).

5.2.2 Wetting

The role of an adhesive is to connect two substrates together, thus the adhesive must first be able to "wet" the surface. The "wetting" here means that adhesives are able to spread well upon the surface and have an intimate contact with it (Blomquist, 1981). In

Table 14. Mc Values of Resin Candidates in Shear Tests (Set L).

Code	Base Resin	Failing Stress (MPa)	Wood Failure (%)	M_c (g/mol)
LMR122	R14	8.64	0	240
LMR125		10.7	0	244
LMR128		11.1	5.63	327
LMR147		11.3	0.38	335
LMR131	R33	12.0	0.13	885
LMR134		13.1	3.63	793
LMR137		11.1	0.63	885
LMR149		10.8	0.5	484
LMR140	R49	4.73	0.5	398
LMR143		6.95	0.25	385
LMR146		10.6	0.88	335
LMR150		8.99	0.25	451

the liquid state, the adhesive can flow into small crevices caused by substrate roughness, and must be able to displace air, dirt, oil and various impurities to prevent the formation of a weak boundary layer.

The wetting function can be roughly classified into two actions: a free spreading of adhesives on the substrate surface and a penetration of liquid resin into the surface crevices or pores which are the remarkable characteristic of wood substrate (Petrie, 2000). The first activity is greatly dependant on the surface tension of both adhesives and substrates. The second activity is closely related to the viscosity of the resin and its working life.

5.2.2.1 Contact Angle

The wetting tendency of resin to the wood surface can be measured by the contact angle between them at equilibrium as indicated by Young's equation (Petrie, 2000):

$$\gamma_{LS} \cos\theta = \gamma_S - \gamma_L \tag{10}$$

where γ_{LS} is the surface tension of the liquid-solid interface, γ_S is the surface tension of the solid, γ_L is the surface tension of the liquid and θ is the contact angle of the liquid against solid surface.

When $\theta = 0°$, the liquid spontaneously spreads over the surface, which is referred to complete wetting. Wetting is favored when cosine $\theta \geq 1$, namely

$$\gamma_S \geq \gamma_L + \gamma_{LS} \tag{11}$$

When the surface tension of the liquid is low, while the surface tension of the substrate surface is high, wetting occurs spontaneously. This explains why polyolefin materials can hardly be wet due to its low surface tension, while metal surfaces and

ceramic surfaces are ready to wet because of their high surface tension. The rule of thumb for good wetting to occur is:

$$\gamma_{adhesive} \prec\prec \gamma_{c-substrate} \tag{12}$$

where $\gamma_{c\text{-substrate}}$ is critical surface tension of the substrate. This concept was proposed by Zisman and is used elsewhere as an important concept of wetting (Petrie, 2000).

The surface tension of the 12 liquid resins were measured using the Wilhelmy method. The results are listed in table 15. The surface tension of all resins ranges from 33 dyne/cm to 48 dyne/cm, roughly the same magnitude of the maple's critical surface tension (46.8 dyne/cm; Gardner, 1996). Thus the wetting degree can not be easily assessed based on the above rule of thumb (equation 12).

Measuring the contact angle might be a more direct approach for determining wetting degree (Blomquist, 1981). The results in table 15 show that the contact angle values vary between 84° to 99° for the different resins against the surface of maple. The contact angle is linear by related to the resin surface tension, as plotted in figure 32. The tendency shows that the lower the resin surface tension, the smaller the contact angle.

Table 16 lists the shear strength of resin-maple bonds as well as contact angle measurement. The resin-wood bonds with best shear performance show the largest contact angles. This is contradictory to the thought. Generally, a small contact angle value means an increased contact area between the adhesive and substrate where the adhesion force is acting. A better spreading of resins over the surface is anticipated. Thus the mechanical performance of bonded joints should be improved. The opposite result indicates that spreading is only one aspect of adhesive wetting characteristics. Other information, such as viscosity, should also be considered together with spreading.

Table 15. Surface Properties of Candidate Resins.

Code	Surface Tension (dyne/cm)	Contact Angle (°)
R122	34	86
R125	33	84
R128	39	88
R131	36	88
R134	48	100
R137	33	85
R140	35	88
R143	38	88
R146	33	85
R147	35	86
R148	45	93
R150	41	90
PVAC	42	92

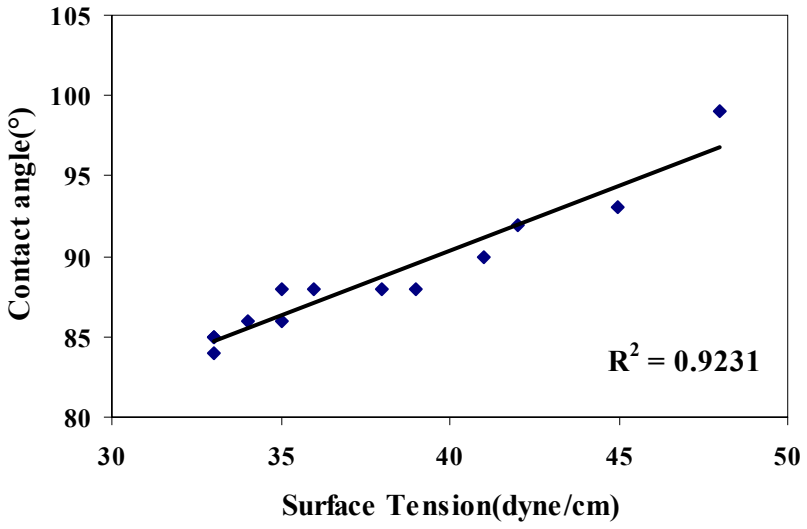

Figure 32. The Relationship between Contact Angle and Surface Tension.

.

Table 16. Contact Angle of Resin Candidates against Maple.

Code	Base Resin	Failing Stress (MPa)	Wood Failure (%)	Contact Angle (°)
LMR122	R14	8.64	0	86
LMR125		10.7	0	84
LMR128		11.1	5.63	88
LMR147		11.3	0.38	86
LMR131	R33	12.0	0.13	88
LMR134		13.1	3.63	100
LMR137		11.1	0.63	85
LMR149		10.8	0.5	93
LMR140	R49	4.73	0.5	88
LMR143		6.95	0.25	88
LMR146		10.6	0.88	85
LMR150		8.99	0.25	90

5.2.2.2 Viscosity

Adhesive viscosity is an essential working property which gives information on how easily the material can be pumped, mixed and spread. By relatively easy viscosity measurements, the change of product composition or quality can be noticed.

The viscosity measurement of Set L resins was carried out at 25°C and recorded in table 17. Each base resin was diluted to some extent by monofunctional monomers and toughener.

The real surface is not perfectly smooth or flat. Crevice, voids and valley caused by the surface roughness of solid substrate prevent adhesive film formation and also affect joint performance. The low viscous resin can flow into voids and displace impurities more easily. For resins that cure rapidly, there is time for competition between the adhesive gap-filling and solidification. Inferior adhesive bonds may be produced because of inadequate contact area between the adhesive and substrate due to insufficient time for the resin to fill in the crevice and displace impurities. This aspect favors for the electron beam curing adhesive where heat is not involved. Unless subject to the high energy radiation, no polymerization occurs. Therefore, a sufficient time is assured for resin gap-filling and spreading.

The situation becomes more complicated when wood is used as a substrate. Wood is a porous, rough, textural and chemical heterogeneous material with great variability, compared to metal or plastic. Even from the same tree, pieces of wood present various composition and properties. Environment surrounding, cutting and storing life are all pertinent to the wood property variation.

Table 17. Viscosity of New Formulations.

Code	Viscosity (cP)
R120	45403
R121	23972
R122	13573
R123	44609
R124	25242
R125	15558
R126	83662
R127	58103
R128	43339
R129	255000
R130	110000
R131	54769
R132	219000
R133	95725
R134	43339
R135	497000
R136	282000
R137	163000
R138	111000
R139	38100
R140	23813
R141	61120
R142	35560
R143	20320
R144	77630
R145	54769
R146	39688
R147	7104
R148	34925
R149	10160
R150	24103
G-2	8271
PVAC	12541

Moisture content, which is an important property affecting both the bulk properties and bondline properties, was carefully monitored in the bonding process. For every set of maple blocks in the tests, moisture content was measured and calculated according to ASTM D4442. The moisture content of all but one set of maple blocks is 7%. Set G is about 5%. The explanation for this particular set is that the panels were oven heated for application of the highly viscous Set G resins.

Porosity is another critical property of wood species. Other than crevice or valley caused by surface roughness, there are considerable pores existing in wood, which greatly influence adhesive penetration. The uneven porosity distribution in different surfaces, such as cross section, tangential surface or surface in latewood or earlywood, complicates our bondline study. Different penetration paths are possible even on the same surface due to the different fiber or trachea concentration in different regions of wood, thus permeability varies dramatically. Generally, resins with small molecular size are easier to penetrate on a clean wood surface of the same substrate.

FTIR imaging is a handy tool for bondline study which is capable of delineating different components of the sample. IR spectra of candidate resins and maple were acquired in advance to detect the difference in absorption bands between maple and resins. The absorption at 1424 cm^{-1} is used to assess all bondline study. This absorption peak, related to C-H deformation with aromatic ring stretching, can clearly distinguish maple and resins. Maple has an obvious absorption at this wave number due to lignin, while all resins are short of this peak because of no aromatic functions in the formulation. Although the family name of R49 is aromatic acid methacrylate half ester, there is no aromatic absorption in the R49 spectra. In IR image, different colors mean different

levels of absorption. Red represents the highest absorption and blue represents the weakest absorption. Thus maple is imaged as red in IR image due to strong absorption; glueline is seen as blue color due to sparse absorption at this wave number.

Figure 33 shows an IR image of bondline made with R14 and figure 34 shows the bondline made with R49. These bonds were grouped under Set G and their IR images were not compared to those of Set L. Maple bonds in Set G were bolted by a manual wrench, therefore resulting in a bondline width that is possibly uneven compared to the samples in Set L, which was assembled by a torque air wrench. To minimize the variability, only bonded joints made with new formations in Set L were compared.

The width of the blue absorption in IR image, which signifies the depth of penetration of the resin to both sides of substrates plus the glueline thickness, was measured. This expression is named as the "width of interphase" in the subsequent study. Three images from different locations of the bondline were collected for each resin. The interphase width was measured five times along the glueline for one image and then averaged for three images. This measurement is only for comparison study. Due to the wood variability, an absolute quantitative analysis seems impossible.

As previously stated, a less viscous resin, which usually means a smaller molecular size, is able to penetrate more deeply in substrate than the viscous formulations. This trend can be observed in figure 35, 36 and 37, which respectively correspond to R14 derivatives, R33 derivatives and R49 derivatives. Figure 38 plots the interphase width as a function of the resin viscosity. The width of interphase increases greatly as the viscosity drops. It indicates that the penetration depth increases as the viscosity decreases with the assumption of an equal glueline thickness.

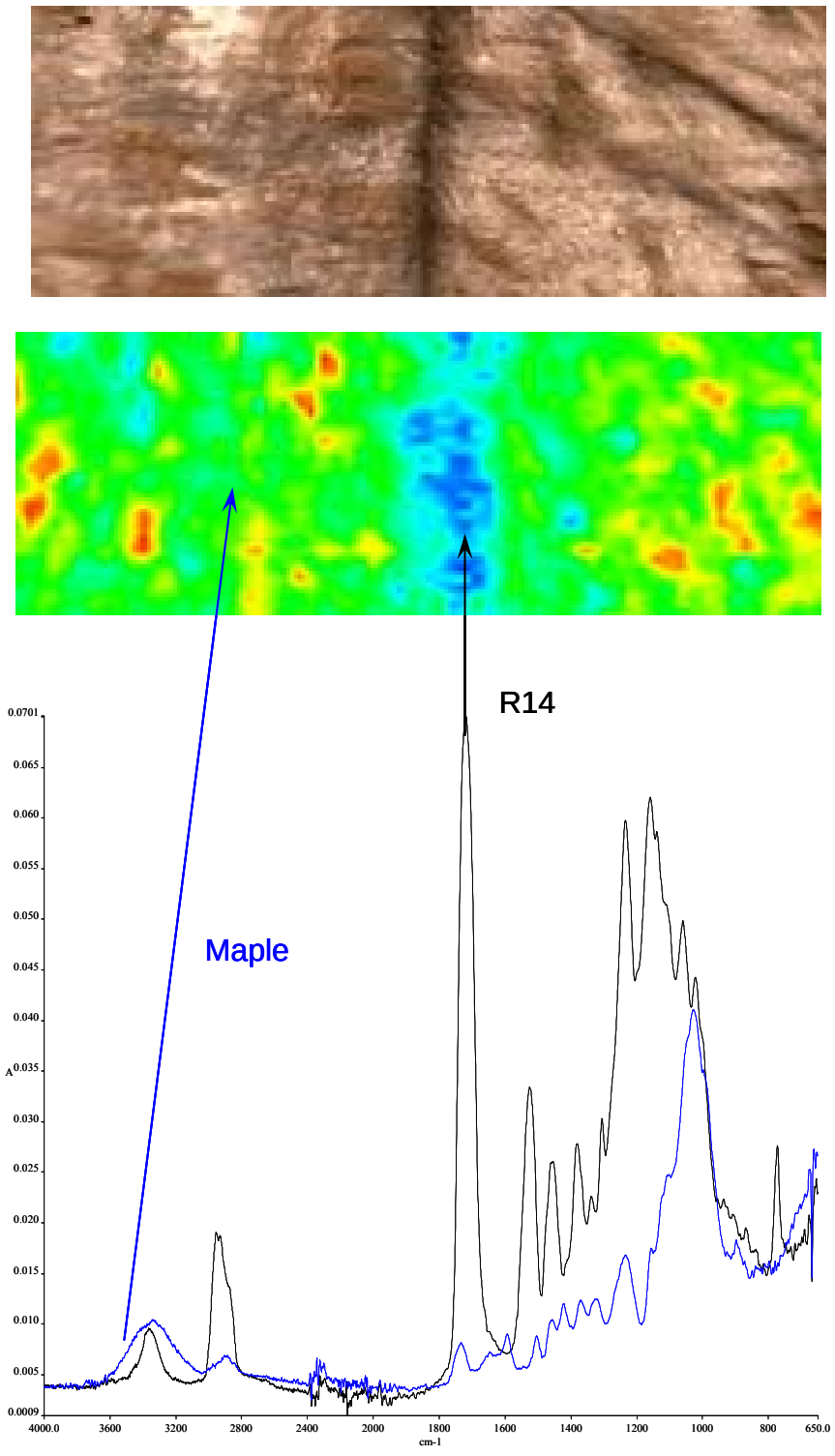

Figure 33. IR Image of Bondline Made with R14.

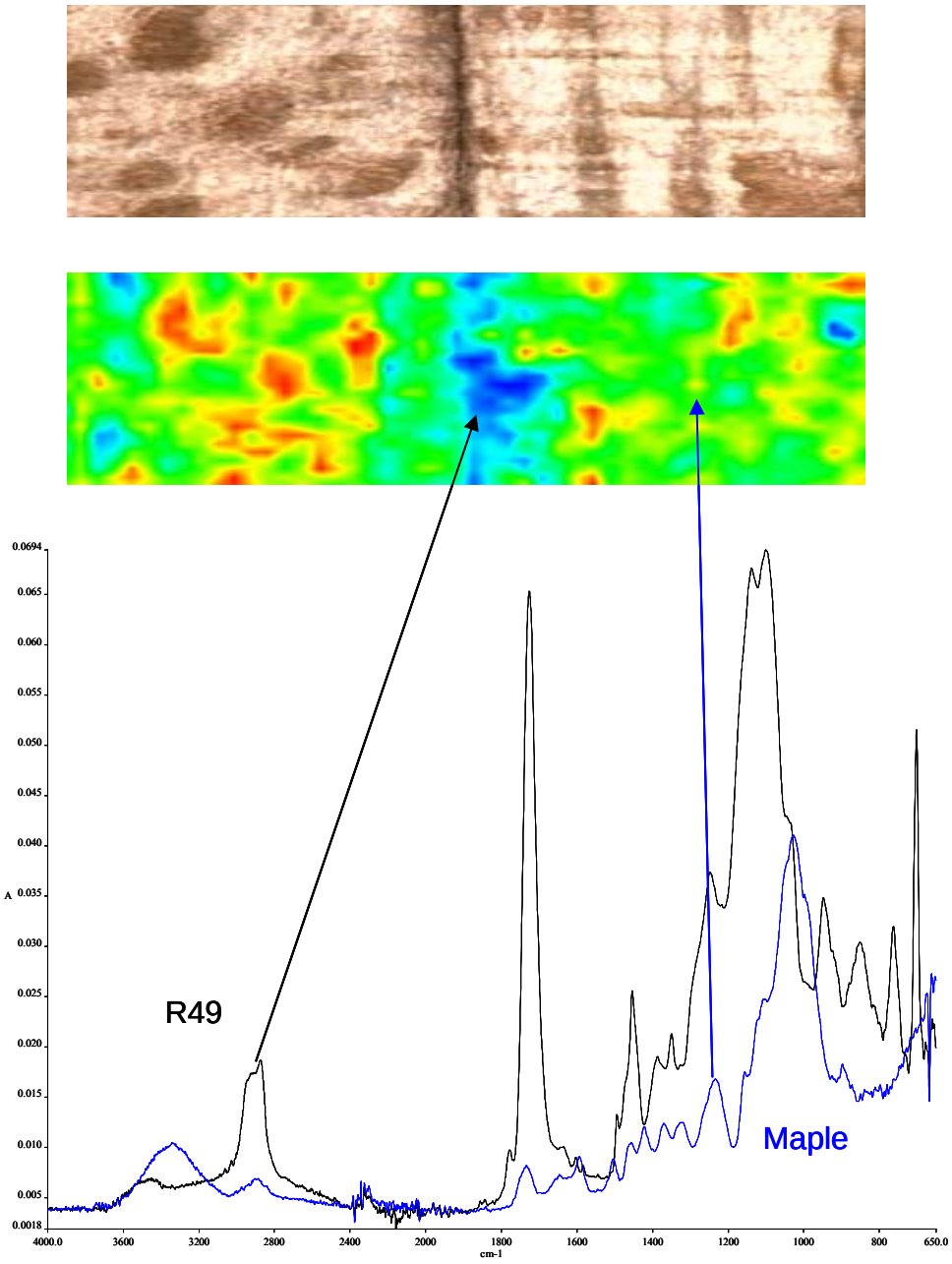

Figure 34. IR Image of Bondline Made with R49.

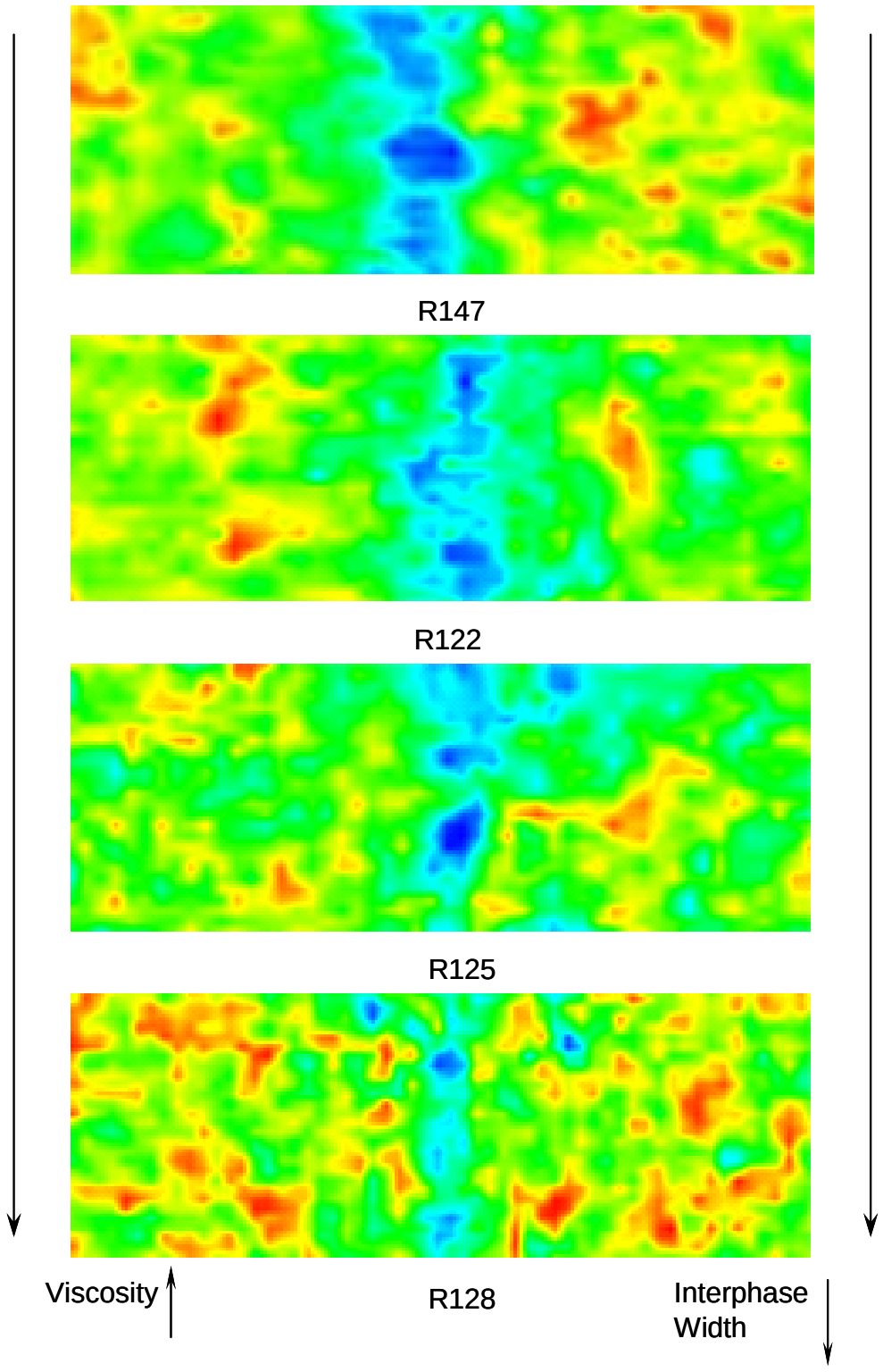

Figure 35. IR Image of Bondline Made with R14 Derivatives.

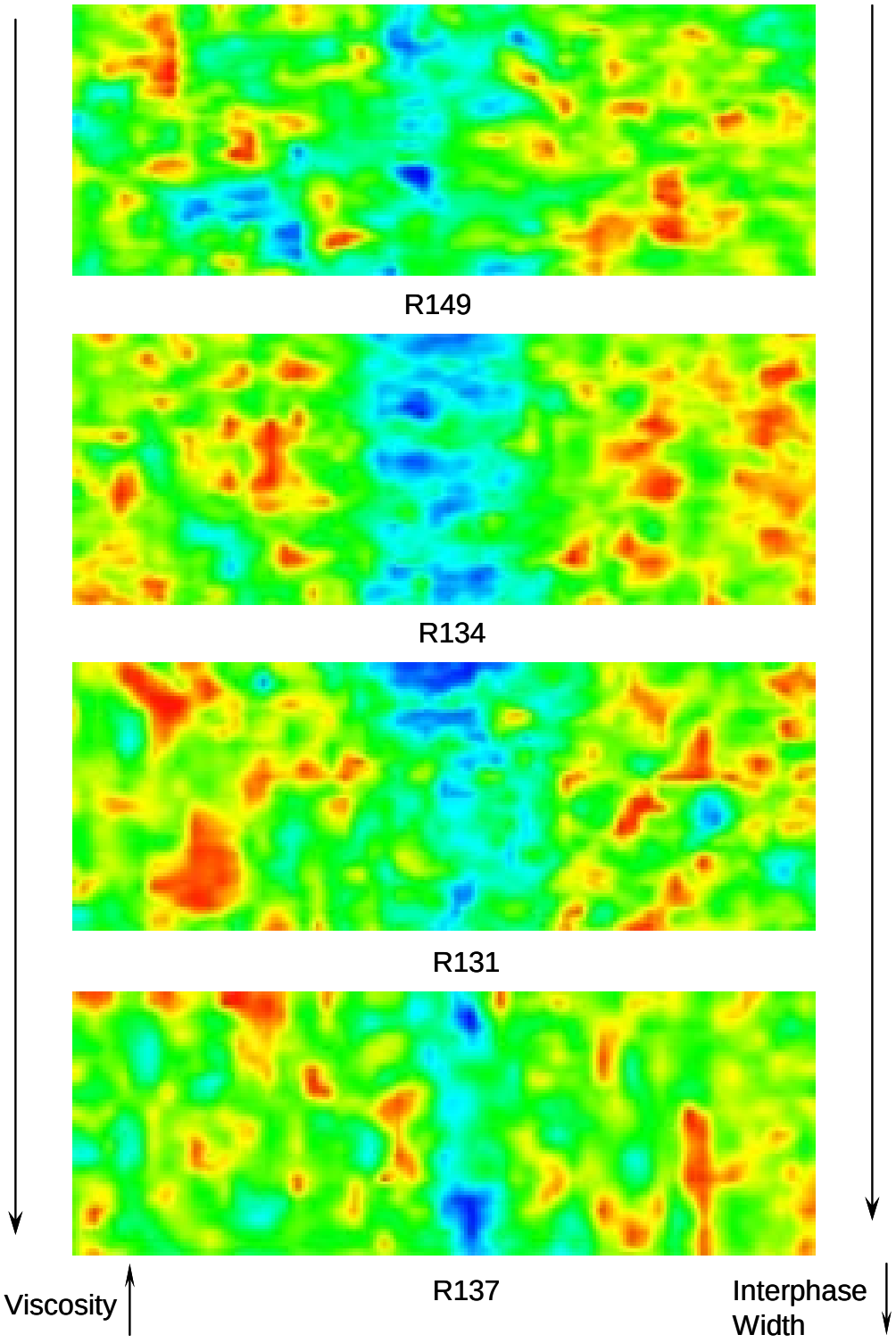

Figure 36. IR Image of Bondline Made with R33 Derivatives.

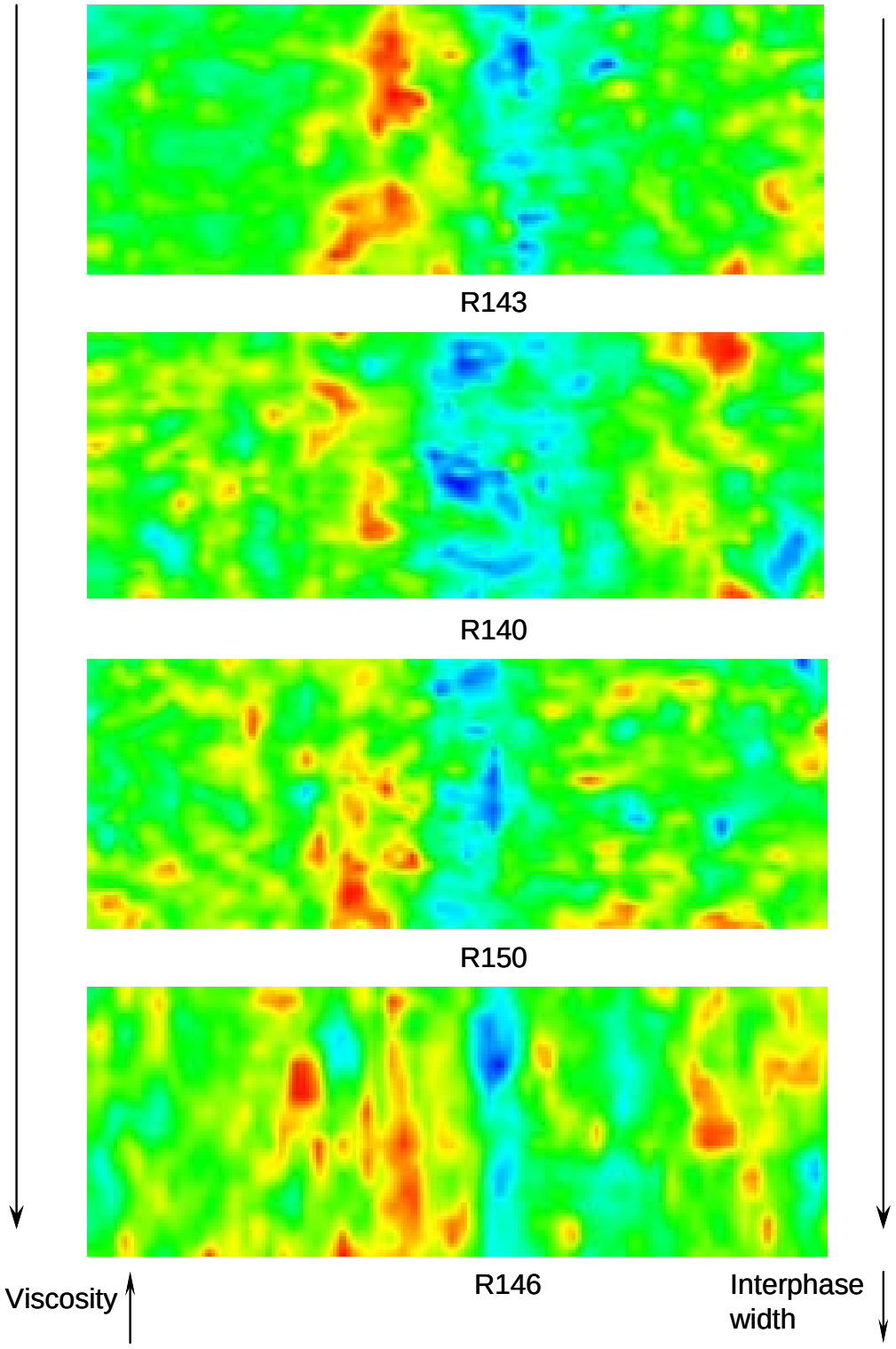

Figure 37. IR Image of Bondline Made with R49 Derivatives.

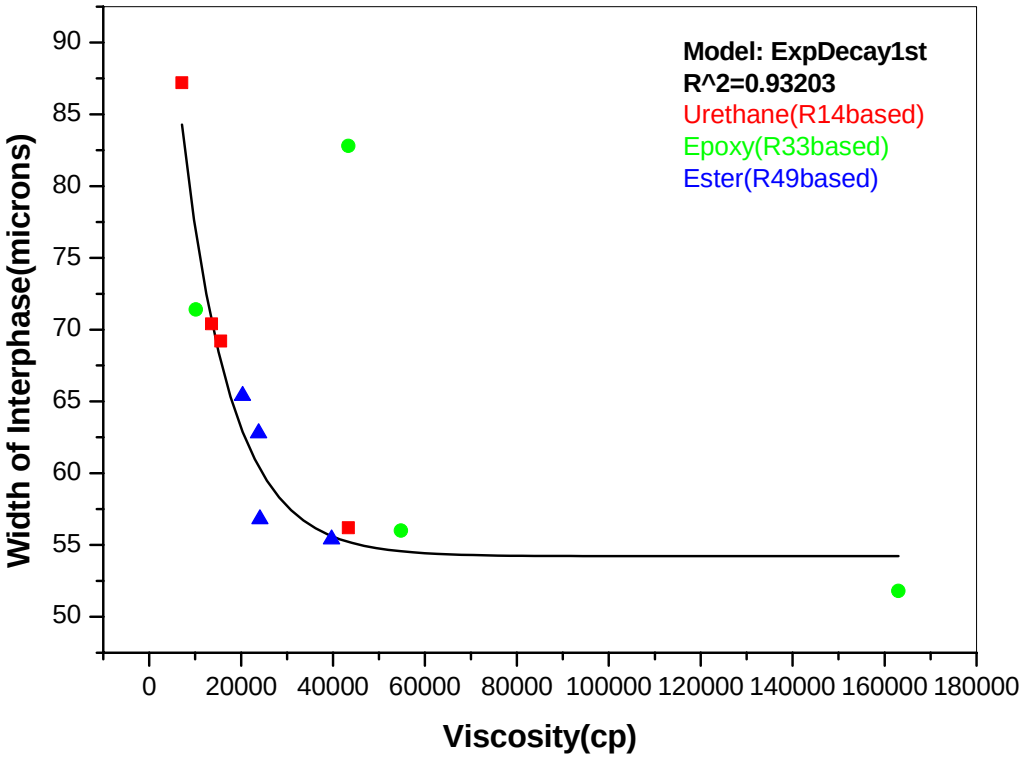

Figure 38. The Interphase Width as a Function of Viscosity.

Table 18 lists shear results of bonded joints and viscosity of resin candidates. There is no clear relationship between shear strength of bonds and viscosity of resins, based on the observation of values in the table.

Surface property investigation indicates no clear relationship between wetting and shear performance of resin-wood bonds. It suggests that other variables are dominating adhesive bond formation and strength. These variables include: technique variability of electron accelerator, environmental factors during shipment of the joints, moisture and temperature differences between resin application and resin cure sites.

Table 18. Viscosity of Resin Candidates in Shear Tests (Set L).

Code	Base Resin	Failing Stress (MPa)	Wood Failure (%)	Viscosity (cp)
LMR122	R14	8.64	0	13573
LMR125		10.7	0	15558
LMR128		11.1	5.63	43339
LMR147		11.3	0.38	7104
LMR131	R33	12.0	0.13	54769
LMR134		13.1	3.63	43339
LMR137		11.1	0.63	163000
LMR149		10.8	0.5	10160
LMR140	R49	4.73	0.5	23813
LMR143		6.95	0.25	20320
LMR146		10.6	0.88	39688
LMR150		8.99	0.25	24103

6 CONCLUSIONS

Totally, 120 unique electron beam curable resins, as individual oligomers or blends, were evaluated.

The e-beam radiation dose for a complete curing of a polymer matrix was optimized for all resins by means of T_g measurements based on DMA spectra as well as attenuation bands in the FTIR spectroscopy. Both studies concluded that the radiation dose for a complete curing was in the range of 20 kGy to 40 kGy for most resins containing acrylate or methacrylate groups. However, a much higher radiation dose was required to cure vinyl ethers. The different curing progress was observed in the resin-wood bondline, where a 40 kGy radiation dose was unable to fully cure resins in the glueline.

The resin formulation studies were focused on the effect of monomers, which not only reduced the viscosity of the oligomers but also participated in the network formation, leading to property modification. The study of dynamic mechanical properties revealed that adding difunctional and trifunctional monomers into base resins resulted in increased E'_{min} values, which signify the increased brittleness of the network. Conversely, the dissipative property of base resins was improved by the presence of monofunctional monomers, indicated by the decreased level of E'_{min}.

The mechanical behavior of resin-wood bonds was evaluated and compared. The correlation between resin properties and bond performance was also explored. The study revealed that energy dissipate capability of resins was a critical factor affecting the mechanical performance of bonded joints. Thus, the adhesive-wood bond strength can be

manipulated by adjusting formulation. With improved energy dissipation of resins, the resin-wood joints exhibited a decent failing strength and deep wood failure. Additionally, the resin-wood bondline and surface properties were investigated. The study showed no direct correlations between wetting (indicated by contact angle and viscosity) and bonds mechanical properties. However, results showed a strong relationship between resin viscosity and penetration into the wood substrate. This suggests that formulation variables can be used to control the breadth of the interphase, and ultimately composite properties.

Finally, the experiments suggest that external, uncontrolled factors created by the conditions of joint preparation may have complicated analysis and interpretation of the data. Specifically, long times between resin application and subsequent cure may have led to over-penetration or other bondline defects.

Two recommendations are addressed here for future research. Surfactants might be employed for further wetting and adhesion mechanism investigation. Specific additives, such as adhesion promoters and coupling agents, might be formulated into resins to promote adhesion between wood and resin matrix. The adhesion study may help to understand the role of lignocelluloses in the progress of electron beam curing.

LIST OF REFERENCES

LIST OF REFERENCES

Aharoni, Shaul M. Corrections between Chain Parameters and the Plateau Modulaus of Polymers. *Macromolecules* 19: 426-434. 1986.

Berejka, Anthony J. and Cliff Eberle. Electron Beam Curing of Composites in North America. *Radiation Physics and Chemistry* 63: 551-556. 2002.

Blomquist, R. F., A. W. Christiansen, R. H. Gillespie, and G. E. Myers. *Adhesive Bounding of Wood and Other Structural Materials.* University Park, PA: The Pennsylvania State University, 1981.

Branalrup, J., E. H. Immergut, and E. A. Grulke. *Polymer Handbook 4th Edition.* New York: John Wiley & Sons, 1999.

Cadlnot, N., B. Boutevin, J. P. Parisi, D. Beziers and E. Chataignier. Electron-beam Curable Structural Adhesives. Part I: Study of Acrylic Resins for Structural Adhesive Applications. *International Journal of Adhesion and Adhesives* 14: 237-241. 1994.

Coqueret, X., B. Defoort, J. M. Dupillier and G. Larnac. Polymerization Kinetics of Acrylate Monomers under UV/EB Radiation: from Lab-scale Monitoring to the Modeling of Industrial Curing. *Radiation Technology Europe Conference*, Berlin. 2003.

Clough, R. L. High-energy Radiation and Polymers: A Review of Commercial Processes and Emerging Applications. *Nuclear Instruments and Methods in Physics Research B* 185: 8-33. 2001.

Errede, L. A. Polymer Swelling. 5. Correlation of Relative Swelling of Poly(styrene-*co*-divinylbenzene) with the Hildebrand Solubility Parameter of the Swelling Liquid.

Macromolecules 19: 1522-1525. 1986.

Flory, Paul J. and John Rehner Jr. Statistical Mechanics of Cross-Linked Polymer Networks. *The Journal of Chemical Physics* 11: 512-526. 1943.

Gardner, Douglas J. Application of the Lifshitz-Van Der Waals Acid Approach to Determine Wood Surface Tension Components. *Wood and Fiber Science* 28(4): 422-428. 1996.

Hale, Arturo and Christopher W. Macosko. Class Transition Temperature as a Function of Conversion in Thermosetting Polymers. *Macromolecules* 24: 2610-2621. 1991.

Hamurcu, E. Elif and Bahattin M Baysal. Solubility Parameter of a Poly(dimethylsiloxane) Network. *Journal of Polymer Science: Part B: Polymer Physics* 32: 591-594. 1994.

Ivanov, V. S. *Radiation Chemistry of Polymers.* Utrecht, Netherlands: VSP, 1992

Liao, D. C., Y. C. Chern, J. L. Han, and K. H. Hsieh Swelling Equilibrium and Sorption Kinetics of Urethane-Modified Bismaleimides Elastomer, *Journal of Polymer Science: Part B: Polymer Physics* 35(11): 1747-1755. 1997.

Lopata, V. J., C. B. Saunders, A. Singh, C. J. Janke, G. E. Wrenn, and S. J. Havens. Electron-beam-curable Epoxy Resins for the Manufacture of High-performance Composites. *Radiation Physics and Chemistry* 56: 405-415. 1999.

Mehnert, R. Electron Beams in Research and Technology. *Nuclear Instruments and Methods in Physics Research B* 105: 348-358. 1995.

Menard, Kevin P. Dynamic Mechanical Analysis: A Practical Introduction. Boca Raton, FL: CRC Press, 1999.

Oberth, Adolf E. Equilibrium Swelling of Polyurethane Elastomers. *Rubber Chemistry*

and Technology 63: 56-65. 1990.

Peacock, Andrew J. ***Handbook of Polyethylene.*** New York: Marcel Dekker, 2000.

Petrie, Edward M. ***Handbook of Adhesives and Sealants.*** New York: McGraw-Hill, 2000.

Ruiz, C. S. B., L. D. B. Machado, E. S. Pino, and M. H. O. Sampa. Characterization of a Clear Coating Cured by UV/EB Radiation. *Radiation Physics and Chemistry* 63: 481-483. 2002.

Sellers, Terry Jr. ***Plywood and Adhesive Technology.*** New York: Marcel Dekker, 1985.

Singh, Ajit. Radiation Processing of Carbon Fiber-reinforced Advanced Composites. *Nuclear Instruments and Methods in Physics Research B* 185: 50-54. 2001.

Singh, Ajit. And J. Silverman. ***Radiation Processing of Polymers.*** New York: Oxford University Press, 1992.

Sturgeon, M. G. and M. L. Lay. Continuous Pressing Medium Density Fiberboard at Nelson Pine Industries New Zealand. *Proceedings 23rd International Particleboard/Composite Materials* Symposium W. S. U.: 179-185. 1989.

Sui, Gang, Zuo-Guang Zhang, C. Q. Chen, and W. H. Zhong. Analyses on Curing Process of Electron Beam Radiation in Epoxy Resins. *Material Chemistry and Physics* 78: 349-357. 2002.

White, James T. Wood Adhesives and Binders: What's the Outlook. *Forest Products Journal* 45(3): 21-28. 1995.

Zosel, A. Mechanical Behavior of Coating Films. *Progress in Organic Coating* 8:47-49. 1980.

VITA

Ting Song was born the first child to Mr. and Mrs. Song in China in 1976. She received her Bachelor of Science Degree in Polymer Engineering after four years in Beijing University of Chemical Technology in 1998. Devoted in the research area of surface modification by UV radiation, her work mainly focused on the UV irritated grafting polymerization on polypropylene surface. In 2001, she received the Maser of Science Degree in Polymer Engineering in the same university.

Ting Song currently is pursuing her second master degree at University of Tennessee, Knoxville. Her research is related to electron beam cured resins for wood composites.